UC San Diego

UC San Diego Electronic Theses and Dissertations

Title

High Frequency Electromagnetic Effects in Micromagnetic Simulations

Permalink

https://escholarship.org/uc/item/8gp3k1dk

Author

Archambault-Couture, Simon

Publication Date

2017

Peer reviewed|Thesis/dissertation

eScholarship.org Powered by the California Digital Library
University of California

UNIVERSITY OF CALIFORNIA SAN DIEGO

High Frequency Electromagnetic Effects in Micromagnetic Simulations

A dissertation submitted in partial satisfaction of the
requirements for the degree
Doctor of Philosophy

in

Electrical Engineering (Applied Physics)

by

Simon Archambault-Couture

Committee in charge:

Professor Vitaliy Lomakin, Chair
Professor Randolph E. Bank
Professor Yeshaiahu Fainman
Professor Eric Fullerton
Professor Ying Shirley Meng

2018

Copyright
Simon Archambault-Couture, 2018
All rights reserved.

The dissertation of Simon Archambault-Couture is approved, and it is acceptable in quality and form for publication on microfilm and electronically:

_____

_____

_____

_____

_____

Chair

University of California San Diego

2018

DEDICATION

For Attieh and Arno

EPIGRAPH

J’ai été nourri aux lettres dès mon enfance, et parce qu’on me persuadait que, par leur moyen, on pouvait acquérir une connaissance claire et assurée de tout ce qui est utile à la vie, j’avais un extrême désir de les apprendre. Mais, sitôt que j’eus achevé tout ce cours d’études, au bout duquel on a coutume d’être reçu au rang des doctes, je changeai entièrement d’opinion. Car je me trouvais embarrassé de tant de doutes et d’erreurs, qu’il me semblait n’avoir fait autre profit, en tâchant de m’instruire, sinon que j’avais découvert de plus en plus mon ignorance.

—René Descartes in *Discours de la Méthode*, 1637

TABLE OF CONTENTS

LIST OF FIGURES

LIST OF TABLES

ACKNOWLEDGEMENTS

I would like to foremost thank my wife, Attieh, who gave me her love and support throughout my doctoral studies, somehow finding the strength to do that after having herself just completed her own doctoral studies. Special thanks also go out to my parents, who always encouraged me to pursue my interests and passions. Thank you to my research advisor, Professor Vitaliy Lomakin, who believed in me and gave me almost complete freedom to pursue my research interests, but yet was always available to provide guidance and insightful technical knowledge when problems arose. Thank you to my labmates, Majd Kuteifan, Sidi Fu, Iana Volvach, Marco Menarini, Ruinan Chang, Marko Lubarda, Marco Escobar and Xueyang Wang for creating an environment where stimulating technical discussions were complemented by just great camaraderie. Thank you to the professors, students and staff of CMRR who organized lectures by specialists in their field from around the world and who participated in the CMRR research conferences where I had the opportunity to get acquainted with the different fields of research being pursued at UC San Diego. Thank you to Professor Eric Fullerton and Sergio Montoya, who gave me the opportunity to participate in their work with magnetic materials in the laboratory and to validate micromagnetic simulation results with actual measurements, and with whom I had many stimulating discussions.

Chapter 3, in part, is currently being prepared for submission for publication, Couture, Simon; Lomakin, Vitaliy. The dissertation author was the primary investigator and author of this material.

Chapter 4, in part, contains material that appears in Coupled Finite-Element Micromagnetic - Integral Equation Electromagnetic Simulator for Modeling Magnetization-Eddy Currents Dynamics, IEEE Trans. Magn., 2017, Couture, Simon; Chang, Ruinan; Volvach, Iana; Goncharov, Alexander; Lomakin, Vitaliy, as well as material that has been submitted for publication, Modeling Eddy Currents in Micromagnetic Simulations: A Coupled Micromagnetic-Maxwell Equations Solver Based on the Finite Element Method, 2018, Couture, Simon; Goncharov,

Alexander; Lomakin, Vitaliy. The dissertation/thesis author was the primary investigator and author of these papers.

VITA

2009	B. Sc. in Electrical Engineering, University of Montreal, Montreal
2011	M. Sc. A. in Electrical Engineering, University of Montreal, Montreal
2018	Ph. D. in Electrical Engineering (Applied Physics), University of California San Diego

ABSTRACT OF THE DISSERTATION

High Frequency Electromagnetic Effects in Micromagnetic Simulations

by

Simon Archambault-Couture

Doctor of Philosophy in Electrical Engineering (Applied Physics)

University of California San Diego, 2018

Professor Vitaliy Lomakin, Chair

This work is concerned with the important connection that exists between micromagnetism and high frequency electromagnetism. As micromagnetic solvers have become important tools in the study and engineering of magnetic devices, and as these devices are increasingly operated at high frequencies, it is important to understand both how micromagnetic simulations can be used in the modeling of magnetic materials for high-frequency applications and how micromagnetic models can be impacted by high-frequency electromagnetic effects.

After an introduction to the theory behind micromagnetism and micromagnetic solvers, the dissertation is divided into two main themes. The first one is the modeling and characterization through micromagnetic simulations of ferromagnetic materials for high frequency applica-

tions. A particular class of materials, namely ferromagnetic nano-granular materials, are studied since they have important technological applications as soft magnetic materials which also exhibit high saturation magnetizations and low electrical resistivities. The extraction of properties such as the hysteresis loop and frequency dependent permeability tensor from micromagnetic simulations is examined. Also, the anisotropy averaging mechanism responsible for the soft magnetic properties of this class of materials is studied and some theoretical results are obtained and presented, such as a derivation of the residual exchange energy between groups of exchange coupled nano-particles and a generalized Stoner-Wohlfarth hysteresis model which accounts for exchange interactions between ferromagnetic particles with random uniaxial anisotropies.

The second theme is the modeling of eddy currents in micromagnetic simulations. Eddy currents, also known as Foucault currents, arise in conductive materials due to rapid variations of the magnetic field and magnetization. A method coupling the Landau-Lifshitz-Gilbert equation of micromagnetics with the magnetoquasistatic Maxwell equations is presented. Based on this method, two coupled micromagnetic-electromagnetic solvers are presented, one based on an integral equation formulation, the other based on the finite element method. A test problem with a known analytical solution is suggested and used to validate the implemented solvers. Also, results concerning the bounds of validity for the magnetostatic approximation to the Maxwell equations, in which case eddy currents are neglected, as well as for the magnetoquasistatic Maxwell equations, where eddy currents are accounted for but electromagnetic wave propagation is neglected, are given. It is found that the magnetoquasistatic approximation is excellent for the vast majority of micromagnetic simulations that are executed today.

Chapter 1

Introduction

1.1 Definitions and basic concepts

Magnetic materials are omnipresent in modern technology. From their use in large scale devices such as power grid transformers and electric car engines, to their dominant role in information recording technologies, mentioning in passing their use in microelectronics with integrated inductors, or their use in telecommunication devices such as RF circulators, it is clear that many of the technologies that today's society relies on require the use of magnetic materials. Despite their widespread use and the fact that magnetic materials have been known for a long time — the first electric motors and transformers appeared at the beginning and end of the 19th century respectively [1, 2] while the first magnetic tape recorders were developed in the 1920's [3] — they are still the subject of research interest. This is due to the existence of a vast array of magnetic alloys and ways to prepare them which can dramatically alter their properties but also to the complexity of the physical laws that govern magnetic phenomena. For instance, the magnetization inside magnetic materials arranges itself in non-trivial way, often in so-called magnetic domains of various shapes and sizes, as shown in Fig. 1.1.

Magnetic domains are the result of competing interactions such as the Heisenberg or ex-

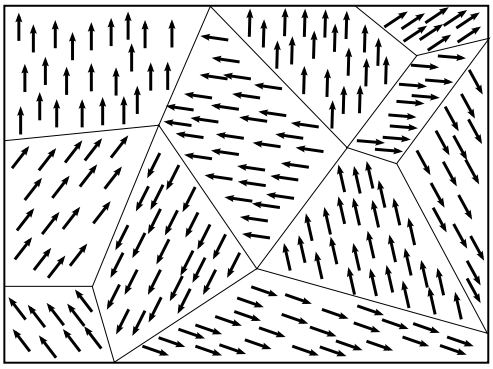

Figure 1.1: Magnetic domains in a ferromagnet. Arrows indicate the direction of magnetization in each domain.

change interaction which favors a parallel alignment of electronic spins of neighboring atoms in ferromagnetic crystals, as shown in Fig. 1.2, the crystalline anisotropy interaction where a spin orientation along certain axes of a crystal lattice is favored, the magnetostrictive interaction where magnetization tends to align based on the direction of strain in the material, or the magnetostatic interaction in which a magnetic field is produced which depends on the macroscopic shape of a magnetic sample and the magnetization's arrangement within that sample.

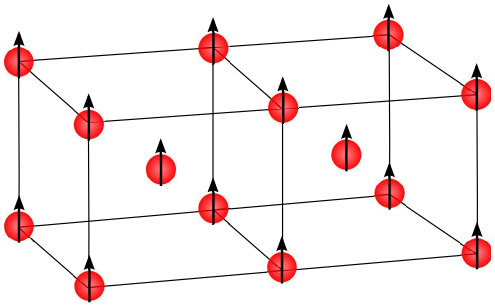

Figure 1.2: The electronic spins at atomic sites in a ferromagnetic crystal tend to align parallel to each other due to the Heisenberg interaction.

An important tool in the study of magnetic materials is the use of computers to simulate their behavior. This subfield of magnetism has come to be known as micromagnetism and the concepts that led to its foundation were summarized and arranged in the form of modern micromagnetic theory in a 1963 monograph by Brown [4]. Micromagnetism is based on the idea that, while the origins of magnetism can be understood in terms of electronic spin at the

atomic level, much understanding of magnetic materials can be gained from considering not microscopic magnetization, that is magnetization at the atomic scale, but rather a macroscopic magnetization consisting of the spatially averaged microscopic magnetization. This is analogous to what is done in electromagnetism, where one customarily works with macroscopic, i.e. spatially averaged versions of the electromagnetic fields, and where the microscopic properties of materials are taken into account by parameters such as the material permittivity and permeability [5, 6]. In fact, in the framework of macroscopic electromagnetism, the magnetization quantity that appears in the equations corresponds to the macroscopic magnetization of micromagnetism.

Using the approach of micromagnetism, the detail of what happens at the atomic level is lost, however the averaged magnetization, which is now treated as a continuous field quantity, can still resolve features of the magnetization such as magnetic domains. In many cases, this is all that is needed in order to study the properties of a magnetic material. This is especially true for ferromagnetic materials, where the exchange interaction forces magnetization to be uniform within regions of up to a few nanometers in size.

The rapid increase in the computational power available to researchers which occured in the last few decades combined with advances in numerical algorithms and methods has enabled micromagnetic studies of increasingly large and complex problems. For instance, in a doctoral dissertation published in 1997, Yang [7] describes the simulation of an array of 16 ellipsoid particles, each discretized using about 4400 tetrahedral element, for a total of about 70,000 elements using a Cray T3D supercomputer with 256 processors. Today, micromagnetic simulations with 10 millions tetrahedral elements are routinely run on desktop computers while problems with hundreds of millions of elements can be solved by more specialized hardware. As micromagnetic solvers gained the ability to handle larger problems, devices such as hard-disk recording heads or magnetic tunnel junctions, which are used in emerging memory technologies [8], were micromagnetically modeled for the purpose of engineering and optimizing them.

1.2 Problems and research aims

Micromagnetism has emerged as a successful technique in the study and design of magnetic materials and devices. As larger problems can now be considered, a challenge within micromagnetism is to identify new ways in which it can be used, new structures that can be studied, or new phenomena that can be incorporated in the model, which perhaps were not achievable previously due to limitations in computing ressources and in the efficiency of solvers. This is the overarching question that guided the present work.

An interesting avenue of investigation appears when micromagnetism is considered from the point of view of electromagnetism. Magnetism is of course intimately related to electromagnetism since the macroscopic magnetization appears explicitly in the Maxwell equations. Despite this, and perhaps not surprisingly, micromagnetic studies usually focus on the physics of magnetism itself, aiming at better understanding the magnetization distribution within magnetic devices, both in terms of the static distribution at equilibrium and magnetizatin dynamics when the system is excited by some external source, while taking into account various magnetic interactions such as the ones previously mentioned but also other, sometimes newly discovered, interactions such as electronic spin transfer [9], the Dzyaloshinsky-Moriya interaction [10] or the different mechanisms which are currently being put forward to explain all-optical switching in magnetic materials [11]. By contrast, from the point of view of electromagnetism, knowledge of the magnetization arrangement inside a magnetic material is not an end in itself but rather is regarded as a response to electromagnetic fields and the focus is placed on how the magnetization and the fields interact together. Electromagnetic theory usually relies on the definition of a material's permeability to characterize its magnetic response. While linear permeability models are adequate in many situations and various more refined models have been used to deal with more complicated aspects of magnetic materials such as hysteresis and non-linearity, very few electromagnetism practitioners have looked at micromagnetism as a tool to better characterize a

magnetic material in terms of its interaction with electromagnetic fields. One of the aims of the present work was therefore to examine to which extent micromagnetic simulations can be used to characterize a magnetic material from the point of view of macroscopic electromagnetism.

Whereas micromagnetism has not been fully exploited in the study of electromagnetism, the same can be said of electromagnetism from the perspective of micromagnetism. Historically, micromagnetic studies have considered only the static Maxwell equations. This is done through the magnetostatic interaction, where the magnetic field produced by the magnetization distribution is taken into account. In so doing however, all electrodynamic effects are effectively neglected. The rationale for this assumption has been that the small size of simulated structures allows the propagation time of electromagnetic wave through the structure, which is determined by the propagation speed corresponding to the speed of light and the size of the structure, to be much shorter than the characteristic time of magnetization dynamics. An aim of the present research was to re-examine this assumption and study electrodynamic effects in micromagnetism.

1.3 Dissertation structure

The dissertation is organized into three main chapters: chapters 2, 3 and 4. In chapter 2, the foundations of micromagnetism are presented. The goal of this chapter is to provide the reader with a basic understanding of the physics of magnetism and micromagnetic modeling so as to set up the discussions in subsequent chapters. The formulation on which the FastMag micromagnetic solver is based, which was used for the present work, is presented. However, details of the implementation such as, for example, how the computation of certain integrals is hardware-accelerated using graphic processing units (GPU) are not given and the reader is instead referred to the relevant publications.

In chapter 3, a particular class of magnetic material consisting of ferromagnetic nanograins in a dielectric host medium is considered. This class of material has important practical

applications such as in integrated inductors due to their high permeability, low losses and capability to operate at high frequencies. As an example of how micromagnetism can be used to characterize magnetic materials in terms of their electromagnetic properties, the hysteresis loop and high frequency permeability tensor of these materials are studied using micromagnetic simulations. The high permeability of this class of materials is due to anisotropy averaging among neighboring, exchange coupled grains. Some results relating to this averaging process were obtained and are presented in this chapter. These include the averaging of groups of nano-particles into so-called effective particles as well as a generalized Stoner-Wohlfarth model for exchange coupled particles.

Chapter 4 couples micromagnetism with Maxwell's equations to account for the dynamic nature of electromagnetic fields. It examines the validity of the static approximation of the Maxwell equations in micromagnetic simulations. It is found that in some cases, the dynamic Maxwell equations must be considered. Whereas it is found that, at least for the time being, the full Maxwell equations are usually not required in micromagnetic simulations, the quasistatic Maxwell equations are found to be an adequate middle ground which allows the modeling of the eddy currents effect. The limits of validity of these different approximations are discussed. The rest of the chapter is devoted to the coupling of the quasistatic Maxwell equations with the micromagnetic model. Formulations based on both integral equations and the finite element method are presented. The effects of eddy currents in micromagnetic simulations are discussed as well as the performance of the different solution methods.

Chapter 2

Micromagnetism

In this chapter, the foundations of micromagnetic simulations are presented. In section 2.1, the Landau-Lifshitz-Gilbert equation is introduced and a justification for it is given based on the Lagrangian formalism. Section 2.2 introduces the concept of effective fields and expressions are given for the effective fields for the exchange interaction and uniaxial crystalline anisotropy. In section 2.3, the magnetostatic field is seen to be induced by the magnetization distribution in the magnetic material and its computation by solving the static Maxwell equations is discussed. The concept of shape anisotropy, closely related to the magnetostatic field, is also introduced. In section 2.4, the space and time discretization schemes used to compute a numerical solution to the Landau-Lifshitz-Gilbert equation are presented.

2.1 The Landau-Lifshitz-Gilbert equation

The governing equation of micromagnetism is the Landau-Lifshitz-Gilbert equation. It is essentially an equation for the conservation of angular momentum applied to a charged particle, more specifically the spinning electron. Lets first consider the origin of this equation for a system without damping using the Lagrangian formalism of classical mechanics.

Consider a particle with mass m_p, charge q and moving with a velocity $\vec{v}$ subjected to a

magnetic field $\vec{B}$ and an electric field $\vec{E}$. Then the Lorentz force acting on this particle is

$$\vec{F} = q\left(\vec{E} + \vec{v} \times \vec{B}\right) \ . \tag{2.1}$$

This force can be derived from the generalized or velocity-dependent potential [12]

$$U = q\phi - q\vec{A} \cdot \vec{v} \tag{2.2}$$

where Φ is the electric scalar potential and $\vec{A}$ is the magnetic vector potential. To show this, first consider the Maxwell equations

$$\nabla \times \vec{E} = -\frac{\partial \vec{B}}{\partial t} \tag{2.3a}$$

$$\nabla \times \vec{H} = \frac{\partial \vec{D}}{\partial t} + \vec{J} \tag{2.3b}$$

$$\nabla \cdot \vec{D} = \rho \tag{2.3c}$$

$$\nabla \cdot \vec{B} = 0 \ . \tag{2.3d}$$

Because of Eq. (2.3d), $\vec{B}$ can be written as the curl of some vector field. The magnetic vector potential is defined such that $\vec{B} = \nabla \times \vec{A}$. Therefore, Eq. (2.3a) can be written as

$$\nabla \times \left(\vec{E} + \frac{\partial A}{\partial t}\right) = 0 \ . \tag{2.4}$$

Since any irrotational vector field can be written as the gradient of some scalar function, the electric scalar potential Φ is introduced such that

$$\vec{E} + \frac{\partial A}{\partial t} = -\nabla\Phi \ . \tag{2.5}$$

To show that the Lorentz force can be derived from the potential of Eq. (2.2), consider cartesian

coordinates. Then, according to Lagrange formalism the ith component of the force must be given by

$$F_i = -\frac{\partial U}{\partial x_i} + \frac{d}{dt}\left(\frac{\partial U}{\partial \dot{x}_i}\right) \tag{2.6}$$

where x_i is the ith cartesian coordinate of the particle and $\dot{x}_i \equiv \partial x_i/\partial t$ is its time derivative, also corresponding to v_i, the ith component of its velocity. Using Eq. (2.2), this becomes

$$F_i = q\sum_{j=1}^{3} v_j \frac{\partial A_j}{\partial x_i} - q\frac{\partial \Phi}{\partial x_i} - q\frac{dA_i}{dt} \ . \tag{2.7}$$

Using the chain rule, the time derivative of A_i can be written in terms of partial derivatives as

$$\frac{dA_i}{dt} = \frac{\partial A_i}{\partial t} + \sum_{j=1}^{3} \frac{\partial A_i}{\partial x_j}\dot{x}_j \tag{2.8}$$

Writing $\dot{x}_j = v_j$ and inserting in Eq. (2.7) gives

$$F_i = q\sum_{j=1}^{3} v_j \left[\frac{\partial A_j}{\partial x_i} - \frac{\partial A_i}{\partial x_j}\right] - q\frac{\partial \Phi}{\partial x_i} - q\frac{\partial A_i}{\partial t} \ . \tag{2.9}$$

It can be seen that this is equivalent to

$$F_i = q\sum_{j=1}^{3} v_j \sum_{k,m,n=1}^{3} \left[\varepsilon_{ijk}\varepsilon_{mnk}\frac{\partial A_n}{\partial x_m}\right] - q\frac{\partial \Phi}{\partial x_i} - q\frac{\partial A_i}{\partial t} \tag{2.10}$$

where ε_{ijk} is the Levi-Civita symbol. Eq. (2.10) can be written as

$$F_i = q\sum_{j=1}^{3} v_j \sum_{k=1}^{3} \varepsilon_{ijk}\left[\nabla \times \vec{A}\right]_k - q\frac{\partial \Phi}{\partial x_i} - q\frac{\partial A_i}{\partial t} \tag{2.11}$$

and using $\vec{B} = \nabla \times \vec{A}$, this becomes

$$F_i = q\left[\vec{v} \times \vec{B}\right]_i - q\frac{\partial \Phi}{\partial x_i} - q\frac{\partial A_i}{\partial t} \ . \tag{2.12}$$

Finally, from Eq. (2.5), the two last terms are seen to correspond to the *i*th component of the $\vec{E}$ field so that

$$F_i = q\left(E_i + \left[\vec{v}\times\vec{B}\right]_i\right) \tag{2.13}$$

which is the Lorentz force Eq. (2.1).

Assuming that the $\vec{B}$ field is uniform around the particle, the magnetic vector potential can be taken as

$$\vec{A} = \frac{1}{2}\vec{B}\times\vec{x} \tag{2.14}$$

where $\vec{x}$ is the position vector of the particle. It is easily verified that $\vec{B} = \nabla\times\vec{A}$ with $\vec{A}$ given by Eq. (2.14). With this, the generalized potential of Eq. (2.2) is given by

$$U = q\Phi - q\left(\frac{1}{2}\vec{B}\times\vec{x}\right)\cdot\vec{v} = q\Phi - \left(\frac{1}{2}\vec{x}\times q\vec{v}\right)\cdot\vec{B}\,. \tag{2.15}$$

The quantity $\frac{1}{2}\vec{x}\times q\vec{v}$ is by definition the magnetic moment $\vec{m}$ associated with the particle. Therefore the generalized potential can be written as

$$U = q\Phi - \vec{m}\cdot\vec{B}\,. \tag{2.16}$$

Now consider as a generalized coordinate in the context of Lagrange formalism the angle θ that the magnetic moment $\vec{m}$ makes with the field $\vec{B}$. A change in this generalized coordinate θ can be regarded as a rotation of the magnetic moment $\vec{m}$ around $\hat{n}$, an axis perpendicular to the plane defined by $\vec{m}$ and $\vec{B}$, as shown in Fig. 2.1a. The Lagrangian for the particle is

$$L = T - U \tag{2.17}$$

where $T = \frac{1}{2}m_p|\vec{v}|^2$ is the particle's kinetic energy and U is the potential of Eq. (2.16). The

Lagrange equation of motion for the generalized coordinate θ is

$$\frac{d}{dt}\left(\frac{\partial L}{\partial \dot{\theta}}\right) = \frac{\partial L}{\partial \theta} \tag{2.18}$$

where $\dot{\theta}$ denotes the time derivative of θ.

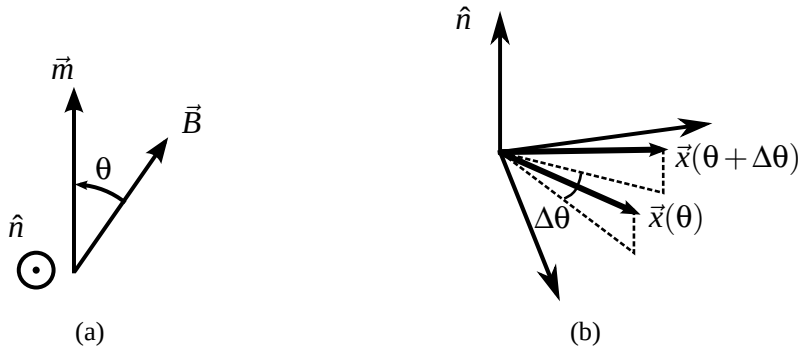

Figure 2.1: (a) Generalized coordinate θ corresponding to the angle between the $\vec{B}$ and $\vec{m}$ vectors. (b) The rotation of $\vec{m}$ by an angle $\Delta\theta$ also implies a rotation of $\vec{x}$, the particle's position vector.

At this point, the potential U is written in terms of θ. Also, while a particle with velocity $\vec{v}$ is being considered, what is really the object of the present discussion is the spinning electron, which classically can be thought of as a spinning body with a finite size. In this picture, the charged particle with velocity $\vec{v}$ that is considered here would be a point of this spinning body. Since we are only concerned with the electron's spin and not a translation movement, and since the electric scalar potential Φ only depends on translation movements and not on the spin, the term $q\Phi$ in the potential of Eq. (2.16) can be neglected. Therefore the potential U of Eq. (2.16) can be written as

$$U = -|\vec{m}||\vec{B}|\cos\theta\ . \tag{2.19}$$

Lets evaluate the left-hand side of the Lagrange equation Eq. (2.18). The quantity inside

parentheses corresponds to

$$\frac{\partial L}{\partial \dot{\theta}} = \frac{\partial T}{\partial \dot{\theta}} - \frac{\partial U}{\partial \dot{\theta}} \tag{2.20}$$

From Eq. (2.19), it is seen that U does not depend on $\dot{\theta}$, therefore $\partial U/\partial\dot{\theta} = 0$. The particle's kinetic energy T can be written $T = \frac{1}{2} m_p \dot{\vec{x}} \cdot \dot{\vec{x}}$ so that

$$\frac{\partial T}{\partial \dot{\theta}} = m_p \dot{\vec{x}} \cdot \frac{\partial \dot{\vec{x}}}{\partial \dot{\theta}} \tag{2.21}$$

If r_i, $i = 1, 2, \ldots, n$, along with θ are independent generalized coordinates that describe the particle system, then the position vector of the particle is $\vec{x} = \vec{x}(\theta, r_1, r_2, \ldots, r_n)$ and its time derivative is given by

$$\dot{\vec{x}} = \frac{\partial \vec{x}}{\partial \theta}\dot{\theta} + \sum_{k=1}^{n} \frac{\partial \vec{x}}{\partial r_k} \dot{r}_k \, . \tag{2.22}$$

From this, it is seen that

$$\frac{\partial \dot{\vec{x}}}{\partial \dot{\theta}} = \frac{\partial \vec{x}}{\partial \theta} \, . \tag{2.23}$$

The rotation of $\vec{m}$ around $\hat{n}$ by an angle $\Delta\theta$ implies the same rotation of the position vector $\vec{x}$. Such a rotation of $\vec{x}$ is depicted in Fig. 2.1b from which one can observe that

$$\frac{\partial \vec{x}}{\partial \theta} = \lim_{\Delta\theta \to 0} \frac{\vec{x}(\theta + \Delta\theta) - \vec{x}(\theta)}{\Delta\theta} = \hat{n} \times \vec{x} \, . \tag{2.24}$$

Using Eqs. (2.23) and (2.24), Eq. (2.21) can be written as

$$\frac{\partial T}{\partial \dot{\theta}} = m_p \dot{\vec{x}} \cdot (\hat{n} \times \vec{x}) \, . \tag{2.25}$$

Since $\dot{\vec{x}} = \vec{v}$, and permutating the triple product, this becomes

$$\frac{\partial T}{\partial \dot{\theta}} = m_p \hat{n} \cdot (\vec{x} \times \vec{v}) \tag{2.26}$$

which is recognized as the $\hat{n}$ component of the angular momentum $\vec{L} = m_p \vec{x} \times \vec{v}$, that is,

$$\frac{\partial T}{\partial \dot{\theta}} = \hat{n} \cdot \vec{L} \ . \tag{2.27}$$

The right-hand side of the Lagrange equation, Eq. (2.18) corresponds to

$$\frac{\partial L}{\partial \theta} = \frac{\partial T}{\partial \theta} - \frac{\partial U}{\partial \theta} \ . \tag{2.28}$$

While a rotation of $\vec{m}$ also implies a rotation of the velocity vector $\vec{v}$, the magnitude of $\vec{v}$ is invariant under the rotation, so that $\partial T / \partial \theta = 0$. From the expression for the potential U, Eq. (2.19), one obtains

$$\frac{\partial U}{\partial \theta} = |\vec{m}||\vec{B}| \sin\theta \tag{2.29}$$

so that the Lagrange equation of movement, Eq. (2.18) reads

$$\frac{d}{dt}(\hat{n} \cdot \vec{L}) = -|\vec{m}||\vec{B}| \sin\theta \ . \tag{2.30}$$

Since $\hat{n}$ is the unit vector in the direction of $\vec{B} \times \vec{m}$, Eq. (2.30) can be written as

$$\frac{d\vec{L}}{dt} = \vec{m} \times \vec{B} \tag{2.31}$$

which says that the rate of change of a charged particle's angular momentum is $\vec{m} \times \vec{B}$, which can then be interpreted as a torque applied on the particle. As mentioned previously, we are in reality interested in the spinning electron instead of the actual motion of a charged particle. In that case, Eq. (2.31) is still valid but $\vec{m}$ has to be interpreted as the magnetic moment of the spinning electron. Then it is useful to consider the relationship between the magnetic moment of a spinning electron and its angular momentum, $\vec{m} = \gamma \vec{L}$ where γ is the electron's gyromagnetic

ratio, given by

$$\gamma = \frac{q_e g}{2m_e} \tag{2.32}$$

where $q_e < 0$ is the electronic charge, m_e is the electron's mass and $g \approx 2$ is the electronic spin g factor. Therefore, Eq. (2.31) can be written as

$$\frac{d\vec{m}}{dt} = \gamma \vec{m} \times \vec{B} \tag{2.33}$$

which is the equation of motion for the magnetic moment in a field $\vec{B}$.

A lossless system is assumed in Eq. (2.33) since it predicts that a magnetic moment subjected to a magnetic field would precess forever around this field. Landau and Lifshitz in a 1935 paper [13] and then Gilbert in his 1956 Ph.D. thesis, the relevant parts of which are summarized in a 2004 paper [14], proposed the addition of a damping term in Eq. (2.33) which would cause the magnetic moment $\vec{m}$ to relax to the lowest energy state which corresponds to alignment with $\vec{B}$. Landau and Lifshitz proposed to add the following term to Eq. (2.33),

$$\frac{d\vec{m}}{dt} = \gamma \vec{m} \times \vec{B} - \frac{\lambda}{|\vec{m}|^2} \vec{m} \times \vec{m} \times \vec{B} \tag{2.34}$$

where λ is a damping coefficient. Gilbert instead argued that a damping term could be introduced based on Lagrangian formalism by adding a term to the Lagrange equation Eq. (2.18), representing a damping generalized force, or in the present case a damping torque,

$$\frac{d}{dt}\left(\frac{\partial L}{\partial \dot{\vec{m}}}\right) = \frac{\partial L}{\partial \vec{m}} - \frac{\partial}{\partial \dot{\vec{m}}}\left(\frac{\eta}{2}\dot{\vec{m}} \cdot \dot{\vec{m}}\right) \tag{2.35}$$

where η is a damping coefficient and where the generalized coordinate here is the magnetic moment $\vec{m}$ instead of the angle θ as in Eq. (2.18) [1]. This is analogous to Rayleigh's dissipation

[1] The damping torque cannot be derived using only the θ generalized coordinate and as Gilbert mentions in his 2004 paper [14], it is in fact not straightforward to derive Eq. (2.33) using the Lagrangian formalism. In fact, the approach that was taken here necessitates certain assumptions, notably in the choice of a complete set of generalized

function $\frac{1}{2}\lambda\dot{\vec{x}}\cdot\dot{\vec{x}}$, the derivative of which with respect to $\dot{\vec{x}}$, corresponding to $\lambda\dot{\vec{x}}$, is added to the Lagrange equation as a friction force for the case of an object moving with velocity $\vec{v}=\dot{\vec{x}}$ [12]. The result of this is that Eq. (2.33) becomes

$$\frac{d\vec{m}}{dt}=\gamma\vec{m}\times\vec{B}+\frac{\alpha}{|\vec{m}|}\vec{m}\times\frac{\partial\vec{m}}{\partial t} \tag{2.36}$$

where α is a damping coefficient related to η. This is the Landau-Lifshitz-Gilbert equation and it can be put in a form similar to the Landau-Lifshitz equation, Eq. (2.34). Indeed, taking the cross product of $\vec{m}$ with Eq. (2.36) gives

$$\vec{m}\times\frac{d\vec{m}}{dt}=\gamma\vec{m}\times(\vec{m}\times\vec{B})+\frac{\alpha}{|\vec{m}|}\vec{m}\times\left(\vec{m}\times\frac{\partial\vec{m}}{\partial t}\right)\ . \tag{2.37}$$

Using the vector identity $\vec{a}\times(\vec{b}\times\vec{c})=(\vec{a}\cdot\vec{c})\vec{b}-(\vec{a}\cdot\vec{b})\vec{c}$, this becomes

$$\vec{m}\times\frac{d\vec{m}}{dt}=\gamma\vec{m}\times(\vec{m}\times\vec{B})+\frac{\alpha}{|\vec{m}|}\left[\left(\vec{m}\cdot\frac{d\vec{m}}{dt}\right)\vec{m}-(\vec{m}\cdot\vec{m})\frac{d\vec{m}}{dt}\right]\ . \tag{2.38}$$

Since it is assumed that the magnitude of $\vec{m}$ is invariant, it follows that $\frac{d\vec{m}}{dt}$ is perpendicular to $\vec{m}$ so that $\vec{m}\cdot\frac{d\vec{m}}{dt}=0$ and Eq. (2.38) reduces to

$$\vec{m}\times\frac{d\vec{m}}{dt}=\gamma\vec{m}\times(\vec{m}\times\vec{B})-\alpha|\vec{m}|\frac{d\vec{m}}{dt}\ . \tag{2.39}$$

Substituting this expression for $\vec{m}\times d\vec{m}/dt$ into Eq. (2.36) yields

$$\frac{d\vec{m}}{dt}=\gamma\vec{m}\times\vec{B}+\frac{\alpha}{|\vec{m}|}\left[\gamma\vec{m}\times(\vec{m}\times\vec{B})-\alpha|\vec{m}|\frac{d\vec{m}}{dt}\right] \tag{2.40}$$

coordinates, which are hinted by Goldstein in [12], p.232, and which complicates the passage from Eq. (2.30) to Eq. (2.31). These complications are not dealt with here and the procedure employed here should be regarded as a justification of the Landau-Lifshitz-Gilbert equation rather than a rigorous proof.

which simplifies to

$$\frac{d\vec{m}}{dt} = \frac{\gamma}{1+\alpha^2}\vec{m}\times\vec{B} + \frac{\gamma\alpha}{(1+\alpha^2)|\vec{m}|}\vec{m}\times(\vec{m}\times\vec{B}) \ . \tag{2.41}$$

This equation is almost identical to the Landau-Lifshitz equation, Eq. (2.34), except that the gyromagnetic ratio is divided by the quantity $1+\alpha^2$. Since experiments have shown that the value of α usually ranges from 0.001 to 1, this difference between the two equations can become significant when dealing with magnetic systems with high damping. The question of which one of Eq. (2.34) or Eq. (2.41) is the correct one is still subject to debate [9]. Nevertheless, it is Eq. (2.41) that is solved through micromagnetic simulations in the present work and it will be referred to as the Landau-Lifshitz-Gilbert (LLG) equation. The fact that the time derivative of $\vec{m}$ only appears on the left-hand side allows the equation to be more easily time-integrated.

Up until now, only the magnetic moment $\vec{m}$ of a single electron has been considered. Following the procedure used in macroscopic electromagnetism [5, 6], the macroscopic magnetization $\vec{M}$ is now introduced and should be regarded as the spatially averaged magnetic moment of all electronic spins within a region large enough to smooth out variations due to the atomic configuration in space but small enough to capture the magnetization distribution within the magnetic material. In electromagnetism, this small enough size will typically be some fraction of the wavelength of electromagnetic fields. In micromagnetism, this small enough size is dictated by the exchange length, which is the length over which magnetization is forced to be mostly uniform due to the exchange interaction. With this averaging procedure in mind, the LLG equation Eq. (2.41) reads

$$\frac{d\vec{M}}{dt} = \frac{\gamma}{1+\alpha^2}\vec{M}\times\vec{B} + \frac{\gamma\alpha}{(1+\alpha^2)|\vec{M}|}\vec{M}\times(\vec{M}\times\vec{B}) \ . \tag{2.42}$$

Here, $\vec{B}$ should also be considered in the context of macroscopic electromagnetism as the spatially averaged magnetic flux density. To couple the LLG equation with the Maxwell

equations, it is convenient to introduce the macroscopic magnetic field which is defined as

$$\vec{H} = \frac{1}{\mu_0}\vec{B} - \vec{M} \, . \tag{2.43}$$

Replacing $\vec{B} = \mu_0(\vec{H} + \vec{M})$ in Eq. (2.42) and noting that $\vec{M} \times \vec{M} = 0$ gives

$$\frac{d\vec{M}}{dt} = \frac{\gamma}{1+\alpha^2}\vec{M} \times \vec{H} + \frac{\gamma\alpha}{(1+\alpha^2)|\vec{M}|}\vec{M} \times (\vec{M} \times \vec{H}) \, . \tag{2.44}$$

where the value of μ_0 is absorbed into γ, depending on the units system that is used. For instance, in cgs units, $\mu_0 = 1$, while in SI units, $\mu_0 = 4\pi \times 10^{-7}$.

2.2 Effective fields

The magnetic field $\vec{H}$ in the LLG equation, Eq. (2.44) has been introduced using the electromagnetic potential of a magnetic moment subjected to a magnetic field. Consequently, interactions such as the magnetostatic interaction or the effect of an externally applied field are taken into account since they involve magnetic fields. On the other hand, important interactions such as the exchange interaction and crystalline anisotropy are not a priori included in the LLG equation. It is however possible to include these interactions using so-called effective magnetic fields.

The idea is to consider the potential due to the magnetic flux density from Eq. (2.16),

$$U = -\vec{M} \cdot \vec{B}. \tag{2.45}$$

Writing this in terms of $\vec{H}$ using $\vec{B} = \mu_0(\vec{H} + \vec{M})$ and in the cgs unit system where $\mu_0 = 1$, one obtains

$$U = -\vec{M} \cdot \vec{H} - \vec{M} \cdot \vec{M} \, . \tag{2.46}$$

Since the magnitude of $\vec{M}$ is assumed to be constant, the second term can be dropped and the potential reads

$$U = -\vec{M} \cdot \vec{H} \tag{2.47}$$

which is of the same form as Eq. (2.45). If the potential associated with another interaction has the same form as Eq. (2.47), then an effective field can be defined for this interaction. However this is generally not the case and an interaction's potential will be some function of $\vec{M}$,

$$U = U(\vec{M}) \ . \tag{2.48}$$

An effective field can be introduced by linearizing this potential around the magnetization distribution $\vec{M}$ of the system at a particular instant in time. Indeed, the Taylor expansion of Eq. (2.48) around $\vec{M} = \vec{M}_0$ is

$$U(\vec{M}) = U(\vec{M}_0) + \left.\frac{\partial U}{\partial \vec{M}}\right|_{\vec{M}=\vec{M}_0} \cdot (\vec{M} - \vec{M}_0) + \ldots \tag{2.49}$$

Neglecting higher order terms and dropping terms that are constant with respect to $\vec{M}$, this becomes

$$U(\vec{M}) = \left.\frac{\partial U}{\partial \vec{M}}\right|_{\vec{M}=\vec{M}_0} \cdot \vec{M} \tag{2.50}$$

which is of the same form as Eq. (2.47) with

$$\vec{H} = -\left.\frac{\partial U}{\partial \vec{M}}\right|_{\vec{M}=\vec{M}_0} \tag{2.51}$$

This linearization procedure is particularly well adapted to micromagnetic simulations where the LLG equation is integrated in time to obtain $\vec{M}$ as a function of time. At each time step, the current magnetization solution is used as the value for $\vec{M}_0$, the effective fields are computed and the LLG is integrated using these linearized interactions. At each time step, the change in $\vec{M}$ is usually small which justifies the above linearization procedure.

2.2.1 Crystalline anisotropy field

Lets take for example uniaxial crystalline anisotropy, where the crystalline structure of the magnetic material causes a preferred direction for the magnetization. The anisotropy vector $\vec{K}$ is defined with its orientation corresponding to the preferred direction and its magnitude K representing the anisotropy energy density, thus the strength of the interaction. This anisotropy interaction is modeled by the potential

$$U_{\text{an}} = K \sin^2 \theta \tag{2.52}$$

where θ is the angle between $\vec{K}$ and $\vec{M}$. Using the identity $\sin^2\theta = 1 - \cos^2\theta$ and dropping the constant term, the potential can be written as

$$U_{\text{an}} = -K \cos^2 \theta = -\frac{(\vec{K} \cdot \vec{M})^2}{K|\vec{M}|^2} \ . \tag{2.53}$$

Using Eq. (2.51), the effective field for uniaxial anistropy is

$$\vec{H}_{\text{an}} = -\left.\frac{\partial U_{\text{an}}}{\partial \vec{M}}\right|_{\vec{M}=\vec{M}_0} = \frac{2}{K|\vec{M}_0|^2}(\vec{K} \cdot \vec{M}_0)\vec{K} \ . \tag{2.54}$$

2.2.2 Exchange interaction field

The crystalline anisotropy is a local interaction in the sense that at a given point, the effective field does not depend on the magnetization distribution elsewhere in the magnetic material. This is not the case for the exchange interaction which favors spatial uniformity of the magnetization. The potential associated with the exchange interaction can be defined as

$$U_{\text{ex}} = \int_\Omega \frac{A_{\text{ex}}}{|\vec{M}|^2} \left[(\nabla M_x)^2 + (\nabla M_y)^2 + (\nabla M_z)^2 \right] dV \tag{2.55}$$

where M_x, M_y and M_z are the x, y and z components of the magnetization $\vec{M}$, A_{ex} is the exchange coefficient and Ω is some volume within the magnetic material. This potential can be understood as penalizing variations in the magnetization in the L^2 norm sense. The functional in Eq. (2.55) does not depend explicitly on $\vec{M}$ so that Eq. (2.51) cannot be used directly to define an effective field. Instead, in the fashion of the calculus of variations, the Taylor expansion of the integrand in Eq. (2.55) in terms of the spatial derivatives is used. Denoting the integrand of Eq. (2.55) by I_{ex} and neglecting higher order terms, this yields

$$U_{\text{ex}}(\vec{M}) = \int_\Omega I_{\text{ex}}(\vec{M}_0) + \left.\frac{\partial I_{\text{ex}}}{\partial \nabla M_x}\right|_{\vec{M}=\vec{M}_0} \cdot (\nabla M_x - \nabla M_{0x}) + \left.\frac{\partial I_{\text{ex}}}{\partial \nabla M_y}\right|_{\vec{M}=\vec{M}_0} \cdot (\nabla M_y - \nabla M_{0y}) + \left.\frac{\partial I_{\text{ex}}}{\partial \nabla M_z}\right|_{\vec{M}=\vec{M}_0} \cdot (\nabla M_z - \nabla M_{0z})\, dV \quad (2.56)$$

where ∇M_{0x} is the x component of $\vec{M}_0$ and where for instance

$$\frac{\partial I_{\text{ex}}}{\partial \nabla M_x} = \frac{\partial I_{\text{ex}}}{\partial P_x}\hat{x} + \frac{\partial I_{\text{ex}}}{\partial P_y}\hat{y} + \frac{\partial I_{\text{ex}}}{\partial P_z}\hat{z} \quad (2.57)$$

with P_x, P_y and P_z denoting the derivatives of M_x with respect to x, y and z respectively. Leaving out terms that are constant with respect to ∇M_x, ∇M_y or ∇M_z, Eq. (2.56) becomes

$$U_{\text{ex}}(\vec{M}) = \int_\Omega \frac{2A_{\text{ex}}}{|\vec{M}|^2}\left[(\nabla M_{0x} \cdot \nabla M_x) + (\nabla M_{0y} \cdot \nabla M_y) + (\nabla M_{0z} \cdot \nabla M_z)\right] dV\ . \quad (2.58)$$

Since $\nabla \cdot (\nabla M_{0x} M_x) = \nabla M_{0x} \cdot \nabla M_x + \nabla^2 M_{0x} M_x$ and similarly for the y and z components, assuming that the magnetization function $\vec{M}$ is sufficiently smooth and using the divergence theorem, Eq. (2.58) can be written as

$$U_{\text{ex}}(\vec{M}) = -\int_\Omega \frac{2A_{\text{ex}}}{|\vec{M}|^2}\left[(\nabla^2 M_{0x} M_x) + (\nabla^2 M_{0y} M_y) + (\nabla^2 M_{0z} M_z)\right] dV + \int_{\partial\Omega} \frac{2A_{\text{ex}}}{|\vec{M}|^2}\left[M_x \nabla M_{0x} + M_y \nabla M_{0y} + M_z \nabla M_{0z}\right] \cdot \hat{n}\, dS\ . \quad (2.59)$$

where $\partial\Omega$ is the surface of the domain Ω and $\hat{n}$ is a outward pointing unit vector perpendicular to this surface. At this point, a limiting procedure is employed whereby the region Ω is taken to be arbitrarily small. If the region is taken to be small enough, the quantity between square brackets in the surface integral can be considered to be constant on the surface $\partial\Omega$. Then this quantity can be moved outside the integral and the surface integral term of Eq. (2.59) becomes

$$\frac{2A_{\text{ex}}}{|\vec{M}|^2}\left[M_x\nabla M_{0x}+M_y\nabla M_{0y}+M_z\nabla M_{0z}\right]\cdot\int_{\partial\Omega}\hat{n}\,dS\ . \tag{2.60}$$

It is easily shown that the integral over any closed surface of $\hat{n}$, the outward-pointing unit normal vector to this surface, is zero so that the surface integral term does not contribute to the potential U_{ex}. Meanwhile, the quantity inside square brackets in the volume integral of Eq. (2.59) is $\nabla^2\vec{M}_0\cdot\vec{M}$. Therefore, Eq. (2.59) becomes

$$U_{\text{ex}}(\vec{M})=-\int_\Omega\frac{2A_{\text{ex}}}{|\vec{M}|^2}\nabla^2\vec{M}_0\cdot\vec{M}\,dV\ . \tag{2.61}$$

From Eq. (2.47), the potential of a magnetic field acting on the magnetization within the region Ω is

$$U=-\int_\Omega\vec{M}\cdot\vec{H}\,dV \tag{2.62}$$

which is of the same form as Eq. (2.61). The effective field for the exchange interaction is therefore

$$\vec{H}_{\text{ex}}=\frac{2A_{\text{ex}}}{|\vec{M}|^2}\nabla^2\vec{M}_0\ . \tag{2.63}$$

2.3 Magnetostatic field

The magnetostatic field, also known as the demagnetizing field and denoted by $\vec{H}_{\text{ms}}$, is part of the effective fields, in the sense that it is included in $\vec{H}$ in the LLG equation. Here it is

given its own subsection to highlight the fact that unlike the anisotropy and exchange fields, the magnetostatic field is a proper magnetic field, in the sense that it is a solution of the Maxwell equations. More will be said on this in chapter 4, but it is the norm in micromagnetism to consider the static Maxwell equations for the magnetic field, the solution of which is then referred to as the magnetostatic field. The justification for using the static approximation is that the size of structures studied in micromagnetism is almost always deeply subwavelength in terms of the electromagnetic wavelength and therefore propagation delay effects can be neglected.

The magnetostatic field is obtained by solving the static Maxwell equations for a given magnetization distribution $\vec{M}$. The static Maxwell equations for the magnetic field are [6]

$$\nabla \times \vec{H}_{\text{ms}} = 0 \tag{2.64a}$$

$$\nabla \cdot \vec{H}_{\text{ms}} = -\nabla \cdot \vec{M} \tag{2.64b}$$

There is a variety of ways in which Eqs. (2.64) can be solved and the topic is treated extensively in the literature, see for instance [15, 16, 17]. In FastMag, the approach taken is based on the fact that since $\nabla \times \vec{H}_{\text{ms}} = 0$, the magnetostatic field can be written in terms of a magnetic scalar potential,

$$\vec{H}_{\text{ms}} = -\nabla \Phi_M \ . \tag{2.65}$$

Inserting this into Eq. (2.64b) gives

$$\nabla^2 \Phi_M = \nabla \cdot \vec{M} \ , \tag{2.66}$$

which is the Poisson equation with source term $\nabla \cdot \vec{M}$. In FastMag, the solution of Eq. (2.66) is obtained by computing the following volume integral [6],

$$\Phi_M = \frac{1}{4\pi} \int \vec{M}(\vec{x}') \cdot \nabla' \left(\frac{1}{|\vec{x} - \vec{x}'|} \right) d\vec{x}' \tag{2.67}$$

where the integration is over all of $\mathbb{R}^3$. The magnetostatic field is then computed from Φ_M using Eq. (2.65).

2.3.1 Shape anisotropy

Shape anisotropy refers to the fact that, due to a magnet's shape and the magnetostatic field, the magnetization inside this magnet will have a preferred direction which minimizes the energy of the system. The potential energy associated with the magnetostatic field $\vec{H}_{\text{ms}}$ generated by a magnetization distribution $\vec{M}$ is

$$U = -\frac{1}{2}\vec{H}_{\text{ms}} \cdot \vec{M} \tag{2.68}$$

This can be compared to the potential energy for a magnet placed in a constant magnetic field, given by Eq. (2.47). The additional factor $\frac{1}{2}$ in Eq. (2.68) is due to the fact that $\vec{H}_{\text{ms}}$ is itself a function, or more precisely a functional, of $\vec{M}$ as seen from Eqs. (2.65) and (2.67). In this case, the Taylor expansion of Eq. (2.50) can be written as

$$\left.\frac{\partial U}{\partial \vec{M}}\right|_{\vec{M}=\vec{M}_0} \cdot \vec{M} = -\frac{1}{2}\left[\vec{H}_{\text{ms}}(\vec{M}_0) \cdot \vec{M} + \left.\frac{\partial \vec{H}_{\text{ms}}}{\partial \vec{M}}\right|_{\vec{M}=\vec{M}_0} \cdot \vec{M}\right] . \tag{2.69}$$

The derivative of the functional $\vec{H}_{\text{ms}}(\vec{M})$ in the second term on the right hand side should be considered in a generalized sense and is known as a Gâteau derivative. It is defined as

$$\left.\frac{\partial \vec{H}_{\text{ms}}}{\partial \vec{M}}\right|_{\vec{M}=\vec{M}_0} \cdot \vec{M} = \lim_{\varepsilon \to 0} \frac{\vec{H}_{\text{ms}}(\vec{M}_0 + \varepsilon \vec{M}) - \vec{H}_{\text{ms}}(\vec{M}_0)}{\varepsilon} \tag{2.70}$$

The functional $\vec{H}_{\text{ms}}$ being linear, Eq. (2.70) evaluates to

$$\left.\frac{\partial \vec{H}_{\text{ms}}}{\partial \vec{M}}\right|_{\vec{M}=\vec{M}_0} = \vec{H}_{\text{ms}}(\vec{M}_0) \tag{2.71}$$

so that Eq. (2.69) simplifies to

$$\left.\frac{\partial U}{\partial \vec{M}}\right|_{\vec{M}=\vec{M}_0} \cdot \vec{M} = -\vec{H}_{\mathrm{ms}}(\vec{M}_0) \cdot \vec{M} \ . \tag{2.72}$$

Comparing this to Eq. (2.51), it is seen that the magnetostatic field $\vec{H}_{\mathrm{ms}}$ can be treated just as a magnetic field $\vec{H}$ produced by external sources when solving the LLG equation.

Having established an expression for the potential associated with the magnetostatic field, Eq. (2.68), it can now be shown that for magnet shapes where the magnetostatic field is uniform inside the magnetic region such as ellipsoids, shape anisotropy is formally equivalent to a uniaxial crystalline anisotropy $\vec{K}_{\mathrm{sh}}$ oriented in the preferred direction of magnetization. For such magnets, the magnetostatic field can be given in terms of the demagnetization factors $N_{\parallel}$ and $N_{\perp}$ [18]. Both the magnetostatic field and the magnetization can be decomposed into parallel and perpendicular components with respect to the preferred direction of magnetization such that $\vec{H}_{\mathrm{ms}} = \vec{H}_{\mathrm{ms}\parallel} + \vec{H}_{\mathrm{ms}\perp}$ and $\vec{M}_{\mathrm{ms}} = \vec{M}_{\mathrm{ms}\parallel} + \vec{M}_{\mathrm{ms}\perp}$. Then the demagnetization factors are defined by

$$\vec{H}_{\mathrm{ms}\parallel} = -N_{\parallel}\vec{M}_{\parallel} \ , \tag{2.73}$$

$$\vec{H}_{\mathrm{ms}\perp} = -N_{\perp}\vec{M}_{\perp} \ . \tag{2.74}$$

Introducing the unit vectors $\hat{n}_{\parallel}$ and $\hat{n}_{\perp}$ parallel and perpendicular to the preferred direction of magnetization as shown in Fig. 2.2, Eqs. (2.73) and (2.74) can be written as

$$\vec{H}_{\mathrm{ms}\parallel} = -N_{\parallel}(\vec{M} \cdot \hat{n}_{\parallel})\hat{n}_{\parallel} \ , \tag{2.75}$$

$$\vec{H}_{\mathrm{ms}\perp} = -N_{\perp}(\vec{M} \cdot \hat{n}_{\perp})\hat{n}_{\perp} \ . \tag{2.76}$$

Inserting these expressions into Eq. (2.68) for the potential energy yields

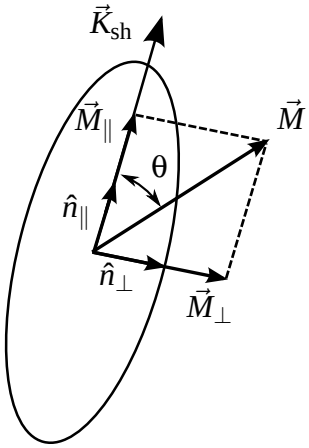

Figure 2.2: The shape anisotropy in an ellipsoidal magnetic particle is equivalent to a uniaxial anisotropy vector $\vec{K}_{\text{sh}}$ which points in the preferred magnetization direction.

$$\begin{aligned} U &= -\frac{1}{2}\left[-N_{\|}(\vec{M}\cdot\hat{n}_{\|})\hat{n}_{\|} - N_{\perp}(\vec{M}\cdot\hat{n}_{\perp})\hat{n}_{\perp}\right]\cdot\vec{M} \\ &= -\frac{1}{2}\left[-N_{\|}(\vec{M}\cdot\hat{n}_{\|})^2 - N_{\perp}(\vec{M}\cdot\hat{n}_{\perp})^2\right] \\ &= -\frac{1}{2}\left[-N_{\|}\cos^2\theta - N_{\perp}\sin^2\theta\right]|\vec{M}|^2 \\ &= -\frac{1}{2}\left[-(N_{\|}-N_{\perp})\cos^2\theta - N_{\perp}\right]|\vec{M}|^2 \end{aligned} \tag{2.77}$$

where θ is the angle subtended by $\vec{K}_{\text{sh}}$ and $\vec{M}$. Dropping the constant term gives

$$U = -\frac{1}{2}(N_{\perp}-N_{\|})\cos^2\theta|\vec{M}|^2\ . \tag{2.78}$$

Comparing this with the potential for crystalline uniaxial anisotropy, Eq. (2.53), it is seen that shape anisotropy is equivalent to a unixial anisotropy with magnitude given by

$$K_{\text{sh}} = \frac{1}{2}(N_{\perp}-N_{\|})|\vec{M}|^2\ . \tag{2.79}$$

While the fact that this result was derived for ellipsoidal magnets may seem to limit its applicability, since ellipsoids can take a wide array of shapes, from a thin needle for a long, prolate spheroid to a circular plane-like volume for a flat, oblate spheroid, the concept of shape

anisotropy can be used to gain insight into the properties of many magnetic structures.

2.4 Space and time discretization

The objective of a micromagnetic solver is to compute a solution $\vec{M}(\vec{x},t)$ to the LLG equation, Eq. (2.44). The LLG equation is a partial differential equation in both space and time and is non-linear in terms of the unknown $\vec{M}$. Different approaches can be used to discretize and solve the LLG equation such as finite differences or the finite element method. The present work was done using and building on the FastMag micromagnetic solver, which is developed by Professor Lomakin's research group at UCSD. The approach that is taken to solve the LLG equation is to discretize the problem in space using the finite element method on a tetrahedral mesh. The magnetization $\vec{M}$ is spatially represented by linear basis functions while point matching is used for the testing functions. This transforms the LLG equation in a system of non-linear ordinary differential equations (ODEs). This system has the same form as the continuous LLG equation, Eq. (2.44), but where $\vec{M}$ represents the vector of values of the components of $\vec{M}$ at the nodes of the tetrahedral mesh and where the effective field $\vec{H}$ is computed at these same nodes. The computation of the effective fields is based on the continuous equations for these fields which were discussed in sections 2.2 and 2.3 and on the representation of the magnetization $\vec{M}$ by linear basis functions.

2.4.1 Computing effective fields at mesh nodes

For the crystalline anisotropy effective field, the field at node i is given by a discretized version of Eq. (2.54) for $\vec{H}_{\text{an}}$,

$$\vec{H}_{\text{an},i} = \frac{2}{K_i M_{s,i}^2}(\vec{K}_i \cdot \vec{M}_i)\vec{K}_i \tag{2.80}$$

where $\vec{K}_i$ is the volume averaged anisotropy vector of tetrahedrons surrounding node i and whose magnitude is K_i, $\vec{M}_i$ is the magnetization at node i and $M_{s,i}$ is the volume averaged saturation magnetization of tetrahedrons surrounding node i. The saturation magnetization is a property of a magnetic material and corresponds to the magnetization's magnitude which is assumed to be constant.

The computation of the effective field for the exchange interaction is complicated by the fact that the magnetization is assumed to be described by linear polynomials whereas the exchange field, given by Eq. (2.63) is proportional to the second order derivative of $\vec{M}$, which is zero locally, i.e. inside a given tetrahedron. Following [19], an approximation of the exchange field at the node i can nonetheless be obtained by assuming that the laplacian of $\vec{M}$ is slowly varying so that it can be regarded as constant within tetrahedrons surrounding node i. Denoting the region corresponding to tetrahedrons around node i by Ω_i and introducing the linear hat basis function centered on node i, ϕ_i, consider the following integral involving $M_{x,i}$, the x component of $\vec{M}_i$,

$$\int_{\Omega_i} \phi_i(\vec{x}) \nabla^2 M_{x,i}(\vec{x}) dV \ . \tag{2.81}$$

Using the divergence theorem, this can be written as

$$\int_{\Omega_i} \phi_i(\vec{x}) \nabla^2 M_{x,i}(\vec{x}) dV = -\int_{\Omega_i} \nabla\phi_i(\vec{x}) \cdot \nabla M_{x,i}(\vec{x}) dV + \int_{\partial\Omega_i} \phi_i(\vec{x}) \nabla M_{x,i}(\vec{x}) \cdot \hat{n} dS \ . \tag{2.82}$$

The surface integral vanishes because the hat basis function ϕ_i is zero on the boundary of Ω_i. Now making use of the assumption that $\nabla^2 M_{x,i}$ is constant within Ω_i, it can be taken out of the left-hand side integral in Eq. (2.82) which yields

$$\nabla^2 M_{x,i}(\vec{x}) = -\frac{1}{\int_{\Omega_i} \phi_i(\vec{x}) dV} \int_{\Omega_i} \nabla\phi_i(\vec{x}) \cdot \nabla M_{x,i}(\vec{x}) dV \ . \tag{2.83}$$

The volume integral of ϕ_i over a tetrahedron is simply a fourth of the tetrahedron's volume and

is easily computed. The other integral is computed by making use of the representation of $\vec{M}$ in terms of basis functions. With identical expressions for the y and z components of $\vec{M}$, the exchange field is obtained by replacing $\nabla^2\vec{M}_0$ in Eq. (2.63) by the expression in Eq. (2.83) for each component.

Before leaving the topic of the exchange field, one will have noticed that if node i is located at the boundary of the magnetic region, the basis function ϕ_i does not vanish on $\partial\Omega_i$. In that case however, the surface integral in Eq. (2.82) still vanishes because $\nabla M_{x,i} \cdot \hat{n} = 0$. Indeed, the directional derivative of $\vec{M}$ in the direction normal to the surface of a magnetic region, $\partial\vec{M}/\partial n$, is zero. This boundary condition is analogous to the boundary condition at the free end of a string which is also an homogeneous Neumann boundary condition [20]. In this analogy, the magnetization's exchange interaction plays the role of the tension in the string.

The computation of the magnetostatic field is based on the computation of the integral in Eq. (2.67) for the magnetic scalar potential. The integral over all the magnetic domain is decomposed into integrals over individual tetrahedrons,

$$\Phi_M(\vec{x}) = \frac{1}{4\pi}\sum_k \int_{\Omega_k} \vec{M}(\vec{x}') \cdot \nabla' \left(\frac{1}{|\vec{x}-\vec{x}'|} \right) d\vec{x}' \tag{2.84}$$

where Ω_k is the region occupied by the kth tetrahedron. An approximation is made where the magnetization is considered to be constant within each tetrahedron and equal to $\vec{M}_k$, the average value of $\vec{M}$ at the 4 nodes of tetrahedron k. Then Eq. (2.84) becomes

$$\Phi_M(\vec{x}) = \frac{1}{4\pi}\sum_k \vec{M}_k \int_{\Omega_k} \nabla' \left(\frac{1}{|\vec{x}-\vec{x}'|} \right) d\vec{x}' \tag{2.85}$$

and using the divergence theorem, this can be written as

$$\Phi_M(\vec{x}) = \frac{1}{4\pi}\sum_k \vec{M}_k \int_{\partial\Omega_k} \frac{\hat{n}}{|\vec{x}-\vec{x}'|} d\vec{x}' \tag{2.86}$$

where the surface integral is over the boundary of tetrahedron k. The magnetic scalar potential Φ_M is computed at each node of the mesh after which its gradient is computed to obtain the magnetostatic field at the nodes.

Special attention must be given to the computation of the integral in Eq. (2.85) when the source point $\vec{x}$ and the observation point $\vec{x}'$ belong to the same tetrahedron. In that case, a singularity extraction procedure must be used, the details of which can be found in [21]. Also, the computation of the magnetic scalar potential from Eq. (2.86) has a N^2 complexity. In FastMag, a non-uniform FFT technique is employed to do this computation with a complexity of $N \log N$. This acceleration technique is described in [22] and [23].

2.4.2 Time integration

At this point, the LLG equation has been cast into a system of ODEs of the form

$$\frac{\partial \vec{M}}{\partial t} = \vec{f}(\vec{M}, \vec{H}) \tag{2.87}$$

where $\vec{M}$ and $\vec{H}$ denote arrays of values of the magnetization and of the effective magnetic field respectively at the mesh nodes and where $\vec{f}(\vec{M}, \vec{H})$ corresponds to an array containing the right-hand side of the LLG equation, Eq. (2.44), evaluated at the mesh nodes. While the dependence of $\vec{f}$ on the effective field $\vec{H}$ is explicit in Eq. (2.87), it is clear that the effective field is itself a function of $\vec{M}$. Furthermore, from Eq. (2.44), it is seen that $\vec{f}$ is a non-linear function of $\vec{M}$.

Different methods can be used for the time integration of Eq. (2.87), for instance explicit methods like the Runge-Kutta method and the Adams-Bashforth method or implicit methods like the Adams-Moulton method. In FastMag, the backward differentiation formula (BDF) method is used. The BDF method is an implicit, multi-step method which is A-stable for order $r = 1$ and $r = 2$. Lets consider the ODE

$$\frac{\partial u}{\partial t} = f(u) \tag{2.88}$$

where the unknown is $u(t)$ and f is a known function of u. The principle of the BDF method is to construct an interpolating polynomial of order r, $p(t)$, which passes through points (t_i, u_i) for $i = n-(r-1), \ldots, n+1$ where u_i is the solution at the discrete time t_i. The method then consists in letting

$$p'(t_{n+1}) = f(u_{n+1}) \tag{2.89}$$

and solving for the solution at the latest time step u_{n+1}.

For order $r = 1$, the interpolating polynomial is

$$p(t) = u_{n+1}\frac{t-t_n}{t_{n+1}-t_n} + u_n\frac{t-t_{n+1}}{t_n-t_{n+1}} \tag{2.90}$$

and its derivative evaluated at $t = t_{n+1}$ is

$$p'(t_{n+1}) = \frac{u_{n+1}-u_n}{t_{n+1}-t_n} \tag{2.91}$$

which also corresponds to the forward Euler method. For order $r = 2$, the interpolating polynomial is

$$p(t) = u_{n+1}\frac{(t-t_n)(t-t_{n-1})}{(t_{n+1}-t_n)(t_{n+1}-t_{n-1})} + u_n\frac{(t-t_{n+1})(t-t_{n-1})}{(t_n-t_{n+1})(t_n-t_{n-1})} + u_{n-1}\frac{(t-t_{n+1})(t-t_n)}{(t_{n-1}-t_{n+1})(t_{n-1}-t_n)} \tag{2.92}$$

and its derivative evaluated at $t = t_{n+1}$ is

$$\begin{aligned} p'(t_{n+1}) =& u_{n+1}\left[\frac{1}{t_{n+1}-t_{n-1}} + \frac{1}{t_{n+1}-t_n}\right] + u_n\left[\frac{1}{t_{n+1}-t_n} + \frac{1}{t_n-t_{n-1}}\right] + \\ & u_{n-1}\left[\frac{t_{n+1}-t_n}{(t_{n+1}-t_{n-1})(t_n-t_{n-1})}\right] . \end{aligned} \tag{2.93}$$

In general, for order r, $p'(t_{n+1})$ is given by

$$p'(t_{n+1}) = \sum_{i=0}^{r} \alpha_i u_{n+1-i} \tag{2.94}$$

where the α_i are coefficients which depend on the time step history. From Eq. (2.89), the BDF method therefore consists in solving

$$\sum_{i=0}^{r} \alpha_i u_{n+1-i} = f(u_{n+1}) \tag{2.95}$$

for u_{n+1}.

Applying the BDF method to the system of ODEs of Eq. (2.87), the following system of equations must be solved for the array of magnetization values at the latest time step, $\vec{M}_{n+1}$,

$$\sum_{i=0}^{r} \alpha_i \vec{M}_{n+1-i} = \vec{f}(\vec{M}_{n+1}) \ . \tag{2.96}$$

This is an implicit system of equations for $\vec{M}_{n+1}$, which also happens to be non-linear since $\vec{f}$ is a non-linear function. Therefore, the Newton method is used to linearize the problem. To apply the Newton method, Eq. (2.96) is written as

$$\vec{g}(\vec{M}_{n+1}) = 0 \tag{2.97}$$

where

$$\vec{g}(\vec{M}_{n+1}) = \sum_{i=0}^{r} \alpha_i \vec{M}_{n+1-i} - \vec{f}(\vec{M}_{n+1}) \ . \tag{2.98}$$

At time step t_{n+1}, starting with an initial guess $\vec{M}_{n+1}^{(0)}$, successive approximations $\vec{M}_{n+1}^{(j)}$ are computed. Given the approximation $\vec{M}_{n+1}^{(j)}$, $\vec{M}_{n+1}^{(j+1)}$ is computed by replacing $\vec{g}(\vec{M}_{n+1})$ in Eq. (2.97) by its Taylor expansion around $\vec{M}_{n+1}^{(j)}$, evaluated at $\vec{M}_{n+1}^{(j+1)}$, where only the first order term has

been kept,

$$\vec{g}(\vec{M}_{n+1}^{(j)}) + \left.\frac{\partial \vec{g}}{\partial \vec{M}_{n+1}}\right|_{\vec{M}_{n+1}=\vec{M}_{n+1}^{(j)}} (\vec{M}_{n+1}^{(j+1)} - \vec{M}_{n+1}^{(j)}) = 0 \; . \tag{2.99}$$

Here, $\partial\vec{g}/\partial\vec{M}_{n+1}$ is the jacobian matrix

$$\frac{\partial \vec{g}}{\partial \vec{M}_{n+1}} = \begin{bmatrix} \frac{\partial g_1}{\partial M_{1,n+1}} & \frac{\partial g_1}{\partial M_{2,n+1}} & \\ \frac{\partial g_2}{\partial M_{1,n+1}} & \frac{\partial g_2}{\partial M_{2,n+1}} & \cdots \\ & \vdots & \ddots \end{bmatrix} \quad . \tag{2.100}$$

where $g_1, g_2, \ldots$ are the components of the $\vec{g}$ function and $M_{1,n+1}$, $M_{2,n+1}$ are the components of the $\vec{M}_{n+1}$ array. The linear system of equations in Eq. (2.99) is solved for $\delta\vec{M} = \vec{M}_{n+1}^{(j+1)} - \vec{M}_{n+1}^{(j)}$ which then allows the computation of the new approximation

$$\vec{M}_{n+1}^{(j+1)} = \vec{M}_{n+1}^{(j)} + \delta\vec{M} \; . \tag{2.101}$$

What was just described is the basis of the BDF-Newton method employed to solve the discretized LLG equation. However, the algorithm that is employed in FastMag has some refinements which will not be presented in details here. The algorithm used is a customized version of the VODE algorithm [24, 25] which was designed to solve systems of initial value ODEs of the form of Eq. (2.87). Both the algorithm used in FastMag and VODE allow the time step to change dynamically during the integration process based on the error and convergence history: when the error exceeds a certain threshold after a certain number of Newton iterations, the time step size is reduced while if convergence is rapidly achieved for a number of consecutive time steps, the time step size is increased. Both the FastMag and VODE algorithms also use a BDF-based predictor to compute the initial guess $\vec{M}_{n+1}^{(0)}$ at a new time step. For the ODE of Eq. (2.88), this predictor is based on the construction of an interpolating polynomial $p(t)$ of degree r which passes through the r points $(t_{n-(r-1)}, u_{n-(r-1)}), \ldots, (t_n, u_n)$ and satisfies $\partial p/\partial t|_{t=t_n} = f(u_n)$.

Chapter 3

Characterization of soft nano-granular ferromagnetic materials

Micromagnetism can be used to characterize magnetic materials in terms of their magnetization response to an applied magnetic field. Two metrics that are used to characterize magnetic materials are introduced in section 3.1, namely the hysteresis loop and the permeability tensor. The hysteresis loop describes the non-linear behavior of magnetization in a magnetic material and conveys key information like the anisotropy field and the coercive field. It also allows magnetic materials to be categorized as either hard or soft magnetic materials. The Stoner-Wohlfarth hysteresis model is described as well as how hysteresis loops can be obtained from micromagnetic simulations. The permeability tensor is the primary mean by which magnetization in magnetic materials is taken into account in electromagnetic problems involving the solution of the Maxwell equations. A method for the extraction of the frequency dependent permeability tensor from micromagnetic simulations is presented. Section 3.2 discusses nano-granular ferromagnetic materials, which are characterized by a low effective anisotropy due to anisotropy averaging amongst ferromagnetic grains with randomly oriented anisotropy axes. The mechanism of anisotropy averaging is described in section 3.3. The concept of effective particles and how

they can be used in micromagnetic simulations of nano-granular ferromagnetic materials is also discussed. Section 3.4 presents some concepts of directional probability theory on the circle which are useful to describe collections of particles with randomly oriented anisotropy axes. In section 3.5, these probability concepts are used to compute hysteresis loops of ensemble of nano-granular ferromagnetic particles by means of a generalized Stoner-Wohlfarth model which accounts for exchange interactions between particles.

3.1 Characterization of magnetic materials with micromagnetic simulations

Two important characteristics of magnetic materials for their use in high frequency applications are the hysteresis loop and frequency dependent permeability tensor which both describe the macroscopic magnetic response of a material to an applied magnetic field.

3.1.1 The hysteresis loop

An example of an hysteresis loop is shown in Fig. 3.1. The hysteresis loop shows the magnetization component in the direction of an applied magnetic field as a function of the magnitude of this applied field as it is sweeped from its maximum positive value to its minimum negative value and back. In the case of Fig. 3.1, the magnetization is shown in terms of m, the magnetization normalized with respect to the saturation magnetization M_s.

Among the many properties that can be defined for an hysteresis loop [18], the coercive field H_c corresponds to the field that must be applied to achieve a state of zero net magnetization after the ferromagnet has been saturated. The coercive field measures how wide the opening of the loop is, and therefore the amount of hysteresis in the system. It is also a way to categorize magnetic materials as being hard or soft, hard magnetic materials being hard to magnetize

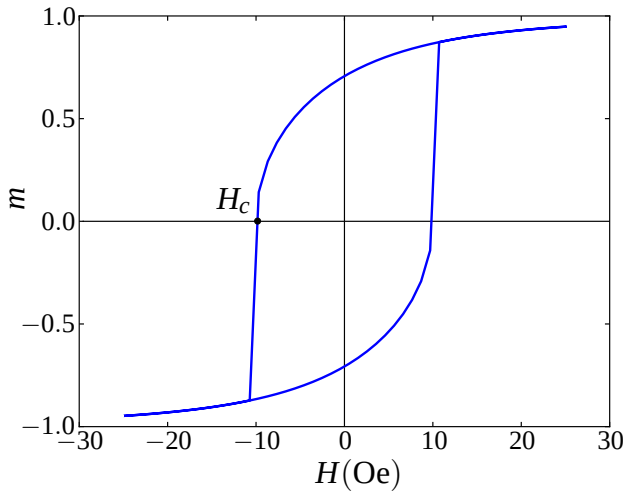

Figure 3.1: Hysteresis loop for a magnetic particle subjected to an applied magnetic field oriented at 45 degrees from the particle's uniaxial anisotropy axis.

and demagnetize while soft materials are easy to magnetize and demagnetize. Hard magnetic materials are used in applications such as permanent magnets and will have coercive fields in the hundreds or thousands of Oe. While a good hard magnetic material is characterized by its non-response to applied magnetic fields, soft magnetic materials are tailored to have specific magnetization responses depending on their application. For instance, magnetic materials for inductor or transformer applications are designed to have a linear behavior, meaning as little hysteresis as possible, or a small H_c field. For those applications, a high permeability, which as will be discussed shortly is equivalent to a high slope of the hysteresis curve, is also desired.

The hysteresis behavior is a combination of the rotation of the magnetization and abrupt reversals at certain values of the applied field which result from the interaction between an applied field and a particle's anisotropy. That was the main proposition of Stoner and Wohlfarth in their seminal 1948 paper [26]. They considered a particle subjected to an applied field $\vec{H}$ and having a uniaxial anisotropy $\vec{K}$, as shown in Fig. 3.2. In their model, Stoner and Wohlfarth neglected inter-particle interactions such as the magnetostatic field and the exchange interaction. Therefore, the total energy associated with the system is the anisotropy energy and the energy associated with the applied field. From Eq. (2.52) and referring to Fig. 3.2, the anisotropy energy

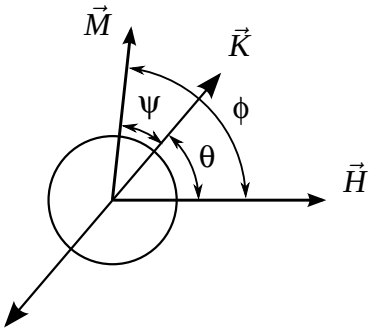

Figure 3.2: Stoner-Wohlfarth hysteresis model for a single particle with uniaxial anisotropy vector $\vec{K}$ subjected to an applied magnetic field $\vec{H}$.

is

$$U_{\text{an}} = K\sin^2\psi \tag{3.1}$$

Using the trigonometric identity $\sin^2\psi = \frac{1}{2} - \frac{1}{2}\cos(2\psi)$ and ignoring the constant term, this becomes

$$U_{\text{an}} = -\frac{K}{2}\cos 2\psi \tag{3.2}$$

From Eq. (2.47), the energy associated with the applied field $\vec{H}$ is

$$U_H = -HM_s\cos\phi \tag{3.3}$$

where M_s is the magnetization amplitude, corresponding to the saturation magnetization. The total energy is therefore

$$U = -\frac{K}{2}\cos 2\psi - HM_s\cos\phi\ . \tag{3.4}$$

The angle ϕ that the magnetization makes with the applied field at equilibrium is found by minimizing this energy. The angle θ between the applied field $\vec{H}$ and the anisotropy direction $\vec{K}$ being a constant of the problem, the angle ψ is written in terms of ϕ as $\psi = \phi - \theta$. Using this in Eq. (3.4), it becomes

$$U = -\frac{K}{2}\cos(2[\phi-\theta]) - HM_s\cos\phi\ . \tag{3.5}$$

The values of ϕ minimizing the total energy are found by solving $\partial U/\partial\phi = 0$ which yields

$$H = \frac{K\sin(2[\theta-\phi])}{M_s\sin\phi}\ . \tag{3.6}$$

Values of ϕ that are solutions of Eq. (3.6) and satisfy the condition $\partial^2 U/\partial\phi^2 > 0$ minimize the energy and correspond to equilibrium states. Given a value for the applied field H and the angle θ, Eq. (3.6) can be solved for ϕ using a root-finding algorithm. There might be two values of ϕ that correspond to states of minimal energy. In the context of hysteresis loop calculations, the correct solution depends on the magnetization history. For example, for $H = 0$, two equilibrium states exist, one with the magnetization pointing in the $+\vec{K}$ direction and the other pointing in the $-\vec{K}$ direction.

Using the Stoner-Wohlfarth model, hysteresis curves can be computed for individual particles or even ensemble of particles. For example, Fig. 3.3 shows the hysteresis loops computed with the Stoner-Wohlfarth model for different values of the angle θ between the applied field and the anisotropy axis. For small angles, the hysteresis loop is seen to have a square shape and a high H_c value. For this reason, the direction of anisotropy is known as the hard axis. For larger values of θ, H_c decreases until the hysteresis loop takes the shape of a straight line for $\theta = 90^\circ$. The direction perpendicular to the anisotropy axis is therefore known as the easy axis. It is important to note that the Stoner-Wohlfarth model is an approximate one as it neglects inter-particle interactions such as the magnetostatic and exchange interactions. In section 3.5, a Stoner-Wohlfarth model that takes into account exchange interaction between particles will be presented.

It is also possible to perform micromagnetic simulations to compute hysteresis loops. Hysteresis loops are usually measured at very low frequencies, that is the magnetic field is sweeped slowly, so that at each field value, the magnetization is at its equilibrium state. This is certainly the case in hysteresis loops computed using the Stoner-Wohlfarth model, and it can also

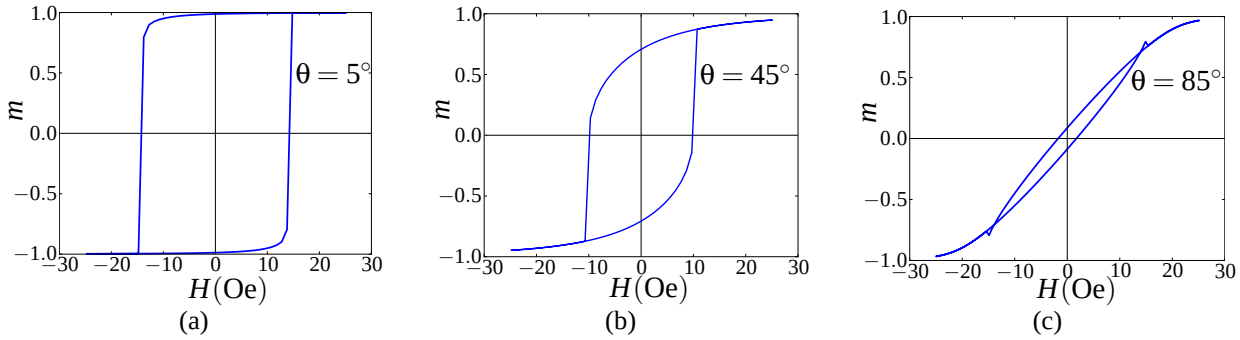

Figure 3.3: Hysteresis loops computed with the Stoner-Wohlfarth model for a particle with uniaxial anisotropy oriented at different angles θ with respect to the applied field.

be achieved in micromagnetic simulations by either varying the applied field at a very slow rate, or by dividing the sweeped values of the field in discrete steps, which are applied successively, with the micromagnetic simulation allowing the system to reach equilibrium at each value of the applied field. For instance, Fig. 3.4a shows the hysteresis loop for a system of 1000 spherical particles with randomly oriented unaxial anisotropies without inter-particle interaction which was obtained with a micromagnetic computation but could very well have been computed using the Stoner-Wohlfarth model. Meanwhile, Fig. 3.4b shows the hysteresis loop for the same system of particles but this time with exchange and magnetostatic interactions between the particles.

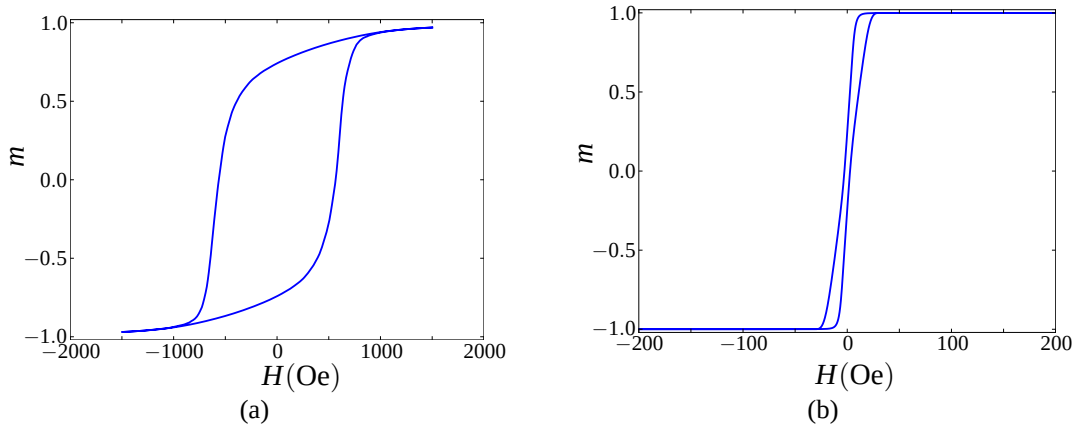

Figure 3.4: Hysteresis loops computed through a micromagnetic simulation for a system of 1000 particles. (a) No inter-particle interactions are considered. (b) Exchange and magnetostatic interactions between particles are taken into account.

As will be seen in subsequent sections, the dramatic decrease in the coercive field (note

the change of scale between the two figures) can be attributed to the exchange interaction which effectively averages out the randomly oriented anisotropies. In cases like this where the exchange interaction plays a dominant role, the Stoner-Wohlfarth model is inadequate and either a more refined model or micromagnetic simulations need to be used to compute the hysteresis loop.

In the above example, the inter-particle exchange interaction was modeled by the exchange interaction energy between two particles i and j,

$$U_{\text{ex}} = -J\vec{m}_i \cdot \vec{m}_j \tag{3.7}$$

where J is the exchange coupling energy and $\vec{m}_i$ and $\vec{m}_j$ are the normalized magnetization vectors of particles i and j. From Eq. (2.51), the effective field acting on particle i due to this exchange interaction is

$$\vec{H}_{\text{ex,i}} = \frac{J}{M_{s,i}V_i}\vec{m}_j \tag{3.8}$$

where $M_{s,i}$ is the saturation magnetization of particle i and V_i is its volume. The volume of particle i appears in the denominator of the effective field because Eq. (2.51) was derived for a point-like magnetic moment while the exchange energy associated with particle i is given by the integral of $-\vec{M}_i \cdot \vec{H}_{\text{ex,i}}$ over the volume of particle i.

3.1.2 The permeability tensor

When the magnetization response to the applied magnetic field is mostly linear as in the hysteresis curve of Fig. 3.4b, permeability can be defined for the material. The permeability of a material, noted μ is defined by the relation between the magnetic flux density $\vec{B}$ and the magnetic field $\vec{H}$,

$$\vec{B} = \mu\vec{H} \ . \tag{3.9}$$

While μ is represented as a scalar in Eq. (3.9), in general it is a tensor which is noted $\overline{\overline{\mu}}$ as different components of the $\vec{H}$ field can affect the different components of $\vec{B}$ differently. Also, the definition of Eq. (3.9) assumes that $\vec{B}$ and $\vec{H}$ are in the frequency domain, that is, they represent the Fourier transform of the corresponding time-domain fields. Because of this, the relation in the time domain equivalent to Eq. (3.9) involves a convolution between the permeability and the magnetic field [27].

In Eq. (3.9), $\vec{B}$ is the spatial average of the microscopic magnetic flux density while the magnetic field $\vec{H}$ is defined as [6]

$$\vec{H} = \frac{1}{\mu_0}\vec{B} - \vec{M} \; . \tag{3.10}$$

Defining the magnetic susceptibility χ_m through the magnetization response to a magnetic field,

$$\vec{M} = \chi_m \vec{H} \; , \tag{3.11}$$

and inserting this into Eq. (3.10) gives

$$\vec{B} = \mu_0(1+\chi_m)\vec{H} \; . \tag{3.12}$$

Comparing this with Eq. (3.9), the permeability can be defined as

$$\mu = \mu_0(1+\chi_m) \; . \tag{3.13}$$

In the above discussion, $\vec{M}$ is the spatially averaged or macroscopic magnetization. In chapter 2 on micromagnetism, the macroscopic magnetization was introduced as the spatially averaged magnetization of individual electronic spins, with the size of the region over which the spatial average is taken being large enough to smooth out individual spin variations but small enough to be able to resolve the magnetization distribution within the ferromagnet. Since permeability is a concept that is used to solve the Maxwell equations in electromagnetic problems,

here $\vec{M}$ corresponds to the magnetization averaged over a region that is small enough to resolve electromagnetic fields, that is, it must correspond to a small fraction of the electromagnetic wavelength. However, the electromagnetic wavelength is usually much larger than the exchange length, which means that the size of the averaging region can be chosen to be much larger than what is possible for micromagnetic simulations. Of course, one could choose to select the size of the averaging region for $\vec{M}$ to be the same as for micromagnetism. However, this would give rise to a permeability with potentially rapid spatial variations, therefore requiring a small spatial discretization size when solving electromagnetic problems numerically and increasing the numerical problem size. For this reason, it is desirable to choose the size of the averaging region to be as large as possible. This means that when computing the permeability using micromagnetic simulations, a large enough volume of the ferromagnet needs to be modeled, and the magnetization $\vec{M}$ that will be considered for computing the permeability will be the volume-averaged magnetization over the whole volume. The choice of the size of the volume will depend on the electromagnetic problem for which a permeability value is sought. For example, if an electromagnetic problem involves a certain ferromagnetic volume with a certain shape, it will be best to simulate that exact shape in the micromagnetic simulation since the shape of the ferromagnet will influence the magnetization response through the magnetostatic field. In other cases, one might be interested in the bulk permeability value of a given ferromagnetic material, that is its permeability if it is assumed that the material has no boundaries and effectively extends to infinity. In that case, it will be useful to use periodic boundary conditions where the simulated region, finite in size, is assumed to interact with periodic reproductions of itself which extend to infinity. Such periodic boundary conditions can be realized by exchange coupling the magnetization at the edge of the problem with magnetization on the opposite edge. Also, the magnetostatic field from the periodic extension of the simulated problem can be computed [23].

From Eq. (3.11), it is seen that by definition, permeability characterizes the linear response of the magnetization $\vec{M}$ to the magnetic field $\vec{H}$. Therefore, materials that have a mostly

linear and closed hysteresis loop lend themselves well to being characterized by permeability. On the other hand, it is difficult to define a truly meaningful permeability when the hysteresis curve is open and wide since in that case the magnetization response simply is not linear. For linear responses, the permeability at zero frequency can be inferred from the slope of the hysteresis curve. An example of a linear magnetization response is the Stoner-Wohlfarth model of a particle where the angle between the magnetic field and the anisotropy axis is $\theta = 90^\circ$. To see this, consider the magnetization $\vec{M}$ and saturation magnetization M_s subjected to a magnetic field $\vec{H}$ in the z direction and a uniaxial anisotropy $\vec{K}$ along the x axis, as shown in Fig. 3.5.

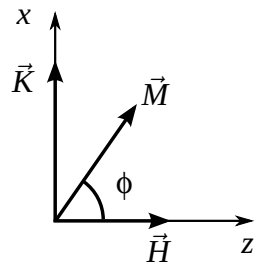

Figure 3.5: Equilibrium magnetization when subjected to a magnetic field along z and a uniaxial anisotropy along x.

From Eq. (2.54) the effective anisotropy field is given by

$$\vec{H}_{\text{an}} = \frac{2}{K|\vec{M}|^2}(\vec{K}\cdot\vec{M})\vec{K}\ . \tag{3.14}$$

In the presence of the field $\vec{H} = H_z\hat{z}$, at equilibrium $\vec{M}$ will point towards the total effective field $\vec{H} + \vec{H}_{\text{an}}$, with the angle ϕ between $\vec{M}$ and $\vec{H}$ given in terms of H_z and the magnitude of $\vec{H}_{\text{an}}$ as

$$\tan\phi = \frac{H_{\text{an}}}{H_z}\ . \tag{3.15}$$

From Eq. (3.14), the magnitude of $\vec{H}_{\text{an}}$ can be written as

$$H_{\text{an}} = \frac{2K}{|\vec{M}|}\cos(\pi/2-\phi) = \frac{2K}{|\vec{M}|}\sin(\phi) \tag{3.16}$$

so that, replacing for H_{an}, Eq. (3.15) becomes

$$\cos\phi = \frac{|\vec{M}|}{2K} H_z \ . \tag{3.17}$$

Noting that the z component of $\vec{M}$ is given by $M_z = \cos\phi |\vec{M}|$, this can be written as

$$M_z = \frac{|\vec{M}|^2}{2K} H_z \tag{3.18}$$

which is the desired result. This can also be written as

$$M_z = \frac{|\vec{M}|}{H_K} H_z \tag{3.19}$$

where

$$H_K = 2K/|\vec{M}| \tag{3.20}$$

is known in the literature as the anisotropy field [18], not to be confused with the anisotropy field of Eq. (3.14), and is the magnitude of the field H_z required to fully align the magnetization along the z axis. Comparing Eqs. (3.19) and (3.11), the magnetic susceptibility is

$$\chi_m = \frac{|\vec{M}|}{H_K} \ . \tag{3.21}$$

While the magnetic susceptibility is stated here as a scalar quantity, Eq. (3.21) in fact corresponds to the $\chi_{m,zz}$ component of the susceptibility tensor $\overline{\overline{\chi}}_m$. Because the magnetization $\vec{M}$ rotates and keeps a constant magnitude, a change in a given component of $\vec{M}$ invariably involves a change in another component. Also, since the relationship between $\vec{H}$ and $\vec{M}$ was established based on the equilibrium state, this susceptibility value corresponds to the zero frequency value. In reality, as described by the LLG equation, the magnetization precesses around the effective magnetic field before aligning itself with it through relaxation. It can be shown that for small

perturbations of $\vec{M}$ around its equilibrium state along the uniaxial anisotropy $\vec{K} = K\hat{x}$ due to a magnetic field $\vec{H} = H_z\hat{z}$, the χ_{mzz} component of the magnetic susceptibility tensor is given by [28]

$$\chi_{m,zz} = \frac{\gamma|\vec{M}|(\gamma H_K + j\omega\alpha)}{(\gamma H_K + j\omega\alpha)^2 - \omega^2} \tag{3.22}$$

where γ is the electron gyromagnetic ratio and α is the damping coefficient in the LLG equation. The magnetization response in the *y* direction is given by the tensor component

$$\chi_{m,yz} = \frac{j\omega\gamma|\vec{M}|}{(\gamma H_K + j\omega\alpha)^2 - \omega^2} \tag{3.23}$$

where the phase difference between $\chi_{m,yz}$ and $\chi_{m,zz}$ due to j in the numerator of Eq. (3.23) indicates precessional motion.

The expressions for the frequency dependent tensor components of Eqs. (3.22) and (3.23) result from the solution of the LLG equation in the frequency domain for a small perturbation around the equilibrium state. The poles of $\chi_{m,zz}$ and $\chi_{m,yz}$ correspond to the ferromagnetic resonance due to precessional motion and the real part of the resonant frequency is

$$\omega_0 = \frac{\gamma H_K}{1+\alpha^2} \ . \tag{3.24}$$

The frequency dependent magnetic susceptibility tensor can be extracted from micromagnetic simulations. Consider Eq. (3.11) which in tensor form reads

$$\vec{M} = \bar{\bar{\chi}}_m \vec{H} \ , \tag{3.25}$$

or in expanded form

$$\begin{bmatrix} M_x \\ M_y \\ M_z \end{bmatrix} = \begin{bmatrix} \chi_{m,xx} \chi_{m,xy} \chi_{m,xz} \\ \chi_{m,yx} \chi_{m,yy} \chi_{m,yz} \\ \chi_{m,zx} \chi_{m,zy} \chi_{m,zz} \end{bmatrix} \begin{bmatrix} H_x \\ H_y \\ H_z \end{bmatrix} \tag{3.26}$$

where the quantities are understood to be in the frequency domain and both $\vec{M}$ and $\vec{H}$ are spatially averaged quantities over the region used to define the macroscopic permeability. If three sets of linearly independent magnetic field excitations, $\vec{H}_1$, $\vec{H}_2$ and $\vec{H}_3$ and their corresponding magnetization responses $\vec{M}_1$, $\vec{M}_2$ and $\vec{M}_3$ are known, then the components of the susceptibility tensor can be obtained. To see this, consider the unit vector

$$\vec{E}_1 = \begin{bmatrix} 1 \\ 0 \\ 0 \end{bmatrix} , \tag{3.27}$$

then the first colum of $\overline{\overline{\chi}}_m$, noted $\vec{\chi}_{m,1}$ is obtained as

$$\vec{\chi}_{m,1} = \overline{\overline{\chi}}_m \vec{E}_1 \ . \tag{3.28}$$

Since the $\vec{H}_1$, $\vec{H}_2$ and $\vec{H}_3$ vectors are linearly independent, $\vec{E}_1$ can be expressed as the linear combination

$$\vec{E}_1 = a_1\vec{H}_1 + a_2\vec{H}_2 + a_3\vec{H}_3 \ . \tag{3.29}$$

Using this to replace $\vec{E}_1$ in Eq. (3.28) and using Eq. (3.25) yields

$$\vec{\chi}_{m,1} = a_1\vec{M}_1 + a_2\vec{M}_2 + a_3\vec{M}_3 \ . \tag{3.30}$$

The a coefficients can be found from the three $\vec{H}$ vectors. Indeed, introducing the $\overline{\overline{H}}$ matrix whose columns correspond to $\vec{H}_1$, $\vec{H}_2$ and $\vec{H}_3$,

$$\overline{\overline{H}} = \begin{bmatrix} & & \\ \vec{H}_1 & \vec{H}_2 & \vec{H}_3 \\ & & \end{bmatrix} , \tag{3.31}$$

Eq. (3.29) can be written in the form

$$\vec{E}_1 = \overline{\overline{H}}\,\vec{A} \tag{3.32}$$

where $\vec{A}$ is the vector of coefficients a_1, a_2 and a_3. Since the $\vec{H}$ vectors are linearly independent, $\overline{\overline{H}}$ is invertible and one can write

$$\vec{A} = \overline{\overline{H}}^{-1}\,\vec{E}_1 \tag{3.33}$$

which allows $\vec{\chi}_{m,1}$ to be computed from Eq. (3.30). The other components of the susceptibility tensor can be computed similarly. Once the susceptibility tensor is known, from Eq. (3.13), the permeability tensor is obtained as $\overline{\overline{\mu}} = \mu_0(\overline{\overline{I}} + \overline{\overline{\chi}}_m)$ where $\overline{\overline{I}}$ is the identity tensor.

This approach can be simplified if each of the three magnetic fields $\vec{H}_1$, $\vec{H}_2$ and $\vec{H}_3$ can be chosen to have only a x, y and z component respectively. This is in general not possible since $\vec{H}$ includes both the applied field and the magnetostatic field. However, when considering the bulk permeability where the finite simulated region is periodically extended to infinity, the volume integral of the magnetostatic field over the simulation region is zero. This is so because, by reciprocity, the contribution of the periodic extensions of the simulated region to the integral of the magnetostatic field within the simulated region is equivalent to the volume integral of the magnetostatic field contributed by the simulated region over all space which is zero. Indeed, the magnetostatic field is given from Eq. (2.65) as $\vec{H}_{\text{ms}} = -\nabla\Phi_M$ and from the divergence theorem we have

$$\int_\Omega \nabla\Phi_M dv = \int_{\partial\Omega} \Phi_M \hat{n} ds \tag{3.34}$$

where the integral is over the region Ω which spans all three-dimensional space and where $\hat{n}$ is the unit vector pointing outward on the surface of Ω. The surface integral is zero in Eq. (3.34) since the potential Φ_M is a constant at infinity and the surface integral of $\hat{n}$ over any closed surface can be shown to be zero. For example, if $\vec{H}_1$ is chosen to be along the x direction, $\vec{H}_1 = H_1\hat{x}$, then from Eq. (3.26) the $\chi_{m,yx}$ component of the susceptibility tensor can be obtained from the y component of the magnetization response $\vec{M}_1 = M_{x1}\hat{x} + M_{y1}\hat{y} + M_{z1}\hat{z}$ as $\chi_{m,yx} = M_{y1}/H_1$.

In practice, the system to be simulated is first allowed to relax to its equilibrium state and, if the full permeability tensor is to be extracted, three micromagnetic simulations are executed, each with a spatially uniform magnetic field pulse $\vec{H}(t)$ is applied in either the x, y or z direction. The pulse $\vec{H}(t)$ is chosen to have the shape of a gaussian pulse, with a frequency content corresponding to the band of frequencies for which the susceptibility is to be extracted. Since the Fourier transform of a gaussian pulse is also a gaussian pulse, this allows the time domain pulse to be designed such that it is band-limited to the desired frequency range. This is important because the broader the frequency range, the more computationally expensive the micromagnetic computation becomes. Indeed, in order to simulate lower frequencies, a longer time must be simulated while a smaller simulation time step must be used to resolve higher frequency content. The time domain magnetization response is then spatially averaged over the domain of simulation and Fourier-transformed in the frequency domain.

For illustration, the above procedure is applied to the simulation of a single spherical particle with uniaxial anisotropy along the z direction. The sphere has a magnetization saturation $M_s = 1400\,\mathrm{emu/cm^3}$, the anisotropy magnitude is $K = 1 \times 10^6\,\mathrm{erg/cm^3}$, the damping coefficient in the LLG equation is $\alpha = 0.1$ and the exchange coefficient is large enough so that the sphere remains uniformly magnetized. With the magnetization at rest in the $+z$ direction, a pulsed magnetic field is applied in the x direction. The applied magnetic field has the shape of a gaussian pulse and is shown in Fig. 3.6a. The magnitude of its Fourier transform, also a gaussian pulse as shown in Fig. 3.6b shows that it has frequency components up to about 12 GHz. The pulse has a peak magnitude of 150 Oe which is seen to be a small perturbation when compared to the anisotropy field H_K of Eq. (3.20) which has a magnitude of 1430 Oe. The three components of the magnetization response are shown in the time domain in Fig. 3.6c and in the frequency domain in Fig. 3.6d in the form of the magnitude of the Fourier transform of the time domain response. From Eq. (3.24), the ferromagnetic resonant frequency is expected to be 3.94 GHz which corresponds to the peak in Fig. 3.6d.

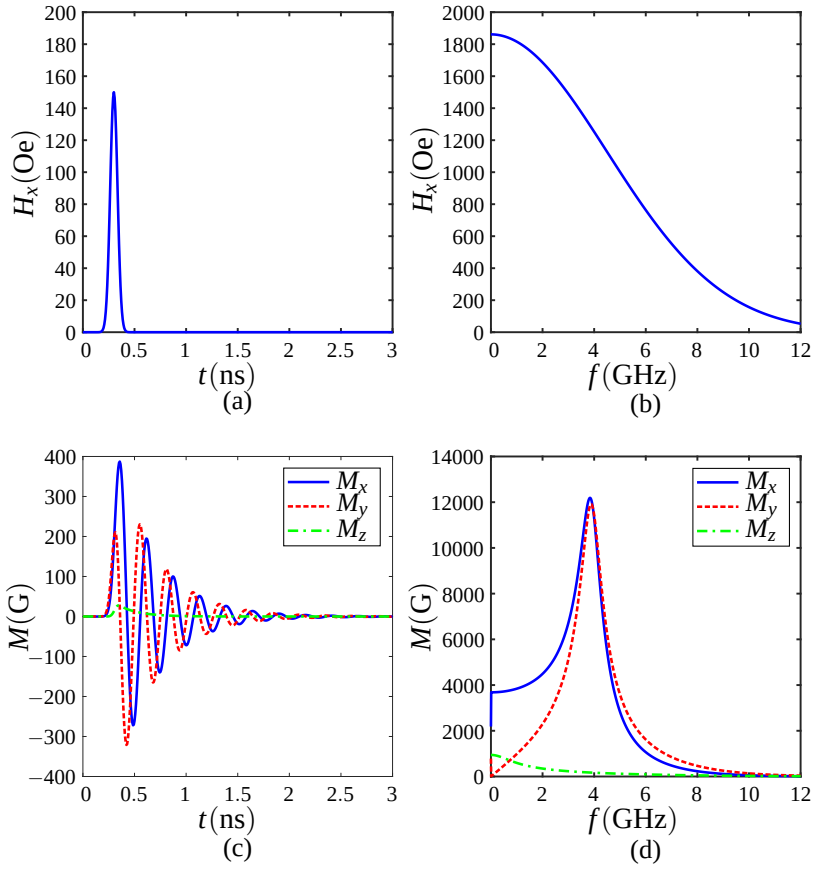

Figure 3.6: Applied magnetic field in the (a) time domain and in the (b) frequency domain for the permeability extraction for a single spherical particle. Magnetization response in the (c) time domain and in the (d) frequency domain of the spherical ferromagnetic particle.

The components of the susceptibility tensor can be obtained by executing two similar simulations with an applied magnetic field along y and z. The result is shown in Fig. 3.7. The tensor components $\chi_{m,xx}$,$\chi_{m,xy}$,$\chi_{m,yy}$,$\chi_{m,yx}$ are compared to the theoretical expressions of Eqs. (3.22) and (3.23). The submatrix representing these four components of the tensor is seen to be anti-symmetric, which is a characteristic of gyrotropic materials. Theoretical results for the $\chi_{m,zx}$ and $\chi_{m,zy}$ components are not readily available since the magnetization response along z is not linear, so that for those components only the numerical result is shown[1]. When the applied field is applied along the z direction, since the magnetization already points towards the z direction

[1]Because the response for those components is not linear, the representation of this response by a susceptibility tensor component is not entirely accurate and can be regarded as a linearization of this response.

corresponding to the equilibrium state, the magnetization response is null which is reflected in the curves for the $\chi_{m,xz}$, $\chi_{m,yz}$ and $\chi_{m,zz}$ components. In section 3.3, it will be seen that permeability extraction can be used as a way to characterize ferromagnetic materials using micromagnetic simulations.

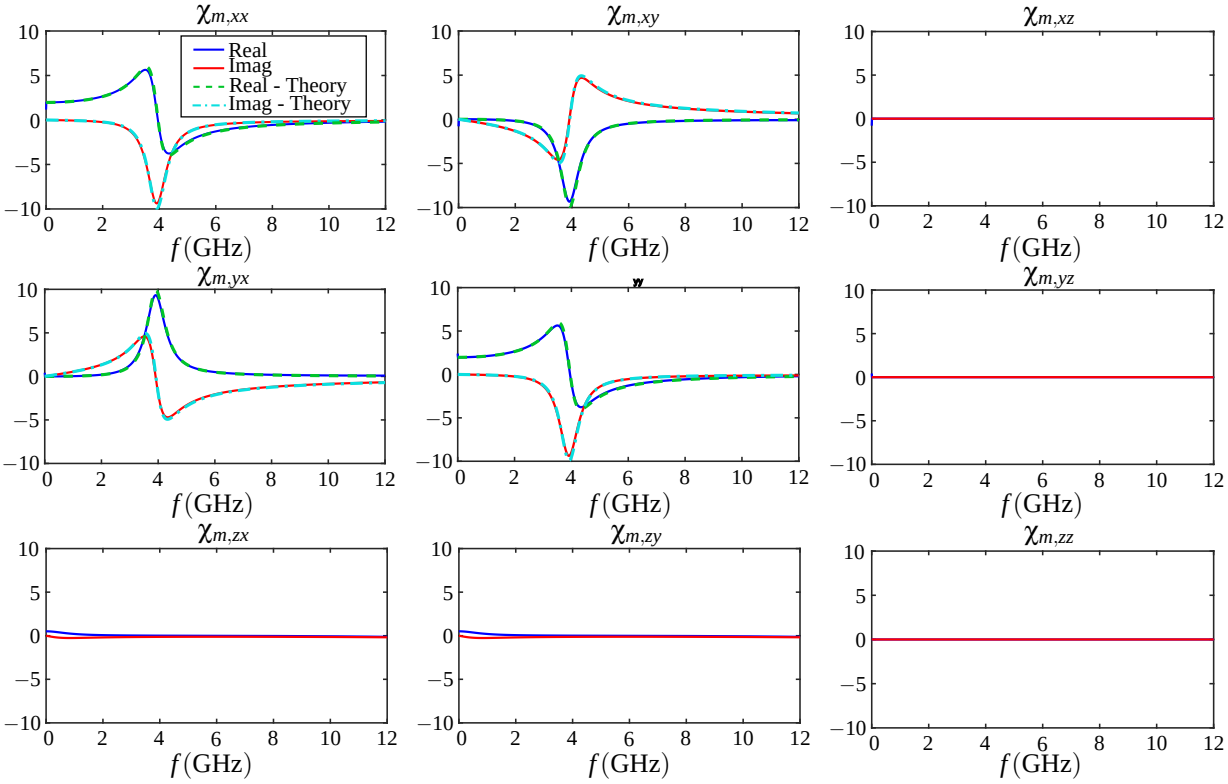

Figure 3.7: Frequency dependent susceptibility tensor components obtained from micromagnetic simulations for a single ferromagnetic sphere.

3.2 Ferromagnetic nano-granular materials

In a 1988 paper, Yoshizawa et al. from Hitachi Metals described nano-crystalline Fe-CuNbSiB alloys which had surprisingly good soft magnetic material properties, that is a low coercive field and high permeability [29]. This is surprising because crystalline ferromagnetic materials are normally associated with a significant crystalline anisotropy. The following quote from their paper describes their assessment of the reasons that could explain this behavior:

> The mechanism whereby FINEMET shows excellent soft magnetic properties is not fully understood. However, it is suggested that this is due to the decrease of local magnetic anisotropy[4] by reducing the grain size and lower magnetostriction than Fe-based amorphous alloys.

Their reference denoted by a superscripted "4" is to a 1973 paper by Hoffmann [30] which states that

> In a polycrystalline film, the local anisotropy mainly consists of the magnetoelastic and magnetocrystalline anisotropy energy of the crystallites. Because of the random orientation of the crystallite axes, this anisotropy is then inhomogeneous.

As it turns out, Yoshizawa et al. were correct: while individual crystalline grains have significant crystalline anisotropies, the overall anisotropy gets averaged out due to the fact that they are randomly oriented. However what they did not mention is that exchange interaction between neighboring grains play a key role in this averaging of the anisotropy.

The idea of considering randomly oriented anisotropy to describe the properties of ferromagnetic material had already been described by Stoner and Wohlfarth [26] in their seminal 1948 paper on the rotation of magnetization due to the interaction between anisotropy and an applied magnetic field. In that paper, the net magnetization of an ensemble of particles with randomly oriented uniaxial anisotropy was considered. While the random orientation of the anisotropy axes was shown to contribute by itself to make the overall response of the particles more soft, Stoner and Wohlfarth did not consider any interaction between particles such as the exchange interaction.

In 1973, Harris et al. proposed a model for magnetization in amorphous ferromagnets in which both randomly oriented uniaxial anisotropy and exchange interaction are considered which they used to predict the Curie temperature and magnetization saturation M_s [31]. In 1978, Alben et al. used this model to predict the "average anisotropy energy density" within a region with a size L corresponding to a "magnetic correlation length" [32] . They obtained the result that the averaged anisotropy density should be proportional to $d^6 K^4 A_{\text{ex}}^{-3}$ where d is a "structural

correlation length", i.e. the length over which the anisotropy is assumed to be uniform and oriented along a given direction, K is the anistropy energy density and A_{ex} is the exchange coefficient.

Herzer used the model proposed by Alben et al. to explain the behavior that had been observed by Yoshizawa et al. for nano-crystalline materials [33, 34]. Using the exchange length, defined as

$$L = \sqrt{\frac{A_{\text{ex}}}{K}}, \tag{3.35}$$

which gives a measure of the length over which magnetization tends to be uniform in the presence of exchange interaction and anisotropy and which corresponds to the magnetic correlation length in the model of Alben et al, and considering a grain size D, the number of grains per volumetric region of size L is

$$N = \left(\frac{L}{D}\right)^3 . \tag{3.36}$$

As will be discussed in section 3.3, from probabilistic considerations, the expected value for the averaged or effective anisotropy's magnitude is

$$K_{\text{eff}} = \frac{K}{\sqrt{N}} . \tag{3.37}$$

In Eq. (3.35) K is the anisotropy energy density. While the exchange length L is usually defined for a spatially uniform and constant anisotropy $\vec{K}$, in the context of ferromagnetic grains with randomly oriented anisotropy directions K in Eq. (3.35) corresponds to the effective anisotropy magnitude which decreases due to the averaging effect. The magnetic correlation length is determined by this new effective anisotropy, therefore

$$L = \sqrt{\frac{A_{\text{ex}}}{K_{\text{eff}}}} . \tag{3.38}$$

Combining Eqs. (3.36), (3.37) and (3.38) and solving for K_{eff} yields

$$K_{\text{eff}} = \frac{D^6 K^4}{A_{\text{ex}}^3} \tag{3.39}$$

which is exactly the result obtained by Alben et al. with the structural correlation length d replaced by the grain size D. This is an important result with practical implications, giving guidelines on how to control a material's microstructure in order to achieve given magnetic parameters. It was validated by Herzer with experimental measurements performed on ribbons of nano-crystalline materials annealed under different conditions, thus yielding different grain sizes [34].

3.3 Micromagnetic simulations and anisotropy averaging in exchange-coupled nano-granular materials

Micromagnetic simulations can be used to compute hysteresis loops and extract the frequency dependent permeability of exchange-coupled nano-granular materials. For example, Fig. 3.4 clearly showed how anisotropy averaging through exchange interaction can drastically close the hysteresis loop of a system of ferromagnetic particles. Such simulations can be very useful to model actual nano-granular materials and to determine the quantitative effects that a change in their properties such as grain size, anisotropy magnitude and direction and exchange interaction strength can have on their macroscopic magnetization response.

Micromagnetic simulations can also be used to validate and better understand the theoretical averaging model described by Herzer and it is this topic that the present section will be concerned with. While Herzer's model predicts trends like the fact that the effective anisotropy magnitude will vary as D^6 where D is the grain size, it is worthwhile to ask if more precise quantitative results can be obtained from the model. For example, for a material consisting

of grains with a size of say 12 nm with randomly oriented uniaxial anisotropies of magnitude $K = 2 \times 10^5\,\mathrm{erg/cm^3}$, can a region with a size L corresponding to the magnetic correlation length of Eq. (3.38) can be assigned an effective uniaxial anisotropy $\vec{K}_{\mathrm{eff}}$ which would accurately represent the material properties? In addition to being a way of validating the anisotropy averaging model and gaining a better understanding of it, doing so would also allow micromagnetic simulations to be executed with such effective regions of size L with a uniform magnetization replacing groups of individual particles, thereby reducing the numerical problem size and resulting in more efficient simulations. For this purpose, lets first have a closer look at the process of anisotropy averaging.

3.3.1 Summing uniaxial anisotropies: a vectorial interpretation

Let N ferromagnetic particles each having volume V_i, $i = 1, \ldots, N$ and uniaxial anisotropy $\vec{K}_i$ randomly oriented in the $x-y$ plane and making an angle θ_i with the positive x axis. Since a uniaxial anisotropy is defined by an orientation rather than a direction, θ_i can be restricted to the $[0, \pi[$ range of values. Assume that these N particles are within a region corresponding to the magnetic correlation length L and that they are intercoupled through exchange interaction such that their normalized magnetization vectors $\vec{m}$ all point in the same direction in the $x-y$ plane, making an angle ϕ with the x axis. Then the N particles can be replaced by a single, larger particle with volume $V = \sum V_i$ with an averaged anisotropy $\vec{K}_{\mathrm{eff}}$. The situation is shown in Fig. 3.8a for the case of $N = 2$.

To obtain an averaged or effective uniaxial anisotropy $\vec{K}_{\mathrm{eff}}$ for the effective region, consider the anisotropy energy associated with the i'th particle, which from Eq. (2.52) reads

$$U_i = K_i V_i \sin^2(\phi - \theta_i)\,. \tag{3.40}$$

Using the trigonometric identity $\sin^2 A = \frac{1}{2} - \frac{1}{2}\cos(2A)$ and dropping the constant term, this

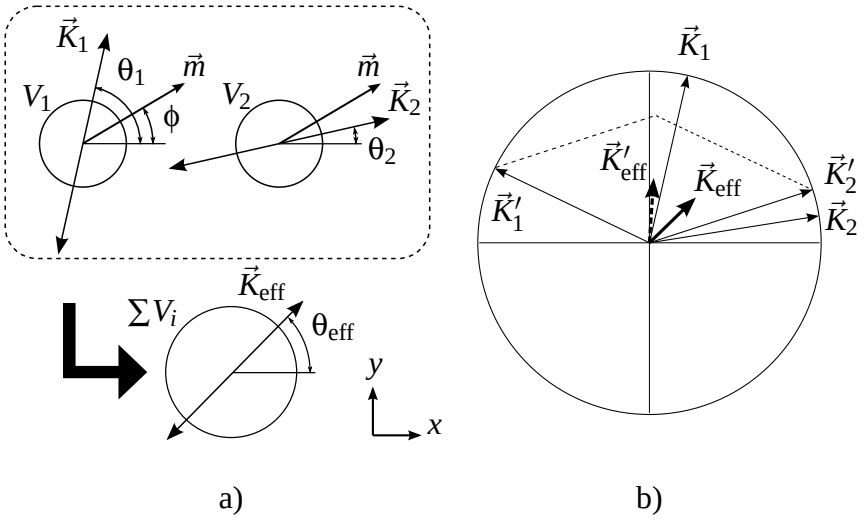

Figure 3.8: Vectorial interpretation of uniaxial anisotropy averaging. (a) Two particles with uniaxial anisotropies $\vec{K}_1$ and $\vec{K}_2$ are equivalent to a single particle with an effective uniaxial anisotropy $\vec{K}_{\text{eff}}$. (b) Relation between $\vec{K}_1$, $\vec{K}_2$ and $\vec{K}_{\text{eff}}$.

becomes

$$U_i = -\frac{1}{2} K_i V_i \cos(2\phi - 2\theta_i) \ . \tag{3.41}$$

Using the trigononmetric identity $\cos(A-B) = \cos A \cos B + \sin A \sin B$, Eq. (3.41) can also be written as

$$U_i = -\frac{1}{2} K_i V_i \left[\cos 2\phi \cos 2\theta_i + \sin 2\phi \sin 2\theta_i\right] \ . \tag{3.42}$$

Introducing the vectors $\vec{K}'_i = K_i \left(\cos 2\theta_i \hat{x} + \sin 2\theta_i \hat{y}\right)$ and $\vec{m}' = \cos 2\phi \hat{x} + \sin 2\phi \hat{y}$ corresponding to the transformed $\vec{K}_i$ and $\vec{m}$ vectors with doubled argument values, Eq. (3.42) can be expressed as

$$U_i = -\frac{1}{2} \vec{m}' \cdot \vec{K}'_i V_i \ . \tag{3.43}$$

Using this, the anisotropy energy for the ensemble of N particles can be written

$$U = \sum_{i=1}^{N} U_i = -\frac{1}{2} \vec{m}' \cdot \sum_{i=1}^{N} \vec{K}'_i V_i \ . \tag{3.44}$$

Using this, the effective averaged anisotropy vector $\vec{K}_{\text{eff}} = K_{\text{eff}} \left(\cos \theta_{\text{eff}} \hat{x} + \sin \theta_{\text{eff}} \hat{y}\right)$ and its trans-

form $\vec{K}'_{\text{eff}} = K_{\text{eff}}\left(\cos 2\theta_{\text{eff}}\hat{x} + \sin 2\theta_{\text{eff}}\hat{y}\right)$ can be defined by

$$\vec{K}'_{\text{eff}} = \frac{1}{V_T}\sum_{i=1}^{N}\vec{K}'_i V_i \tag{3.45}$$

where $V_T = \sum_{i=1}^{N} V_i$ is the total volume of the particles over which the averaging is being performed. The total anisotropy energy in Eq. (3.44) can therefore be written as

$$U = -\frac{1}{2}\vec{m}' \cdot \vec{K}'_{\text{eff}} V_T. \tag{3.46}$$

Comparing this with Eq. (3.43), it is seen that the system of N particles is equivalent to a single particle of volume V_T with an effective averaged uniaxial anisotropy $\vec{K}_{\text{eff}}$ corresponding to the average of transformed K'_i vectors weighted by the particles' volumes. The procedure of transforming the $\vec{K}_i$ vectors by doubling their argument, summing them and transforming them back by halving the resulting vector's argument is illustrated in Fig. 3.8b for the case of $N = 2$ particles. It is seen that the resulting anisotropy energy density K_{eff} is reduced as compared to that of the individual particles. This vectorial approach is an intuitive way of understanding why for example two uniaxial anisotropies of equal magnitude oriented perpendicularly to each other cancel each other out.

Up to this point, only uniaxial anisotropies and magnetization vectors confined to a plane were considered. In the general 3-dimensional case where 2 or more anisotropy vectors and the magnetization vector do not necessarily lie within the same plane, an equivalent uniaxial anisotropy cannot be defined. Luckily, for technological reasons, namely the fact that nanocrystalline ferromagnetic materials are usually used in the form of thin films, the materials are subjected to a strong shape anisotropy [18] which forces the magnetization to be mostly parallel with the thin film's plane. In that case, it can be shown that a given uniaxial anisotropy $\vec{K}$ making an angle θ with the film plane is equivalent to a uniaxial anisotropy with an axis parallel to the plane in the direction corresponding to the projection of $\vec{K}$ into the plane with a magnitude

$K\cos^2\theta$. For this reason, the anisotropy of the individual grains in ferromagnetic nano-granular materials can be considered to lie within a single plane along with the magnetization.

3.3.2 Effective anisotropy and exchange coupling

If the exchange coefficient A_{ex} of the material, the size D of the ferromagnetic grains and the anisotropy magnitude K are known, Eqs. (3.38) and (3.39) suggest that a precise value of the magnetic correlation length can be obtained. However, these relations are only approximate. In updates to his theory, Herzer suggests that Eq. (3.38) should be replaced by

$$L = \phi_0 \sqrt{\frac{A_{\text{ex}}}{K_{\text{eff}}}} \tag{3.47}$$

where ϕ_0 is a prefactor given by $\phi_0 = \alpha\sqrt{\frac{8}{3\beta}}$ with α being "an effective average angle between the easiest directions of the exchange coupled units" and β being "a constant basically related to the symmetry and distribution of the random anisotropy axis" [35]. As Herzer notes in [35],

> It should be noted, that the pre-factors α and β via their combination in ϕ_0 can be rationalized into the basic exchange length L_0. The latter ultimately remains the only open parameter within the above scaling analysis. It is therefore more appropriate to write down the results for $< K1 >$ or L_{ex} in a rationalized form involving the ratio (D/L_0) rather than in the explicit form as given in the original papers involving all the individual material parameters and, in particular, more or less arbitrary pre-factors.

Therefore it seems that specifying an exact size L of the region over which the anisotropy of particles should be averaged poses a difficulty. While numerical value of the pre-factors can be assigned by fitting numerical simulations results [35] or experimental results [34] to the theory, this is somewhat unsatisfying. An approach that avoids this problem is to consider that there is a residual exchange interaction between the regions of size L over which anisotropy is averaged. This approach is illustrated in Fig. 3.9. The individual particles of Fig. 3.9a are exchange coupled with coupling energy J and with the exchange interaction energy between two particles given by

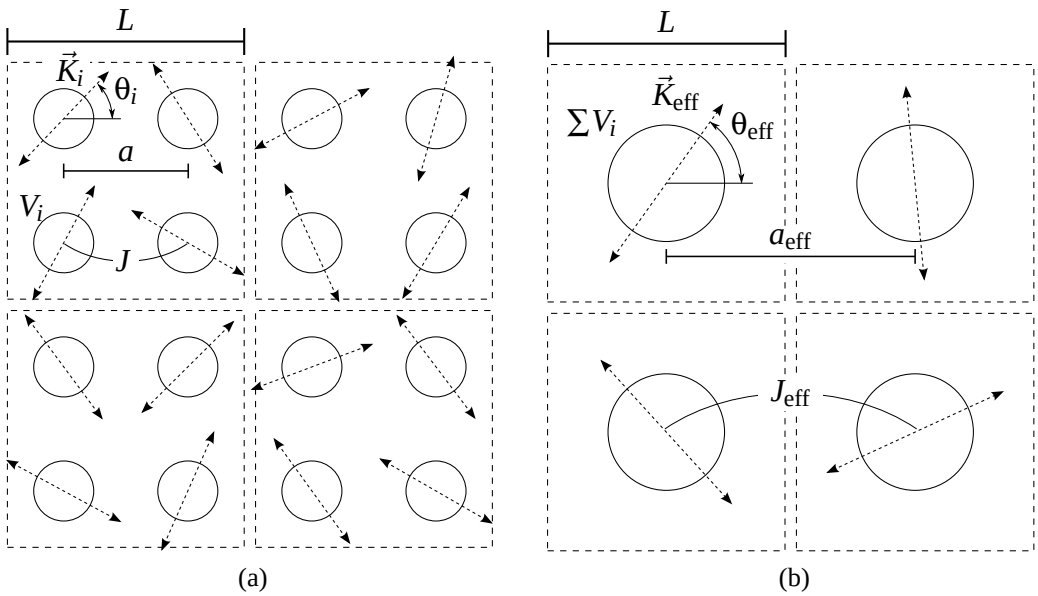

Figure 3.9: Anisotropy averaging over regions of size L. (a) Individual particles with anisotropies $\vec{K}_i$, volumes V_i and exchange coupling energy J. (b) Effective particles with anisotropy $\vec{K}_{\text{eff}}$ corresponding to the averaged anisotropy, volume $\sum V_i$ and residual exchange coupling energy J_{eff}.

Eq. (3.7). Within a region of size L where the exchange coupling is strong enough that all particles can be assumed to have a magnetization pointing in the same direction, the individual particles can be grouped together into a single region that can be treated as a single effective particle, as shown in Fig. 3.9b. This effective particle is assigned an anisotropy corresponding to the average anisotropy of the individual particles and has a volume corresponding to the sum $\sum V_i$ of the particles' volumes. Whereas individual particles are separated by a distance a, the effective particles are separated by a distance $a_{\text{eff}} = L$ corresponding to the size of the averaging regions. The model allows for a residual exchange coupling energy J_{eff} between the effective particles. The strength of this residual exchange coupling will depend on the averaging region size L so that, as long as the condition that particles within the averaging region have a mostly homogeneous magnetization due to exchange interaction is satisfied, L can be chosen arbitrarily.

The relationship between the exchange energy J between individual particles, the residual exchange energy J_{eff} between effective particles, and the averaging region size L can be

obtained by requiring that the volumetric exchange energy density remains the same between the original system with individual particles and the effective particles system. This exchange energy density is exactly the exchange coefficient A_{ex} of continuous micromagnetism introduced in section 2.2.2. The procedure is then exactly the reverse of the procedure used to introduce a continuous exchange energy density A_{ex} from individual atomic spins, with the atomic spins replaced by nano-particles [4, 36], and is as follows.

For a system of exchange coupled particles the exchange energy associated with particle i is

$$U_{\text{ex},i} = -\frac{1}{2} J \sum_{j=1}^{k} \vec{m}_i \cdot \vec{m}_j \tag{3.48}$$

where the sum is over particle i's k nearest neighbors and the factor $\frac{1}{2}$ is present because only half the exchange energy between two particles is associated with particle i. Since $\vec{m}_i \cdot \vec{m}_j = \cos\theta_{ij}$ where θ_{ij} is the angle between $\vec{m}_i$ and $\vec{m}_j$, and using the first two terms of the Taylor expansion $\cos\theta_{ij} \simeq 1 - \frac{1}{2}\theta_{ij}^2$, valid for small θ_{ij}, Eq. (3.48) can be written as

$$U_{\text{ex},i} \simeq \frac{1}{4} J \sum_{j=1}^{k} \theta_{ij}^2 \tag{3.49}$$

where the constant term was dropped. Now, since the $\vec{m}_i$'s are unit vectors, again for small θ_{ij} the approximation $|\theta_{ij}| \simeq |\vec{m}_j - \vec{m}_i|$ holds, so that the energy can be written

$$U_{\text{ex},i} \simeq \frac{1}{4} J \sum_{j=1}^{k} |\vec{m}_j - \vec{m}_i|^2 \,. \tag{3.50}$$

Defining the continuous magnetization $\vec{m}(\vec{x})$ which interpolates the magnetization of the individual particles and letting $\vec{r}_{ij}$ be the vector from particle i to j, Eq. (3.50) can be written

$$U_{\text{ex},i} \simeq \frac{1}{4} J \sum_{j=1}^{k} \left(\vec{r}_{ij} \cdot \nabla m_x\right)^2 + \left(\vec{r}_{ij} \cdot \nabla m_y\right)^2 + \left(\vec{r}_{ij} \cdot \nabla m_z\right)^2 \tag{3.51}$$

where ∇m_x, ∇m_y and ∇m_z are the gradients of the continuous magnetization components evaluated at the center of particle i. Assuming that for example particles are arranged in a simple cubic lattice with lattice constant a, each particle has 6 nearest neighbors, 2 along each x, y and z directions, and since $|\vec{r}_{ij}| = a$, Eq. (3.51) becomes

$$U_{\text{ex},i} \simeq \frac{1}{2} a^2 J \left[(\nabla m_x)^2 + (\nabla m_y)^2 + (\nabla m_z)^2 \right] . \tag{3.52}$$

The energy in Eq. (3.52) represents the exchange coupling energy associated with particle i. To define an exchange energy density, this energy must be divided by the volume of space associated with particle i, which for particles arranged in a simple cubic lattice is a^3. Doing this and comparing with the integrand of the expression for the exchange energy in a continuous magnetization system, Eq. (2.55), it results that the equivalent exchange energy coefficient A_{ex} for the ensemble of particles is

$$A_{\text{ex}} = \frac{J}{2a} . \tag{3.53}$$

A relation like Eq. (3.52) can be obtained for particles arranged in other configurations than a simple cubic lattice. For instance, for a body-centered cubic lattice with an underlying cubic lattice of size a where nearest-neighbor exchange coupling occurs with 8 particles, it can be shown that Eq. (3.53) becomes

$$A_{\text{ex}} = \frac{J}{a} . \tag{3.54}$$

For the case of a face-centered cubic lattice with an underlying cubic lattice of size a, if each particle is exchange coupled to its 12 nearest neighbors, the corresponding result is

$$A_{\text{ex}} = \frac{2J}{a} . \tag{3.55}$$

It should be noted that in reality, particles in nano-granular materials do not organize in a regular lattice but instead tend to be randomly scattered throughout the material. It is also expected

that the exchange coupling energy J between particles will not be constant for every pair of particles but will instead be some function of the inter-particle distance. Finding a relation such as Eq. (3.53) for this case would require probabilistic arguments and is not a trivial task. In this work, we will be satisfied with considering regular arrays of particles with nearest-neighbor coupling.

The relation between the exchange coupling energy J between individual particles and the residual exchange coupling energy J_{eff} between effective particles is obtained by considering Eq. (3.53) for each system and enforcing the equality of the equivalent continuous exchange coefficient A_{ex}. If both the individual particles and the effective particles are arranged in a simple cubic lattice, the result is the relation

$$J_{\text{eff}} = \frac{a_{\text{eff}}}{a} J. \tag{3.56}$$

where $a_{\text{eff}} = L$, the size of the averaging region. Since the number of particles over which the averaging occurs is given by $N = L^3/a^3$, Eq. (3.56) can also be written as

$$J_{\text{eff}} = N^{\frac{1}{3}} J. \tag{3.57}$$

While the exchange coupling energy between the effective particles J_{eff} is larger than J, a better measure is the exchange coupling energy density since it can be compared to the other energy terms which are expressed in terms of energy density. For instance, the energy density due to an external magnetic field is proportional to the saturation magnetization M_s and is the same for the original and effective particles systems since the saturation magnetization M_s is unchanged. Meanwhile, due to averaging, the anisotropy energy density K_{eff} of the effective particles is reduced as compared to the anisotropy energy density K of the original particles. Similarly, the exchange energy density $j = J/V_i$, where V_i is the volume of particle i, is in fact reduced for the system of effective particles. Indeed, for the effective particles, $j_{\text{eff}} = J_{\text{eff}}/V$ so

that using $V = \sum V_i$ as the volume of an effective particle as well as Eq. (3.57) and assuming that all particle volumes V_i are identical yields

$$j_{\text{eff}} = \frac{j}{N^{\frac{2}{3}}}. \tag{3.58}$$

To illustrate the anisotropy averaging of nano-granular materials in micromagnetic simulations, Fig. 3.10a shows the hysteresis curves of a $144 \times 144 \times 12$ simple cubic array of particles computed with no exchange coupling between the particles, corresponding to $j = 0$ and with an inter-particle exchange coupling with an energy density of $j = 1.8 \times 10^5\,\text{erg/cm}^3$. The particles are assumed to be small enough to be uniformly magnetized, have saturation magnetization $M_s = 1000\,\text{emu/cm}^3$ and have a uniaxial anisotropy of magnitude $K = 2 \times 10^5\,\text{erg/cm}^3$ with a direction that is randomly distributed in the $x-y$ plane. It is seen that a significant reduction of the effective anisotropy occurs due to anisotropy averaging.

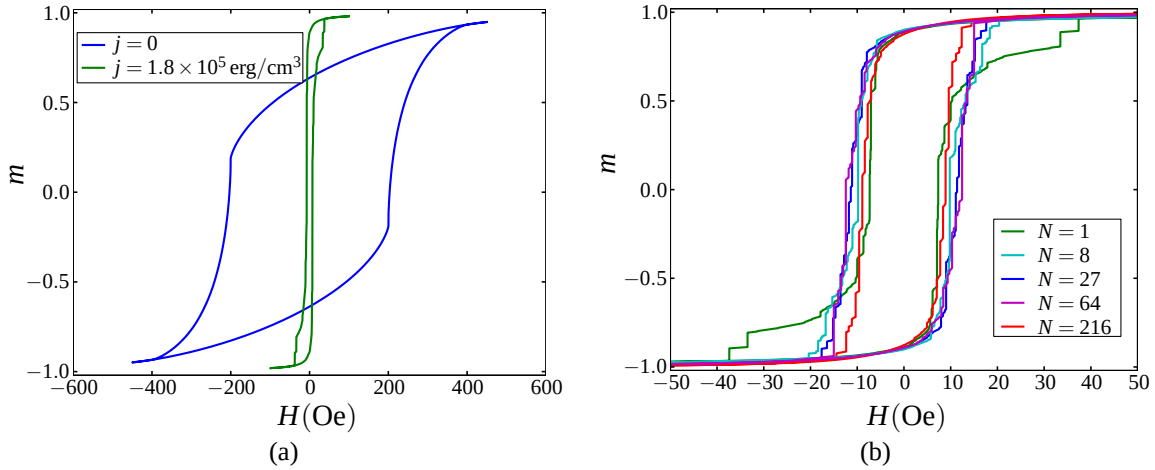

Figure 3.10: (a) Hysteresis loops computed for a $144 \times 144 \times 12$ array of particles with and without inter-particle exchange coupling. (b) Hysteresis loops computed for effective particles corresponding to anisotropy averaging over N particles. The corresponding residual exchange energy densities j_{eff} are given in table 3.1.

Shown in Fig. 3.10b are hysteresis loops computed using arrays of averaged particles based on the system of individual particles with $j = 1.8 \times 10^5\,\text{erg/cm}^3$ of Fig. 3.10a. The case $N = 1$ corresponds to the original system with individual particles while the other values of

N correspond to the number of particles inside each averaging region. The values of N are seen to correspond to the sequence of integers 1, 2, 3, 4 and 6 to the power three, so that the averaging regions have the shape of a cube with side lengths corresponding to multiples of the spacing between individual particles and the entire $144 \times 144 \times 12$ array of particles can be neatly subdivided in averaging regions. Based on Eq. (3.58), the residual exchange energy densities j_{eff} corresponding to each value of N are shown in table 3.1. It is seen that the hysteresis loops for these averaged systems are very similar to each other. Yet, the individual particles system corresponding to $N = 1$ has 250 K particles while the averaged particles system with $N = 216$ has only 1152 particles and can be computed much more quickly.

Table 3.1: Residual exchange energy densities corresponding to the effective particles for the different numbers of averaged particles N of Fig. 3.10b.

N	j_{eff} [erg/cm^3]
1	1.80×10^5
8	4.50×10^4
27	2.00×10^4
64	1.13×10^4
216	5.00×10^3

In the previous example, the micromagnetic simulation did not account for the magnetostatic field. This is because the averaged anisotropy model does not take into account that the magnetostatic field generated by an ensemble of particles will be different than the magnetostatic field generated by a single larger effective particle. The magnetostatic field could accurately be accounted for with the effective particle model by computing the magnetostatic field generated by the particles inside an averaging region while assuming that their magnetization is homogeneous. However, this was not done in this work as the primary goal was to study the anisotropy averaging due to exchange interaction.

3.4 Directional probability on the circle

As was discussed in section 3.3.1, the problem of anisotropy averaging in nano-granular ferromagnetic materials is a 2-dimensional problem where we are interested in the averaged value, or expected value in probability terminology, of the sum of vectors with randomly distributed orientations and magnitudes. Interestingly, this type of problem gave rise to a branch of probability theory known as directional probability on the circle which, while it shares the same fundamental concepts as standard probability theory on the line, has quite distinct features. For instance, when defining the mean direction of two unit vectors which are naturally defined by the angles θ_1 and θ_2 that each vector makes with the positive x axis, the use of the arithmetic mean as used for numbers on the real line is not adequate. For example, for the two unit vectors shown in Fig. 3.11 with $\theta_1 = \pi/4$ and $\theta_2 = 7\pi/4$, the arithmetic mean would correspond to a mean direction of π whereas the mean direction which "makes sense" corresponds to the zero angle.

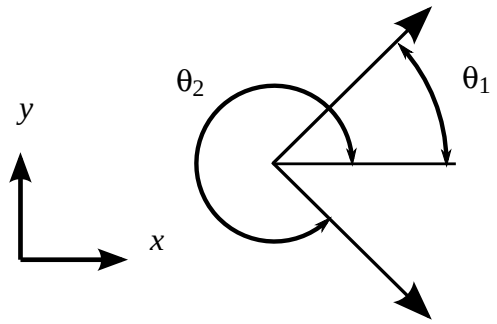

Figure 3.11: The mean direction of two unit vectors is not adequately determined by the arithmetic mean of the angles that they make with the positive x axis.

In what follows, some results of directional probability theory will be stated without proof. The interested reader can consult the excellent work on the topic by Mardia [37]. It is interesting to consider the same problem of summing two unit vectors but this time from a probabilistic point of view. Indeed, consider two random vectors on the unit circle characterized by the two random variables θ_1 and θ_2 representing the angles that the unit vectors make with

the positive x axis. Lets consider that both θ_1 and θ_2 are idenpendent and identically distributed with a uniform distribution, that is, they are characterized by the probability density function

$$f(\theta) = \frac{1}{2\pi} \tag{3.59}$$

which, unlike random variables defined on the whole real line, is defined on the set $[0, 2\pi[$ and is such that

$$\int_0^{2\pi} f(\theta) d\theta = 1 \ . \tag{3.60}$$

What is the probability distribution of the resulting sum vector? While it can be shown rigorously, intuitively and from the circular symmetry of the problem it is clear that the direction ϕ of the resulting vector is a random variable that is uniformly distributed, that is, there is no preferred direction in which the resulting vector is more likely to point. One might wonder what this implies in terms of the expected value of ϕ. If the definition of the expected value from probability theory on the line is applied, we obtain

$$E[\phi] = \int_0^{2\pi} \phi f(\phi) d\phi \ . \tag{3.61}$$

With ϕ uniformly distributed so that $f(\phi) = \frac{1}{2\pi}$, this gives $E[\phi] = \pi$, which again shows the inadequacy of simply applying linear probability concepts to probabilities on the circle. In directional probability theory, the mean or expected direction of an angular probability distribution is the direction with respect to which the circular dispersion is minimized. The circular dispersion is a measure of the dispersion of points on the unit circle corresponding to random angles with respect to a point corresponding to a given angle α and is defined as

$$D = \int_0^{2\pi} f(\theta)[1 - \cos(\theta - \alpha)] d\theta \ . \tag{3.62}$$

From this expression, it is seen that when θ is uniformly distributed with the probability density

function of Eq. (3.59), the circular dispersion is $D = 1$. Since in this case the expression for D is independent of α, no value of α minimizes it and no expected direction exists. For distributions where an expected direction exists corresponding to $\alpha = \theta_0$, the circular dispersion with respect to θ_0 is known as the circular variance and is given by

$$V = \int_0^{2\pi} f(\theta)[1 - \cos(\theta - \theta_0)]d\theta \ . \tag{3.63}$$

It can be shown that for any distribution, $0 \leq V \leq 1$, with $V = 1$ corresponding to no directional preference, i.e. a uniform distribution, and $V = 0$ corresponding to a Dirac distribution probability distribution function concentrated on the point θ_0.

What about the expected magnitude of the sum of two random vectors on the unit circle? Whereas on the real line the sum of two uniformly distributed random variables has an expected value of zero, it can be shown that the expected value of the resulting vector magnitude is $4/\pi \approx 1.27$. In the general case of the sum of N random and uniformly distributed vectors each with a fixed magnitude K_0, the direction of the resulting vector is still uniformly distributed, and the probability density function for the resulting vector's magnitude normalized by the number of random vectors N, K, can be shown to be to be

$$f(K) = K \int_0^{\infty} xJ_0(Kx) \left[J_0\left(\frac{xK_0}{N}\right) \right]^N dx \tag{3.64}$$

where $J_0(x)$ is the Bessel function of the first kind and order 0. From Eq. (3.45), this is seen to be the probability distribution for the averaged anisotropy K_{eff} when averaging uniformly distributed anisotropies with fixed magnitude K_0. For N large, using the central limit theorem, it can be shown that the probability density function for K tends towards

$$f(K) = \frac{2NK}{K_0^2} e^{-NK^2/K_0^2} \ . \tag{3.65}$$

From this expression, the expected value of K can be obtained for large N and is given by

$$E[K] = \frac{\sqrt{\pi}}{2\sqrt{N}} K_0 \ . \tag{3.66}$$

It is this result that justifies the expression of Eq. (3.37) for the magnitude of the averaged anisotropy.

Aside from the uniform distribution, another distribution that plays an important role in directional probability is the equivalent of the normal distribution on the line, known as the von Mises distribution. Its probability density function is

$$f(\theta) = \frac{1}{2\pi I_0(k)} e^{k\cos(\theta-\theta_0)} \tag{3.67}$$

where $I_0(k)$ is the modified Bessel function of the first kind and order 0, θ_0 is the distribution's mean direction and k is the concentration parameter. A concentration parameter $k = 0$ corresponds to the uniform distribution while large k values correspond to a high probability density concentration around the mean direction angle θ_0. The circular variance of the distribution is given in terms of the concentration parameter as

$$V = 1 - \frac{I_1(k)}{I_0(k)} \tag{3.68}$$

The probability density function for the von Mises distribution is plotted in Fig. 3.12 for the mean direction $\theta_0 = 0$ and concentration parameter values $k = 0$, $k = 0.4$ and $k = 1.5$.

The von Mises distribution can be useful to model nano-granular materials in which there is a preferred direction of the anisotropy axis, like for example if the material is annealed in the presence of an applied magnetic field, in which case the particles' anisotropy axes will tend to align with the applied field. When summing N independent random vectors characterized by a von Mises distribution, the direction θ and magnitude K of the resulting vector normalized

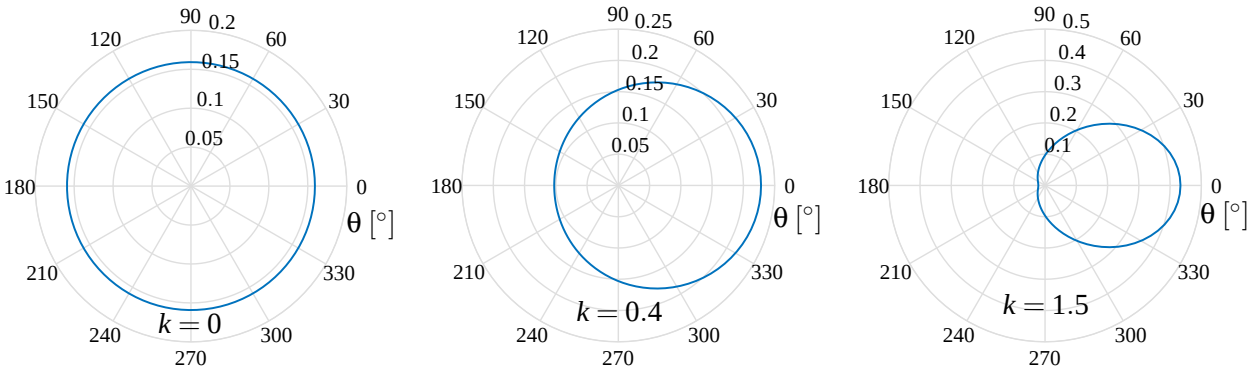

Figure 3.12: Probability density function of the von Mises distribution for a mean direction $\theta_0 = 0$ and a concentration parameter value of (a) $k = 0$, (b) $k = 0.4$ and (c) $k = 1.5$.

by the number of random vectors N are characterized by the following joint probability density function,

$$f(\theta, K) = \frac{K}{2\pi [I_0(k)]^N} e^{\frac{kNK}{K_0}\cos(\theta - \theta_0)} \int_0^\infty x J_0(xK) \left[J_0\left(\frac{xK_0}{N}\right)\right]^N dx \,. \tag{3.69}$$

For large N, it can be shown that the expected value of the resulting vector's normalized magnitude K is

$$E[K] = K_0 \left[\frac{I_1(k)}{I_0(k)} + \frac{1}{2N} + O(N^{-3/2}) \right] \,. \tag{3.70}$$

While K decreases as $N^{-\frac{1}{2}}$ as per Eq. (3.66) for the case of the uniform distribution, from Eq. (3.70) it is seen that in the case of the von Mises distribution, a portion of the uniaxial anisotropy cannot be averaged out regardless of the number of random vectors N, while the remaining portion quickly decreases as N^{-1}.

The probability density functions for the sum of N random vectors that were presented in this section can be useful to generate samples of effective particles with averaged anisotropies, therefore avoiding the need to generate samples of individual particles and individually summing their anisotropy vectors to obtain an averaged vector. As will be seen in the next section, it can also be used to compute hysteresis loops using a Stoner-Wohlfarth model which accounts for exchange interaction between particles using probability distributions.

To illustrate the effect of random anisotropy vectors with a von Mises distribution, consider a $500 \times 500 \times 80$ nm thin film consisting of 21,000 particles, each with a saturation magnetization $M_s = 1422\,\text{emu}/\text{cm}^3$, intercoupled with an exchange energy density $j = 1 \times 10^6\,\text{erg}/\text{cm}^3$ and with uniaxial anisotropies of magnitude $K_0 = 2 \times 10^5\,\text{erg}/\text{cm}^3$ and random orientations distributed according to a von Mises distribution with mean direction corresponding to the y axis and concentration parameter k. The hysteresis loops for a magnetic field applied in the x direction, that is perpendicular to the preferred direction of anisotropy, for $k = 0$, $k = 1$ and $k = 2$ are shown in Fig. 3.13.

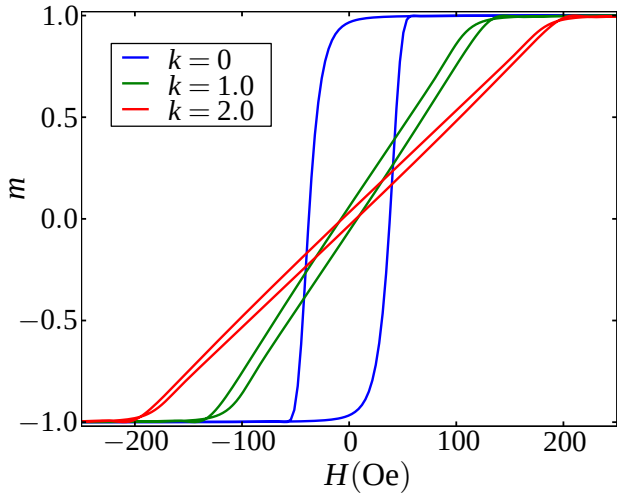

Figure 3.13: Hysteresis loops computed for a $500 \times 500 \times 80$ nm thin film consisting of 21,000 particles with a saturation magnetization $M_s = 1422\,\text{emu}/\text{cm}^3$, intercoupled with an exchange energy density $j = 1 \times 10^6\,\text{erg}/\text{cm}^3$ and with uniaxial anisotropies of magnitude $K_0 = 2 \times 10^5\,\text{erg}/\text{cm}^3$ with randomly oriented directions in the $x-y$ plane following a von Mises distribution with mean direction in the y direction and concentration parameter $k = 0$, $k = 1$ and $k = 2$.

It is seen that the case $k = 0$, corresponding to a uniform random distribution, requires the least strength of the applied field to completely switch the magnetization direction. However, it also exhibits the most open hysteresis loop and therefore the least linear behavior, highlighting the advantage of having a certain amount of anisotropy perpendicular to the direction of the applied field, effectively creating a magnetic soft direction. The system with concentration parameter $k = 2$ has more anisotropy in the direction perpendicular to the applied field than the

system with $k = 1$, which is why it requires a stronger magnetic field to completely switch the direction of the magnetization. It also results in a smaller slope of the hysteresis curve, which translates to a lower value of the permeability or magnetic susceptibility.

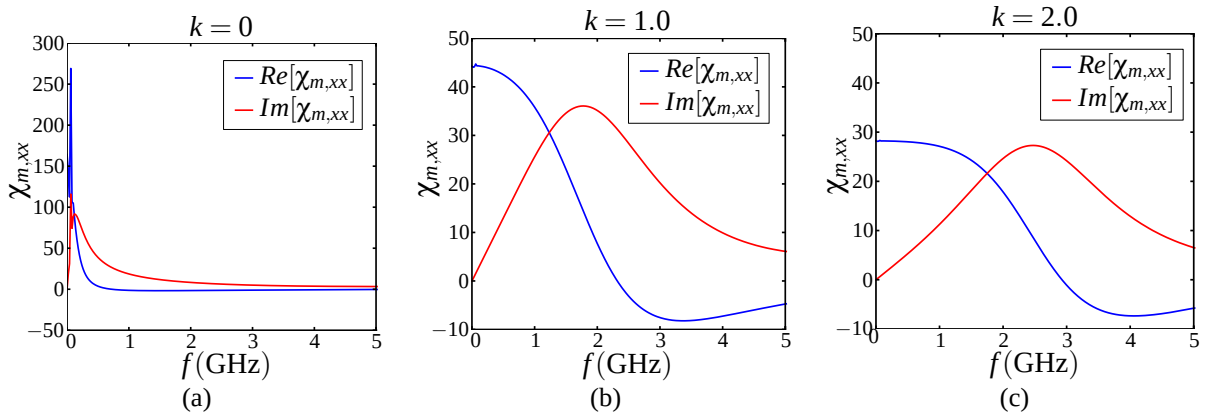

Figure 3.14: Extracted $\chi_{m,xx}$ component of the magnetic susceptibility tensor for the three nano-granular materials with random anisotropy distributions corresponding to $k = 0$, $k = 1$ and $k = 2$.

The $\chi_{m,xx}$ component of the magnetic susceptibility tensor is extracted for the three systems of particles with $k = 0$, $k = 1$ and $k = 2$. The results are shown in Figs. 3.14a, 3.14b and 3.14c respectively. Having an open hysteresis loop with a significant non-linear behavior, the magnetic susceptibility for the $k = 0$ case is not a good representation of the material's magnetic response. Yet, the extracted susceptibility response still yields useful information. For instance, the susceptibility value at low frequencies is quite high, reflecting the fact that the effective anisotropy of the material is small due to anisotropy averaging. This is also reflected in the high slope value of the corresponding hysteresis loop. Due to the weak effective anisotropy, the resonant frequency occurs at relatively low frequencies, and the susceptibility at higher frequencies is very weak. For $k = 1$, the higher slope value translates to a higher permeability value than for the $k = 2$ case. This is due to the stronger anisotropy in the $k = 2$ case, which also has the effect of pushing the ferromagnetic resonance to a higher frequency value, thereby allowing the $k = 2$ material to maintain its susceptibility value over a broader frequency range. This effect is the well known trade-off between high permeability value and the ability of the material to maintain

that high permeability value at high frequencies. The low frequency permeability in the $k = 1$ and $k = 2$ cases can be obtained from the slope of the hysteresis curves of Fig. 3.13. In both cases, the filling ratio of the particles in the simulations was 0.31, so that the spatially averaged magnetization amplitude is $|\vec{M}| = 0.31 M_s$. For the $k = 1$ case, from Fig. 3.13 the anisotropy field is seen to be $H_k = 130\,\mathrm{Oe}$. Then, with $M_s = 1422\,\mathrm{emu/cm^3}$ and with Eq. (3.21) taking the form

$$\chi_m = \frac{4\pi|\vec{M}|}{H_K} \tag{3.71}$$

in cgs units for a magnetization amplitude expressed in $\mathrm{emu/cm^3}$, one obtains $\chi_m = 42.6$ which is close to the value observed in Fig. 3.14b at low frequencies. In the $k = 2$ case, the anisotropy field is $H_k = 200\,\mathrm{Oe}$ from which Eq. (3.71) yields $\chi_m = 27.7$, which again is close to the value observed at low frequencies in Fig. 3.14.

3.5 Generalized Stoner-Wohlfarth model for exchange-coupled ferromagnetic grains

In section 3.1.1 about the hysteresis loop, the Stoner-Wohlfarth model describing the magnetization rotation in a particle with a uniaxial anisotropy subjected to an applied magnetic field was introduced. The model was used to compute the hysteresis loop for a single particle, and it was mentioned that it can also be used to compute the hysteresis loops of ensembles of particles. The 1948 paper of Stoner and Wohlfarth [26] was such a significant contribution to our understanding of the mechanism of magnetization rotation in ferromagnets that it is perhaps less well known that in that same paper, Stoner and Wohlfarth used their model to compute the hysteresis loop of an ensemble of particles with anisotropy axes randomly and uniformly distributed on the unit sphere.

For a single particle and referring to Fig. 3.2, the Stoner-Wohlfarth hysteresis model

relies on finding the value of the angle ϕ between the magnetization and the applied magnetic field which minimizes the total energy. This value of ϕ corresponds to the solution of Eq. (3.6) in which the other quantities, namely the applied magnetic field magnitude H, the anisotropy magnitude K, the angle θ between the applied magnetic field $\vec{H}$ and the particle's saturation magnetization M_s, are assumed to be known. The hysteresis loop is computed by sweeping the applied magnetic field H from its maximum value to its minimum value and then back, and computing $\cos\phi$ for each discrete H value, which corresponds to the component of the normalized magnetization along the direction of the applied field.

In the case of an ensemble of randomly oriented particles, the angle θ between $\vec{H}$ and the anisotropy vector $\vec{K}$ becomes a random variable and the computation of the hysteresis loop then involves the expected value of $\cos\phi$,

$$E[\cos\phi] = \int_0^{2\pi} \cos\phi f(\theta) d\theta \ , \tag{3.72}$$

where $f(\theta)$ is the probability density function of the random variable θ and which is to be computed for each discrete value of the H sweep. The angle ϕ being obtained from the solution of Eq. (3.6), it can be considered as a function (albeit without an explicit form) of θ, K and H, so that

$$\phi = \phi(H, \theta, K) \ . \tag{3.73}$$

With this, Eq. (3.72) can be written as

$$E[\cos\phi] = \int_0^{2\pi} \cos\phi(H, \theta, K) f(\theta) d\theta \tag{3.74}$$

and the integral can be computed using a numerical integration scheme such as Simpson's rule. The probability density function $f(\theta)$ will depend on the distribution of the random anisotropy direction. In the case of randomly oriented $\vec{K}$ vectors with a uniform distribution on the sphere

of radius K, it is straightforward to show that the probability density function is $f(\theta) = \frac{1}{2}\sin\theta$. Using this, just as Stoner and Wohlfarth did in their 1948 paper [26], the hysteresis loop of Fig. 3.15 can be obtained where the particles were assumed to have a fixed anisotropy magnitude of $K = 1 \times 10^6\,\mathrm{erg/cm^3}$ and a saturation magnetization $M_s = 1400\,\mathrm{emu/cm^3}$. Also shown for comparison is the hysteresis computed using a micromagnetic simulation for an ensemble of 1000 particles with the same characteristics, which is seen to agree quite well with the result obtained with the Stoner-Wohlfarth model, the difference between the curves being due to the finite number of particles in the micromagnetic simulation.

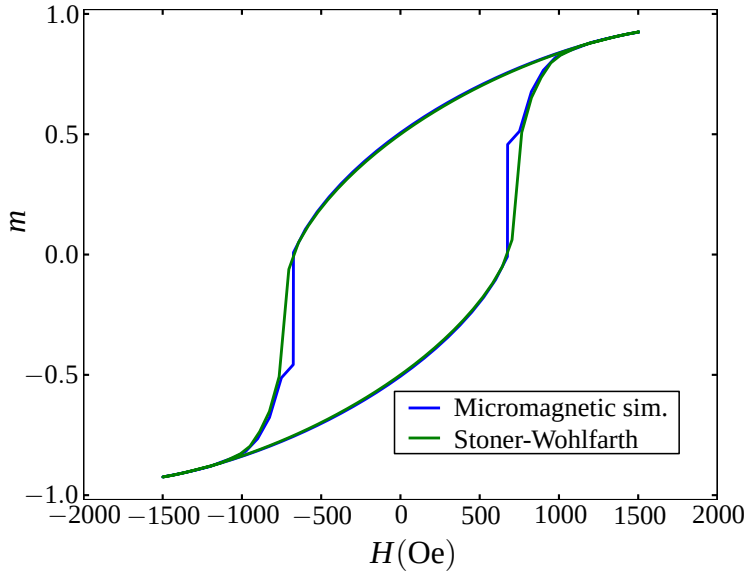

Figure 3.15: Comparison of hysteresis loops for an ensemble of particles with randomly oriented anisotropy following a uniform distribution on the unit sphere computed by a micromagnetic simulation with 1000 particles and the probabilistic Stoner-Wohlfarth hysteresis model.

In the case where the anisotropy magnitude K is not fixed but is also a random variable, Eq. (3.74) takes the form

$$E[\cos\phi] = \int_0^{2\pi}\int_0^{\infty} \cos\phi(H,\theta,K)\, f(\theta,K)\, d\theta \tag{3.75}$$

where $f(\theta,K)$ is the joint probability density function of the random variables θ and K. Given $f(\theta,K)$, the corresponding hysteresis loop can then be computed just as in the previous example.

A limitation of the Stoner-Wohlfarth model is that it does not take into account interactions between particles such as the exchange interaction. Since the exchange interaction and the anisotropy averaging that results from it can have a drastic effect on the magnetic properties of materials, a generalized Stoner-Wohlfarth model which takes into account exchange interaction between particles would be a valuable tool. Such a model can be obtained by adding the exchange energy density to the total energy density of Eq. (3.5). Since the Stoner-Wohlfarth model does not rely on a Monte Carlo simulation involving a realization of a large ensemble of particles, which can then easily be inter-coupled, but instead relies on a probabilistic description of a particle, how can the exchange coupling be introduced in the model? Taking the probabilistic approach one step further, the particle whose energy is under consideration can be exchange coupled to a second probabilistic particle representing the random ensemble of particles, with the exchange energy corresponding to the expected value of the exchange energy between the particle under consideration and the probabilistic particle. Another way of stating this is that the particle under consideration is exchange coupled to each and every particle in an ensemble with infinitely many particles, each with its own anisotropy vector, with the number of particles having a given anisotropy vector proportional to the probability density function of the anisotropy distribution. The exchange energy acting on the particle under consideration is then taken to correspond to the expected value or mean of this continuum of exchange energies. This idea is illustrated in Fig. 3.16, where the unprimed particle is the particle under consideration, the energy of which we seek to minimize, and the primed particle represents the probabilistic ensemble of particles to which it is exchange coupled.

Based on Eq. (3.7), the exchange energy between the primed and unprimed particles of Fig. 3.16 is $-j\vec{m}\cdot\vec{m}' = -j\cos(\phi-\phi')$. However, since $\phi' = \phi'(H,\theta',K')$ is a random variable, as discussed above it is the expected value of this energy that must be added to the unprimed particle's total energy without exchange interaction, Eq. (3.5), so that with exchange coupling,

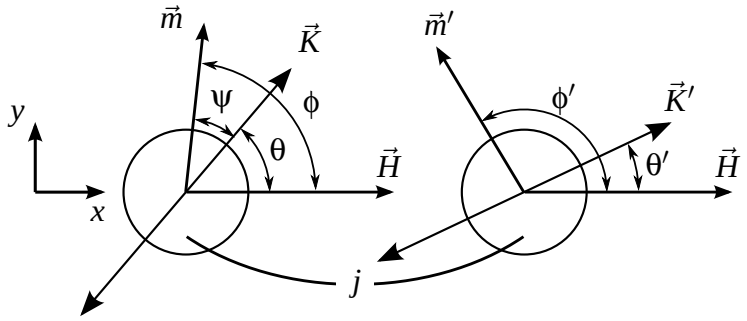

Figure 3.16: Stoner-Wohlfarth model with exchange coupling. The unprimed particle is the particle under consideration, for which the energy minimum is sought. The primed particle represents the probabilistic ensemble of particles to which the unprimed particle is coupled.

the total energy becomes

$$U = -\frac{K}{2}\cos(2[\phi-\theta]) - HM_s\cos\phi - j\int_0^{2\pi}\int_0^{\infty} f(\theta',K')\cos\left[\phi-\phi'(H,\theta',K')\right]dK'd\theta' \ . \quad (3.76)$$

where $f(\theta',K')$ is the joint probability density function of the anisotropy's random distribution. In the same way that in the Stoner-Wohlfarth model without exchange, ϕ is given by the function $\phi(H,\theta,K)$ where this function represents the solution of the non-linear equation of Eq. (3.6), minimizing the energy of Eq. (3.76) by letting $\partial U/\partial\phi = 0$ yields a non-linear equation that must be solved for ϕ given values of H, θ and K, that is,

$$K\sin(2[\phi-\theta]) + HM_s\sin\phi + j\int_0^{2\pi}\int_0^{\infty} f(\theta',K')\sin\left[\phi-\phi'(H,\theta',K')\right]dK'd\theta' = 0 \quad (3.77)$$

with only solutions such that $\partial^2 U/\partial\phi^2 > 0$ corresponding to minima of the energy, that is

$$2K\cos(2[\phi-\theta]) + HM_s\cos\phi + j\int_0^{2\pi}\int_0^{\infty} f(\theta',K')\cos\left[\phi-\phi'(H,\theta',K')\right]dK'd\theta' > 0 \ . \quad (3.78)$$

However, and here comes the key argument, the probabilistic ensemble of particle represented by primed quantities in Fig. 3.16 is in fact the same ensemble of particles of which the unprimed particle is a part of. Therefore, the function $\phi'(H,\theta',K')$ which gives the ϕ' angle value

of the primed particle is the same function $\phi(H,\theta,K)$ giving the ϕ angle value of the particle under consideration, i.e. we effectively have $\phi'(H,\theta',K') = \phi(H,\theta',K')$. Using this and writing occurences of ϕ in Eq. (3.77) in their explicit function form yields

$$K\sin(2[\phi(H,\theta,K)-\theta]) + HM_s\sin\phi(H,\theta,K) + j\int_0^{2\pi}\int_0^{\infty} f(\theta',K')\sin\left[\phi(H,\theta,K)-\phi(H,\theta',K')\right]dK'd\theta' = 0\,. \quad (3.79)$$

Comparing this with Eq. (3.6) for the case without exchange coupling, it is seen that while Eq. (3.6) is a scalar non-linear equation where H, θ and K are assumed to be given, Eq. (3.79) involves a functional of $\phi(H,\theta,K)$ and as such is a non-linear integral equation to be solved for $\phi(H,\theta,K)$. Just as in the Stoner-Wohlfarth hysteresis model, the value of H will be sweeped, and for each discrete H value Eq. (3.79) needs to be solved. To solve this equation numerically, the function $\phi(H,\theta,K)$ is discretized in the space $\{\theta \in [0,2\pi[, K \in [0,R]\}$. While the probability density function $f(\theta,K)$ is in theory defined for $K \in [0,\infty[$, in practice it is very close to zero above a certain value R, chosen depending on the distribution, so that $\phi(H,\theta,K)$ can be discretized over a finite domain. By this discretization procedure, the function $\phi(H,\theta,K)$ can be written as

$$\phi(H,\theta,K) = \sum_{j=1}^{N} \phi_j(H)\psi_j(\theta,K) \quad (3.80)$$

where the ψ_i's, $i = 1,\ldots,N$ are the N basis functions and the ϕ_i's are the unknown coefficients, here shown as functions of H to highlight the fact that a different set of these coefficients must be determined for each H value. A total of N equations are then obtained by multiplying Eq. (3.79) by N test functions and integrating over the domain of solution. In our implementation of this method, flat basis functions with unit magnitude on a rectangular grid and point matching, the equivalent of choosing Dirac distributions as testing functions, were used. However, any other type of basis function, test function and discretization grid could in principle be used.

With Eq. (3.80), Eq. (3.79) can be written as

$$K\sin\left(2\left[\sum_{j=1}^{N}\phi_j(H)\psi_j(\theta,K)-\theta\right]\right)+HM_s\sin\left(\sum_{j=1}^{N}\phi_j(H)\psi_j(\theta,K)\right)$$
$$+\,j\int_0^{2\pi}\int_0^{\infty}f(\theta',K')\sin\left[\sum_{j=1}^{N}\phi_j(H)\psi_j(\theta,K)-\sum_{j=1}^{N}\phi_j(H)\psi_j(\theta',K')\right]dK'd\theta'=0\,. \quad (3.81)$$

Introducing the N test functions $\lambda_i(\theta,K)=\delta(\theta-\theta_i)\delta(K-K_i)$ for $i=1,\ldots,N$ where δ denotes the Diract distribution and (θ_i,K_i) corresponds to the center point of each flat basis function $\psi_i(\theta,K)$, and multiplying Eq. (3.81) by each test function $\lambda_i(\theta,K)$ successively and performing a double integration over $\{\theta\in[0,2\pi[,K\in[0,R]\}$ yields a non-linear system of N equations for $i=1,\ldots,N$,

$$K_i\sin(2[\phi_i(H)-\theta_i])+HM_s\sin\phi_i(H)$$
$$+\,j\int_0^{2\pi}\int_0^{\infty}f(\theta',K')\sin\left[\phi_i(H)-\sum_{j=1}^{N}\phi_j(H)\psi_j(\theta',K')\right]dK'd\theta'=0\,. \quad (3.82)$$

Denoting the vector of unknown coefficients ϕ_i by $\vec{\phi}$, starting from an initial guess $\vec{\phi}^{(0)}$, which in the context of hysteresis loop computations would be the solution $\vec{\phi}(H)$ for the previous discrete value of the applied magnetic field H, the system of equations corresponding to Eqs. (3.82) is solved iteratively with the constraint of Eq. (3.78) by computing an updated approximation of the solution $\vec{\phi}^{(m+1)}$ from the previous approximation $\vec{\phi}^{(m)}$. A number of methods to solve non-linear systems of equations could be used. In our implementation, we used a fixed-point method where each component $\phi_i^{(m+1)}$ of the solution vector $\vec{\phi}^{(m+1)}$ is computed sequentially and the most recent approximation of each component is used in the computation, therefore making the algorithm used a non-linear fixed-point variant of the Gauss-Seidel method for linear systems.

Based on Eq. (3.82), the fixed-point method that we used in our implementation was,

$$K_i \sin(2[\phi_i^{(m+1)} - \theta_i]) + HM_s \sin\phi_i^{(m+1)} + j\int_0^{2\pi}\int_0^{\infty} f(\theta',K') \sin\left[\phi_i^{(m+1)} - \sum_{j=1}^{N} \phi_j^{(m)} \psi_j(\theta',K')\right] dK'd\theta' = 0\,. \quad (3.83)$$

where the functional dependence of the $\vec{\phi}$ components on H was omitted from the notation for clarity. Using the trigonometric identity $\sin(A-B) = \sin A\cos B - \cos A\sin B$, Eq. (3.83) can be written as

$$K_i \sin(2[\phi_i^{(m+1)} - \theta_i]) + HM_s \sin\phi_i^{(m+1)} - j\left[S\cos\phi_i^{(m+1)} - C\sin\phi_i^{(m+1)}\right] \quad (3.84)$$

where

$$C = \int_0^{2\pi}\int_0^{\infty} f(\theta',K') \cos\sum_{j=1}^{N} \phi_j^{(m)} \psi_j(\theta',K') dK'd\theta' \quad (3.85)$$

and

$$S = \int_0^{2\pi}\int_0^{\infty} f(\theta',K') \sin\sum_{j=1}^{N} \phi_j^{(m)} \psi_j(\theta',K') dK'd\theta' \quad (3.86)$$

which is a non-linear scalar equation for $\phi_i^{(m+1)}$, not unlike Eq. (3.6) for the original Stoner-Wohlfarth model, that can be solved using a root finding algorithm.

To validate the proposed approach, the hysteresis loop for a system of exchange coupled particles with exchange energy density $j = 3\times10^5\,\mathrm{erg/cm^3}$, saturation magnetization $M_s = 1400\,\mathrm{emu/cm^3}$ and random anisotropy vectors $\vec{K}$ with both the magnitude and the direction being random with a distribution corresponding to the sum of the anisotropy of 12 particles[2] with uniformly oriented anisotropy directions in the $x-y$ plane and fixed anisotropy magnitude $K_0 = 1\times10^6\,\mathrm{erg/cm^3}$. In this case, the resulting anisotropy direction is uniformly distributed in the $x-y$ plane while the probability density function for K is given by Eq. (3.64). The re-

[2]This number of 12 is chosen arbitrarily and simply serves to define the joint probability density function $f(\theta,K)$.

sult obtained using the generalized Stoner-Wohlfarth model with exchange coupling is shown in Fig. 3.17 and compared with the result obtained using the Stoner-Wohlfarth hysteresis model without exchange coupling and two hysteresis loops obtained from the micromagnetic simulation of an ensemble of 10,000 particles, with and without exchange coupling respectively. Exchange coupling is seen to have an appreciable effect on the hysteresis loop and the micromagnetic simulation results are seen to be in good agreement with the results obtained with both the generalized and original Stoner-Wohlfarth hysteresis models.

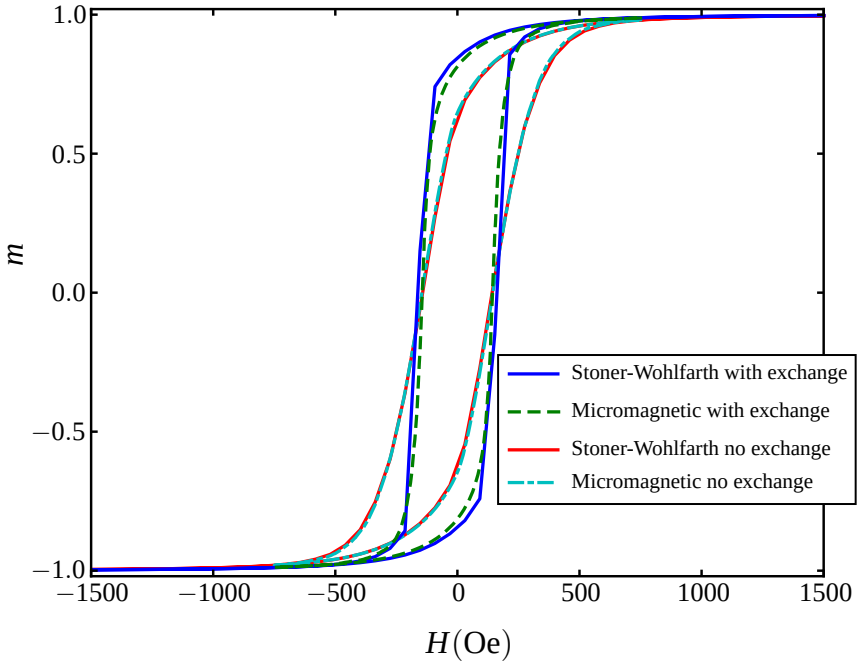

Figure 3.17: Comparison of hysteresis loops for an ensemble of particles with randomly oriented anisotropy following a uniform distribution on the unit sphere computed by a micromagnetic simulation with 1000 particles and the probabilistic Stoner-Wohlfarth hysteresis model.

It should be noted that the iterative method used to solve the non-linear equation in the generalized Stoner-Wohlfarth method performs best when the exchange energy density j is not dominant compared to the other terms in Eq. (3.76). In cases where exchange coupling is dominant, the system of equations becomes ill-conditioned. Because of this, the definition of effective particles through anisotropy averaging is a tool that can be usefully combined with the above generalized Stoner-Wohlfarth method with exchange coupling since it lowers the effec-

tive exchange coupling energy between effective particles. Also, it should be noted that when comparing the result obtained from the generalized Stoner-Wohlfarth model with the result of micromagnetic simulations, j in Eq. (3.76) being the exchange energy density associated with a given particle, it should correspond to the energy density between 2 exchange coupled particles in the micromagnetic simulation multiplied by the number of nearest-neighbors with which a particle is coupled. In the simulation used to produce the results of Fig. 3.17, while an exchange energy density of $j = 3 \times 10^5 \,\mathrm{erg/cm^3}$ was used for the Stoner-Wohlfarth model, since in the micromagnetic simulation a simple cubic array of particles was considered where each particle is exchange coupled to its 6 nearest neighbor, the exchange energy between two particles is set to $j/6 = 5 \times 10^4 \,\mathrm{erg/cm^3}$.

Chapter 3, in part, is currently being prepared for submission for publication, Couture, Simon; Lomakin, Vitaliy. The dissertation author was the primary investigator and author of this material.

Chapter 4

Coupling micromagnetism and electrodynamics: modeling eddy currents in micromagnetic simulations

The LLG equation states that the time derivative of the angular momentum associated with a spinning electron is equal to the torque due to the interaction between the electron's magnetic moment and a magnetic field. As discussed in chapter 2, while the LLG equation is derived from electromagnetism and considers the magnetic field as obtained from the solution of the Maxwell equations, it is possible through a linearization procedure to introduce effective magnetic fields to account for other interactions which are not governed by electromagnetism. Chapter 3 focused on two of these effects, namely the exchange interaction and crystalline anisotropy. The present chapter is concerned with the true or maxwellian magnetic field, in the sense that it satisfies the Maxwell equations, and how it is coupled with the LLG equation of micromagnetism.

Historically, only the static Maxwell equations were considered, leading to the magnetostatic field, also known as the demagnetizing field or dipolar interaction. On p.17 of his 1963

book *Micromagnetics*, Brown writes, "The magnetostatic energy was taken into account in some of these early calculations in micromagnetics. In domain theory, meanwhile, it had been almost completely ignored." In a 2000 review on the current state of the art in micromagnetism [38], the magnetostatic field is considered as one of the effective fields along with the exchange and anisotropy fields, without justifying the magnetostatic approximation. This situation is probably due to a number of factors, one of which being the fact that originally, the works that led to micromagnetism were concerned with the equilibrium state of magnetization, with studies on magnetization dynamics coming somewhat later. Another factor to explain the prevalence of the magnetostatic approximation is the small size of the magnetic regions that were considered which justifies neglecting any electrodynamic effect. Lastly, the problem of computing the magnetostatic field for a given magnetization configuration is in itself far from trivial and computationally costly, and therefore provided a sufficient challenge for researchers, numerical algorithms and computers.

As the size of problems that can be handled computationally has grown and as the frequency of operation of magnetic devices has increased and consequently researchers have become more interested in modeling the high frequency behavior of magnetic devices, some researchers pursued the idea of going beyond the magnetostatic approximation and including electrodynamic effects in micromagnetic simulations. Given that ferromagnetic materials are good conductors, one such effect is eddy currents, which are induced by time varying magnetic fields and magnetization, and themselves induce a magnetic field which will interact with the magnetization through the LLG equation. Eddy currents are known to have potentially significant effects in magnetic materials, introducing losses to the system and altering the magnetization dynamics.

In section 4.1, the phenomenon of eddy currents and how they arise from the Maxwell equations is discussed. The different approximations to the Maxwell equations and how they couple to the LLG equation are also presented. Section 4.2 offers a review of the works that have been done on modeling eddy currents effects in micromagnetic simulations. In section 4.3, the

limits of validity of the quasistatic approximation of the Maxwell equations, which is sufficient to account for eddy currents, are examined. The limits of validity of the static approximation, in which case eddy current effects can safely be neglected, are also given. Section 4.4 discusses the mechanism for coupling the LLG and Maxwell equations so that eddy currents, including the diffusion effect, are accounted for. In section 4.5, the formulation for an integral equation solver for the Maxwell equations is presented. A test problem which is used to validate the proposed solver is described in section 4.6. Section 4.7 introduces an alternative Maxwell equations solver based on the finite elements method. Lastly, section 4.8 presents simulation results that illustrate the effects of eddy currents in micromagnetic simulations.

4.1 Eddy currents and the Maxwell equations

Eddy currents, also known as Foucault currents, occur in conductors subjected to a time-varying magnetic flux density $\vec{B}$. The effect can be understood in terms of Faraday's law,

$$\nabla \times \vec{E} = -\frac{\partial \vec{B}}{\partial t} \tag{4.1}$$

where the time-varying magnetic flux density $\vec{B}$ induces an electric field $\vec{E}$ whose rotation is equal to $\partial\vec{B}/\partial t$. In a material with conductivity σ, this electric field will give rise to a current field due to Ohm's law,

$$\vec{J} = \sigma\vec{E} \tag{4.2}$$

with the current lines rotating around $\partial\vec{B}/\partial t$, hence their name eddy currents. The eddy currents phenomenon is illustrated in Fig. 4.1.

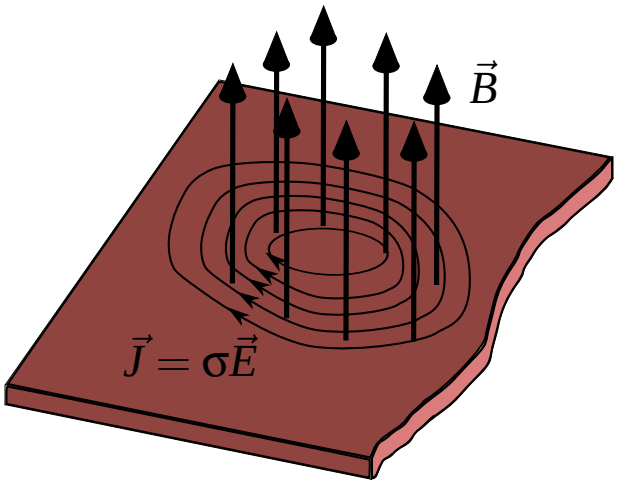

Figure 4.1: A time-varying magnetic flux density $\vec{B}$ in a conductive material with conductivity σ induces a rotating electric field $\vec{E}$ and a corresponding current density $\vec{J}$, known as eddy currents

Faraday's law is one of the Maxwell equations, which read

$$\nabla \times \vec{E} = -\frac{\partial \vec{B}}{\partial t} \tag{4.3a}$$

$$\nabla \times \vec{H} = \frac{\partial \vec{D}}{\partial t} + \vec{J} \tag{4.3b}$$

$$\nabla \cdot \vec{D} = \rho \tag{4.3c}$$

$$\nabla \cdot \vec{B} = 0\ . \tag{4.3d}$$

In these equations, the magnetic field is defined as

$$\vec{H} = \frac{1}{\mu_0}\vec{B} - \vec{M} \tag{4.4}$$

with μ_0 the free space permeability while the electric flux density is defined as

$$\vec{D} = \varepsilon_0\vec{E} + \vec{P} \tag{4.5}$$

with ε_0 the free space permittivity and where the material's electric polarization $\vec{P}$ has been in-

troduced [6]. The electric polarization is a macroscopic field quantity which is defined as the spatially averaged molecular dipole moment inside a material and measures the spatial distribution of bound charges inside molecules or atoms of a material. When an electric field is applied, positive and negative charges will tend to separate from each other, and for many materials, the electric polarization can be expressed as a linear function of the electric field,

$$\vec{P} = \varepsilon_0 \chi_e \vec{E} \tag{4.6}$$

where χ_e is the electric susceptibility [1]. Inserting this into Eq. (4.5) gives

$$\vec{D} = \varepsilon_0 (1 + \chi_e) \vec{E} = \varepsilon \vec{E} \tag{4.7}$$

where the material's permittivity is defined as $\varepsilon = \varepsilon_0 (1 + \chi_e)$. This linear relationship between $\vec{D}$ and $\vec{E}$ greatly eases the solution of the Maxwell equations.

When treating magnetic materials in electromagnetic problems, establishing a linear relationship between $\vec{H}$ and $\vec{M}$ is highly desireable. When it is possible, the magnetic susceptibility χ_m is defined, as was done in chapter 3, such that

$$\vec{M} = \chi_m \vec{H} \ . \tag{4.8}$$

Inserting this into Eq. (4.4) gives

$$\vec{B} = \mu_0 (1 + \chi_m) \vec{H} = \mu \vec{H} \tag{4.9}$$

where the material's permeability is defined as $\mu = \mu_0 (1 + \chi_M)$. In many problems involving magnetic materials however, this is not possible due to effects such as magnetic hysteresis and

[1] Note that the electric susceptibility is usually defined in the frequency domain, so that in the time domain the product of χ_e and $\vec{E}$ would be replaced by their convolution. Also, in general both χ_e and χ_m are tensors.

in general to the non-linear nature of the equations governing magnetization dynamics. Indeed, what is needed to solve the Maxwell equations is a constitutive relation between $\vec{M}$ and $\vec{H}$, i.e. a function f such that $\vec{M} = f(\vec{H})$. Clearly, such a constitutive relation consists in the solution of the LLG equation with the associated mechanics of micromagnetism. This leads to the important idea that, whereas from the point of view of micromagnetism, the Maxwell equations are solved to determine the magnetic field induced by a given magnetization distribution, from the point of view of an electromagnetic problem, the LLG equation needs to be solved to determine the magnetization for a given magnetic field. The LLG and Maxwell equations should therefore be regarded as a coupled set of equations where neither the LLG equation nor the Maxwell equations is subordinate to the other but instead should be considered on an equal footing.

To see how the Maxwell equations and the LLG equation are coupled, Eq. (4.4) is used to write the Maxwell equations in the form

$$\nabla \times \vec{E} = -\mu_0 \frac{\partial}{\partial t}\left(\vec{H} + \vec{M}\right) \tag{4.10a}$$

$$\nabla \times \vec{H} = \frac{\partial \vec{D}}{\partial t} + \vec{J} \tag{4.10b}$$

$$\nabla \cdot \vec{D} = \rho \tag{4.10c}$$

$$\nabla \cdot \left(\vec{H} + \vec{M}\right) = 0\ . \tag{4.10d}$$

When the static approximation is made, the time derivative terms in Eqs. (4.10a) and (4.10b) are neglected and the Maxwell equations become

$$\nabla \times \vec{E} = 0 \tag{4.11a}$$

$$\nabla \times \vec{H} = \vec{J} \tag{4.11b}$$

$$\nabla \cdot \vec{D} = \rho \tag{4.11c}$$

$$\nabla \cdot \left(\vec{H} + \vec{M}\right) = 0\ . \tag{4.11d}$$

where the equations in terms of $\vec{E}$ and $\vec{H}$ are seen to be completely decoupled. In the context of micromagnetics, the electrostatic equations, Eqs. (4.11a) and (4.11c), can be ignored and only the magnetostatic equations, Eqs. (4.11b) and (4.11d), are solved. In Eqs (4.11), the current density $\vec{J}$ should be regarded as an impressed current, given as a data of the problem. To differentiate the field arising from this impressed current and the field induced by the magnetization, $\vec{H}$ is decomposed into

$$\vec{H} = \vec{H}_i + \vec{H}_{\text{ms}} \tag{4.12}$$

where the impressed field $\vec{H}_i$ is solution of

$$\nabla \times \vec{H}_i = \vec{J} \tag{4.13a}$$

$$\nabla \cdot \vec{H}_i = 0 \tag{4.13b}$$

and where the magnetostatic field is solution of

$$\nabla \times \vec{H}_{\text{ms}} = 0 \tag{4.14a}$$

$$\nabla \cdot \left(\vec{H}_{\text{ms}} + \vec{M} \right) = 0 \, . \tag{4.14b}$$

Summing Eqs. (4.13) and (4.14), it is easily seen that $\vec{H}$ of Eq. (4.12) satisfies Eqs. (4.11b) and (4.11d). The equations for $\vec{H}_i$, Eqs. (4.13), are completely independent of the magnetization $\vec{M}$ and can be solved for a given source current distribution $\vec{J}$. The equations for $\vec{H}_{\text{ms}}$, Eqs. (4.14) correspond to the equations of section 2.3 on the magnetostatic field and can be solved for a given magnetization distribution $\vec{M}$. From the point of view of electromagnetism, the problem of Eqs. (4.14) is relatively straightforward: given the magnetization $\vec{M}$ everywhere in space, compute the field $\vec{H}_{\text{ms}}$ also everywhere in space. Since Eqs. (4.14) do not depend on time other than through $\vec{M}$, the magnetostatic field effectively propagates instantaneously and all the system dynamics lie with the LLG equation. It is not surprising then that when the static Maxwell

equations are used in micromagnetism, the magnetostatic field is treated as just another effective field with the Maxwell equations being subordinate to the LLG equation.

This picture changes when the dynamic Maxwell equations of Eqs. (4.10) are considered. Through Faraday's law, Eq. (4.10a), a time-varying magnetization will induce an electric field and corresponding eddy currents, which will in turn induce a magnetic field through Ampere's law, Eq. (4.10b). Unlike in the static case, here the electric field is coupled with the magnetic field and needs to be considered. The displacement current term $\partial\vec{D}/\partial t$ in Eq. (4.10b), which was famously postulated by Maxwell, also gives rise to wave propagation of the electric and magnetic fields. While it is certainly possible to consider the solution of the full Maxwell equations in the context of micromagnetic simulations, even today the size of the magnetic devices that are modeled are deeply subwavelength. For instance, for dynamics with a frequency of 10 GHz, which is quite typical of magnetic materials, the freespace wavelength is 3 cm whereas micromagnetic problems rarely exceed tens of microns in size. For this reason and because of other arguments that will be presented in section 4.3, there is no need to solve the full Maxwell equations. Instead, the magnetoquasistatic Maxwell equations, where the displacement current term is neglected, is a good compromise which accounts for the eddy currents effect.

The magnetoquasistatic Maxwell equations read as follows,

$$\nabla \times \vec{E} = -\mu_0 \frac{\partial}{\partial t}\left(\vec{H} + \vec{M}\right) \tag{4.15a}$$

$$\nabla \times \vec{H} = \vec{J} \tag{4.15b}$$

$$\nabla \cdot \vec{D} = \rho \tag{4.15c}$$

$$\nabla \cdot \left(\vec{H} + \vec{M}\right) = 0\ . \tag{4.15d}$$

In addition to the electromagnetic wave propagation effect that is lost, it is interesting to note that neglecting the displacement current also breaks the conservation of charges law that is contained in the full Maxwell equations. Indeed, taking the divergence of Eq. (4.10b) and making use of

Eq. (4.10c), one obtains

$$\nabla \cdot \vec{J} = -\frac{\partial \rho}{\partial t} \tag{4.16}$$

which is the conservation law for the free charge density ρ in its differential form. With the magnetoquasistatic approximation, taking the divergence of Eq. (4.15b) yields

$$\nabla \cdot \vec{J} = 0 \tag{4.17}$$

or, using Ohm's law,

$$\nabla \cdot (\sigma \vec{E}) = 0 \, . \tag{4.18}$$

In regions where the conductivity σ is non-zero and uniform, this gives $\nabla \cdot \vec{E} = 0$. In ferromagnets, electric polarizability is weak so that $\vec{D} = \varepsilon_0 \vec{E}$ can be assumed. Then from Eq. (4.15c), it follows that in regions of uniform conductivity, $\rho = 0$. In regions where the conductivity is zero, no such conclusion can be made and there can exist distributions of charges that are specified for a problem and which will produce a corresponding electrostatic field that is added to the field induced from Faraday's law, Eq. (4.15a). In the literature on eddy currents, one often sees Eq. (4.15c) written as $\nabla \cdot \vec{D} = 0$ for conductive regions. However, as pointed out by Brown [39], the volumetric charge density ρ in Eq. (4.15c) should be replaced by a surface charge density at surfaces where a discontinuity in the conductivity occurs, for example at the boundary of a conductive region or at the boundary between two conducting regions with different conductivities. To see this, consider Eq. (4.15b) and lets assume that the current density $\vec{J}$ has no singularity such as a surface Dirac distribution [2] . The curl operator would cause any discontinuity in the component of $\vec{H}$ tangential to the surface across which the discontinuity occurs to generate such a singularity. This can be understood in terms of distribution theory, where the generalized curl operator on some function $\vec{u}$ is defined based on the inner product of the curl of $\vec{u}$ with a test

[2] Such a singularity would represent a surface current density which arises in perfectly conducting materials or infinitely thin conductors, both of which are not considered here.

function $\vec{\phi}$. Indeed, referring to Fig. 4.2, it can be shown that

$$< \nabla \times \vec{u}, \vec{\phi} >= \int_{\Omega_1} \nabla \times \vec{u} \cdot \vec{\phi} dV + \int_{\Omega_2} \nabla \times \vec{u} \cdot \vec{\phi} dV + \int_C [\hat{n} \times (\vec{u}_2 - \vec{u}_1)] \cdot \vec{\phi} dS \tag{4.19}$$

where $\vec{u}_2 - \vec{u}_1$ represents the jump in $\vec{u}$ at the surface C [40]. Since $\vec{J}$ has no surface singularity, it follows that $\hat{n} \times \vec{H}$ is continuous across any surface with $\hat{n}$ being a unit vector normal to this surface. From this, it follows that the normal component of $\nabla \times \vec{H}$ is also continuous across any surface. From Eq. (4.15b), this means that the normal component of $\vec{J}$, which can be expressed as

$$\hat{n} \cdot \vec{J} = \hat{n} \cdot (\sigma \vec{E}) \ , \tag{4.20}$$

is continuous across any surface. This includes surfaces where a jump discontinuity of the conductivity σ occurs. From Eq. (4.20), it is seen that a discontinuity in σ must therefore be accompanied by a jump discontinuity of the normal $\vec{E}$ component, $\hat{n} \cdot \vec{E}$.

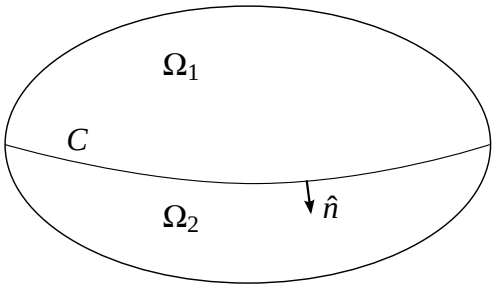

Figure 4.2: Two-dimensional representation of a three-dimensional domain Ω divided into two domains, Ω_1 and Ω_2 which are separated by a surface C.

As was done for the curl operator, a generalized divergence operator can be defined by

$$< \nabla \cdot \vec{u}, \vec{\phi} >= \int_{\Omega_1} \nabla \cdot \vec{u} \phi dV + \int_{\Omega_2} \nabla \cdot \vec{u} \phi dV + \int_C \hat{n} \cdot (\vec{u}_2 - \vec{u}_1) \phi dS \tag{4.21}$$

from which it is seen that a jump discontinuity across any surface of the component of a vector field $\vec{u}$ normal to that surface introduces a surface Dirac distribution. Applying this to the electric

field at a surface with a jump discontinuity of the conductivity, from Eq. (4.15c) with $\vec{D} = \varepsilon_0 \vec{E}$, it is seen that the charge density ρ must include a surface charge density ρ_s corresponding to the jump in $\vec{E}$.

A case which is of particular interest is at the boundary of a conductor region, outside of which the conductivity σ is zero. For the normal component of $\vec{J}$ in Eq. (4.20) to be continuous, the normal component of $\vec{E}$ inside the conductor at the boundary must be zero, that is,

$$\hat{n} \cdot \vec{E} = 0 \; . \tag{4.22}$$

Meanwhile, outside the conductor, the $\vec{E}$ field can be obtained by solving Eqs. (4.15a) and (4.15c) and will depend on $\vec{H}$ and $\vec{M}$. However, because the electric field there will not generate any current, it will have no effect on the solution for $\vec{H}$, which would not be the case if the displacement current term was not neglected. The $\vec{E}$ field in non-conductive regions is therefore not needed when solving the magnetoquasistatic Maxwell equations and can be regarded as a by-product of the solution process, along with the corresponding surface charge density.

From the discussion so far, it is seen that the magnetoquasistatic Maxwell equations allow the modeling of eddy currents at the cost of neglecting electromagnetic wave propagation effects as well as capacitive effects resulting from electric charge dynamics. While the electromagnetic wave propagation effect is lost, propagation of the fields by diffusion is still dictated by the magnetoquasistatic Maxwell equations. Indeed, considering a conductive region which for simplicity is assumed to have a uniform conductivity, taking the curl of Eq. (4.15b) with $\vec{J} = \sigma \vec{E}$ gives

$$\nabla \times \nabla \times \vec{H} = \sigma \nabla \times \vec{E} \tag{4.23}$$

Using Eq. (4.15a) to replace for $\nabla \times \vec{E}$ and using the identity $\nabla \times \nabla \times \vec{H} = \nabla(\nabla \cdot \vec{H}) - \nabla^2 \vec{H}$ along

with $\nabla \cdot \vec{H} = -\nabla \cdot \vec{M}$ from Eq. (4.15d), Eq. (4.23) becomes

$$\frac{\partial \vec{H}}{\partial t} = \frac{1}{\sigma \mu_0} \nabla^2 \vec{H} - \frac{\partial \vec{M}}{\partial t} + \frac{1}{\sigma \mu_0} \nabla \nabla \cdot \vec{M} \tag{4.24}$$

which is a diffusion equation for the magnetic field $\vec{H}$. A diffusion equation can also be obtained for $\vec{J}$ from the magnetoquasistatic Maxwell equations. Indeed, taking the curl of Eq. (4.15a) and using Eq. (4.15b) to replace for $\nabla \times \vec{H}$ gives

$$\frac{\partial \vec{J}}{\partial t} = \frac{1}{\sigma \mu_0} \nabla^2 \vec{J} - \frac{\partial}{\partial t} \nabla \times \vec{M} \ . \tag{4.25}$$

In both Eqs. (4.24) and (4.25), the diffusion constant is $(\sigma \mu_0)^{-1}$ and both are a vector version of the scalar diffusion equation, which in its simplest one-dimensional form reads

$$\frac{\partial u(x,t)}{\partial t} = k \frac{\partial^2 u}{\partial x^2} \tag{4.26}$$

where k is the diffusion constant. The solution of Eq. (4.26) has the functional form [20]

$$u(x,t) \sim e^{-x^2/4kt} \ . \tag{4.27}$$

A comparison between this and Eqs. (4.24) and (4.25) motivates the definition of the magnetic time constant

$$\tau_m = \sigma \mu L^2 \tag{4.28}$$

where L is a characteristic length over which diffusion occurs (for example, the size of a conductor region). The magnetic time constant corresponds to the characteristic time over which diffusion dynamics occur. The same comparison between the scalar diffusion equation and Eqs. (4.24)

and (4.25) can be used to characterize the diffusion length scale. The skin depth is defined as

$$\delta = \sqrt{\frac{1}{\pi f \mu \sigma}} \tag{4.29}$$

where f is the system's characteristic frequency. These constants will be used in section 4.3 when discussing the limits of validity of the magnetoquasistatic approximation and also when analyzing simulation results involving eddy currents.

4.2 State of the art of eddy currents modeling in micromagnetic simulations

To this author's knowledge, the first work describing the inclusion of eddy currents effects in micromagnetic simulations is that of Della Torre and Eicke in 1997 who proposed a 2D finite difference solver [41]. In their approach, the diffusion effect is neglected since the term $\partial\vec{H}/\partial t$ in the right-hand side of Eq. (4.15a) is discarded and only the $\partial\vec{M}/\partial t$ term is considered. Their approach consists in iteratively solving the LLG equation, and at each iteration computing $\partial\vec{M}/\partial t$ through finite differences, which is then used to compute the $\vec{E}$ field and the eddy currents. The $\vec{H}$ field induced by eddy currents is then computed and fed back into the LLG equation.

Also in 1997, Sandler and Bertram introduced a similar method to include eddy currents in a 1D micromagnetic model of a hard disk recording head [42]. They also neglected the diffusion effect. In 2004, Torres et al. proposed a scheme similar to that of Della Torre and Eicke to include eddy currents in a 3D finite difference micromagnetic solver [43]. They too neglected diffusion effect. They presented simulation results which showed that eddy currents accelerate the switching of the magnetization in a ferromagnetic cube from a up state to a down state.

In 2005, Hrkac et al. proposed a hybrid finite element method / boundary elements

method for a 3D eddy currents micromagnetic solver which did include diffusion effects, even though it neglected the time derivatives of externally applied fields and of the magnetostatic field[3] [44, 45]. Including the $\partial\vec{H}/\partial t$ term in the right-hand side of Eq. (4.15a) to account for diffusion makes the problem of solving the Maxwell equations for the $\vec{H}$ field more difficult. The earlier works described above circumvented this by neglecting this term, which allowed the Maxwell equations to be solved given the magnetization $\vec{M}$ and its time-derivative $\partial\vec{M}/\partial t$ as a set of partial differential equations involving only the spatial derivatives of $\vec{H}$. When the time derivative of $\vec{H}$ is included in the Maxwell equations, these become a set of partial differential equation in terms of both space and time for $\vec{H}$. Then the strategy employed by the works cited above of time integrating the LLG equation and iteratively solving the Maxwell equations based only on the latest solution for the magnetization and its time derivative does not work. To address this problem, Hrkac et al. considered a system of equations composed of the LLG and Maxwell equations and integrated it in time as a whole, using the IDA solver [25] which solves differential-algebraic systems of equations which are systems with the form $F(t,u,\dot{u}) = 0$, with $\dot{u}$ denoting the time derivative of the unknown $u(t)$.

In 2007, Takano et al. presented micromagnetic simulation results which included eddy currents effects for a hard-disk recording head [46]. Their solver was based on a edge elements finite elements formulation and included the diffusion effect, however in their paper the details on the formulation and how time integration is performed are scarce. Lastly, in 2012 Chang et al. proposed a formulation similar to that of Torres et al. but based on a finite element formulation. Their solver was based on the FastMag micromagnetic solver and neglected the diffusion effect.

[3] As will be seen later in this chapter, discarding the time derivative of the magnetostatic field from the eddy currents formulation is actually justified and does not constitute an approximation.

4.3 Bounds for the validity of the static and quasistatic Maxwell equations

Before discussing the strategy used to solve the coupled LLG and Maxwell equations and presenting the solver's formulation, the present section aims to give bounds for the validity of the static and quasistatic approximations to the Maxwell equations. The discussion follows the approach used by Haus and Mercher [47] which consists in comparing the fields obtained using the full Maxwell equations with those obtained using the approximate Maxwell equations to evaluate the error associated with the approximation.

The full Maxwell equations, Eqs. (4.3), can be written in the frequency domain in terms of the $\vec{E}$ and $\vec{H}$ fields as

$$\nabla \times \vec{E} = -j\omega\mu\vec{H} \tag{4.30a}$$

$$\nabla \times \vec{H} = j\omega\varepsilon\vec{E} + \vec{J} \tag{4.30b}$$

$$\nabla \cdot \vec{E} = \frac{\rho}{\varepsilon} \tag{4.30c}$$

$$\nabla \cdot \vec{H} = 0. \tag{4.30d}$$

where ω is the angular frequency and where the linear constitutive relations $\vec{D} = \varepsilon\vec{E}$ and $\vec{B} = \mu\vec{H}$ are used. There are two underlying assumptions to these constitutive relations. The first one is the linearity of the electric polarization and magnetization response. In the context of micromagnetics, the magnetization response evidently cannot in general be considered as a linear function of $\vec{H}$ as in Eq. (4.8). However, an approximate magnitude for μ can be obtained by linearizing the behavior of $\vec{M}$ around a given state based on how much the magnetization would vary if an applied field was applied, and since the discussion will rely on order of magnitude arguments, such an approximate value as the definition of μ is perfectly acceptable. The second one is that while in general the permittivity and permeability are tensors, for the order of magnitude

arguments of this section, they will be assumed to be scalars.

Let us begin by deriving the condition for the validity of the magnetoquasistatic approximation. Assuming that the spatial variations of $\vec{E}$ over a characteristic length L are of the same order of magnitude as $\vec{E}$ itself, the curl of $\vec{E}$ will have a magnitude on the order of

$$\nabla \times \vec{E} \sim \frac{E}{L} \tag{4.31}$$

where E denotes the magnitude of $\vec{E}$. The characteristic length L that should be considered for the purpose of setting a bound for the magnetoquasistatic approximation is the largest linear dimension of the problem and will be discussed in more details shortly. With this, in terms of the magnitudes of $\vec{E}$ and $\vec{H}$, Eq. (4.30a) yields

$$E \sim \omega \mu L H \, . \tag{4.32}$$

The magnetoquasistatic Maxwell equations are obtained by neglecting the displacement current term in Eq. (4.30b) which becomes

$$\nabla \times \vec{H} = \vec{J} \, . \tag{4.33}$$

The error $\Delta\vec{H}$ introduced by this approximation therefore satisfies

$$\nabla \times \Delta\vec{H} = j\omega\varepsilon\vec{E} \tag{4.34}$$

or, in terms of magnitudes and characteristic length,

$$\Delta H \sim \omega \varepsilon L E \, . \tag{4.35}$$

Using Eq. (4.32), the magnitude of the relative error on the $\vec{H}$ field is on the order of

$$\frac{\Delta H}{H} \sim \omega^2 \varepsilon \mu L^2 \ . \tag{4.36}$$

In terms of the relative permittivity and permeability, and introducing the characteristic time $\tau = 1/\omega$ for a given frequency component ω, Eq. (4.36) can be written as

$$\frac{\Delta H}{H} \sim \frac{1}{\tau^2} \frac{L^2}{c^2/\varepsilon_r \mu_r} \ . \tag{4.37}$$

Since $c^2/\varepsilon_r \mu_r$ corresponds to the speed of propagation of electromagnetic waves, Eq. (4.37) states that the error introduced by the magnetoquasistatic approximation is small when the time required for an electromagnetic wave to propagate a distance corresponding to the characteristic length L is much smaller than the characteristic time. The validity of the magnetoquasistatic approximation therefore depends on the highest frequency component that characterize the system dynamics, corresponding to the shortest characteristic time τ. Concerning the characteristic length L, Eq. (4.37) and the use of L to characterize the spatial derivatives of the fields imply that it is variations of the fields over large distances that are critical to determine the error associated with the magnetoquasistatic approximation. Intuitively, this can be understood from the fact that the magnetoquasistatic approximation essentially disregards electromagnetic wave propagation. Therefore, variations of the fields over small distances propagate very quickly and the propagation delay can be neglected. On the other hand, it is propagation over large distances that can incur a significant time delay. For this reason, as stated before it is the largest linear dimension of the problem that should be considered as the characteristic length L[4].

The relative error in Eq. (4.36) can also be written in terms of the electromagnetic wave-

[4] An equivalent, but perhaps more rigorous approach would be to consider the Fourier transform in space of the fields, in which case the curl of a vector field $\vec{A}$ is equivalent to $\vec{k} \times \vec{A}$ and involves the spatial frequency $\vec{k}$, to which a characteristic length can be associated by $L \sim 1/k$.

length, given by $\lambda = 1/2\pi\omega\sqrt{\mu\varepsilon}$,

$$\frac{\Delta H}{H} \sim (2\pi)^2 \frac{L^2}{\lambda^2} \ . \tag{4.38}$$

This states that the error introduced by the magnetoquasistatic approximation is small when the characteristic length is much smaller than the electromagnetic wavelength,

$$L \ll \lambda \ . \tag{4.39}$$

It is interesting to note that the same condition of validity holds for the electroquasistatic approximation, where the $\partial\vec{B}/\partial t$ term is neglected, which corresponds to the $-j\omega\mu\vec{H}$ term in Eq. (4.30a). Indeed, assuming that we are in a region removed from any current source $\vec{J}$ (note that eddy currents will not be present in the electroquasistatic approximation), Eq. (4.30b) yields

$$H \sim \omega\varepsilon LE \ . \tag{4.40}$$

From Eq. (4.30a), the error introduced by the electroquasistatic approximation will be on the order of

$$\Delta E \sim \omega\mu LH \tag{4.41}$$

which, when combined with Eq. (4.40) becomes

$$\frac{\Delta E}{E} \sim \omega^2\varepsilon\mu L^2 \tag{4.42}$$

which is identical to the relation of Eq. (4.36) for the magnetic field. One might wonder, if the condition for the electroquasistatic and magnetoquasistatic are in fact the same, which one should be used? The answer to this question is that it depends on the problem that is considered. In both approximations, the wave propagation effect is neglected, but the price paid for that is the loss of an accurate representation of the dynamics of electric charges in the magnetoquasistatic

approximation and the loss of the Faraday and eddy currents effects in the electroquasistatic approximation. If the problem is concerned with magnetic induction, as in eddy currents problems, the magnetoquasistatic approximation must be used. If the problem is instead about dynamic capacitive effects, the electroquasistatic approximation is the correct choice. If both effects are equally important, the full Maxwell equations need to be used and wave propagation considered.

At this point, it is interesting to look at how good the quasistatic approximation is in the context of micromagnetic simulations. Micromagnetic simulations are seldom done on devices exceeding a few tens of microns, so that $L = 50\,\mu\text{m}$ can be considered an upper limit. The frequency content of magnetization dynamics is usually limited to a few tens of GHz so that $\omega = 2\pi \times 50 \times 10^9\,\text{s}^{-1}$ can be considered an upper limit. Then, considering a relative permittivity $\varepsilon_r = 1$ and for instance a relative permeability $\mu_r = 10$, from Eq. (4.36) the relative error on the magnetic field is $\Delta H/H \sim 0.03$. From this rough calculation, it can be concluded that the magnetoquasistatic approximation is an excellent one for the vast majority of micromagnetic simulations carried out today.

Now that the magnetoquasistatic approximation was shown to be a comfortable one for virtually all micromagnetic simulations, the next task is to determine when the magnetostatic approximation is acceptable, that is, when is it acceptable to use the long standing assumption that the static Maxwell equations are sufficient in micromagnetic simulations and when on the other hand can eddy currents effects be expected to have a non-negligible effect. In the magnetoquasistatic approximation inside conductor regions, the current density $\vec{J}$ in Eq. (4.33) includes eddy currents $\vec{J}_{\text{eddy}}$ while they are excluded in the magnetostatic approximation. Because of this, the magnitude of the error on $\vec{H}$ introduced by the magnetostatic approximation is on the order of

$$\Delta H \sim L\, J_{\text{eddy}} \tag{4.43}$$

where the characteristic length L here corresponds to the largest linear dimension of the largest conducting body in the problem. The eddy current density is given by $\vec{J}_{\text{eddy}} = \sigma\vec{E}$ with $\vec{E}$ be-

ing given by Faraday's law, Eq. (4.30a), which leads to the relation for the magnitude of $\vec{E}$ of Eq. (4.32). Combining this with Eq. (4.43) gives the relative error as

$$\frac{\Delta H}{H} \sim \sigma\omega\mu L^2 \ . \tag{4.44}$$

This can be written more simply using the magnetic time constant of Eq. (4.28) and the characteristic time $\tau = 1/\omega$,

$$\frac{\Delta H}{H} \sim \frac{\tau_m}{\tau} \tag{4.45}$$

which states that the error introduced by the magnetostatic approximation is negligible when the diffusion time constant is much smaller than characteristic time of the system dynamics,

$$\tau_m \ll \tau \ . \tag{4.46}$$

In other words, eddy currents can be neglected if diffusion throughout conductors occurs much faster than the characteristic time. The relative error can also be written in terms of the skin depth δ, defined in Eq. (4.29), in which case Eq. (4.44) becomes

$$\frac{\Delta H}{H} \sim 2\frac{L^2}{\delta^2} \ . \tag{4.47}$$

This states that the magnetostatic approximation is sufficient when the skin depth is much larger than the size of conductors,

$$L \ll \delta \ . \tag{4.48}$$

Again, it is interesting to consider some parameters that might be used in a typical micromagnetic simulation to get an idea of the validity of the magnetostatic approximation. Considering the largest conductor size to be a modest $L = 1\,\mu\text{m}$, a conductivity $\sigma = 1 \times 10^7\,\text{S/m}$ which roughly corresponds to the conductivity of iron, a modest relative permeability value $\mu_r = 5$ and

the highest frequency component to be 5 GHz, Eq. (4.44) gives

$$\frac{\Delta H}{H} \sim 2.0 \tag{4.49}$$

which indicates that neglecting eddy current effects by considering the magnetostatic approximation could introduce a significant error in the magnetic field in this case. It is important to note that while satisfying the conditions of Eqs. (4.46) and (4.48) guarantees the validity of the magnetostatic approximation, depending on the specific problem, the use of the magnetostatic approximation in a micromagnetic simulation might still yield accurate results even if they are not satisfied. This might be the case for instance when effective fields other than the magnetic field induced by eddy currents or the magnetostatic field dominate the dynamics, or when the dominant field variations occur over a scale smaller than the largest conductor size L. Determining whether or not the eddy currents can be neglected for a specific problem is a complex question, and the bounds given above should serve as a guide. If they are satisfied, the magnetostatic approximation is definitely valid. If they are not, then one should proceed with care when using the magnetostatic approximation and consider the possibility that eddy currents effects could be non-negligible.

4.4 Coupling the Landau-Lifshitz-Gilbert and magnetoquasistatic Maxwell equations

The modeling of eddy currents effects in micromagnetic simulations requires the solution of the LLG equation coupled to the magnetoquasistatic Maxwell equations. For convenience, the LLG equation is repeated here from Eq. (2.44),

$$\frac{d\vec{M}}{dt} = \frac{\gamma}{1+\alpha^2}\vec{M}\times\vec{H} + \frac{\gamma\alpha}{(1+\alpha^2)|\vec{M}|}\vec{M}\times(\vec{M}\times\vec{H}) \tag{4.50}$$

while from the discussion of section 4.1, the magnetoquasistatic Maxwell equations read

$$\nabla \times \vec{E} = -\mu_0 \frac{\partial}{\partial t}\left(\vec{H} + \vec{M}\right) \tag{4.51a}$$

$$\nabla \times \vec{H} = \vec{J} \tag{4.51b}$$

$$\nabla \cdot \vec{E} = \frac{\rho_s}{\varepsilon_0} \tag{4.51c}$$

$$\nabla \cdot \left(\vec{H} + \vec{M}\right) = 0\ . \tag{4.51d}$$

Referring to section 2.4.2 on the time integration of the LLG equation, the LLG is an equation of the form

$$\frac{\partial \vec{M}}{\partial t} = \vec{f}(\vec{M}, \vec{H}) \tag{4.52}$$

where $\vec{f}$, corresponding to the right-hand side of (4.50), is a non-linear function of the magnetization $\vec{M}$ and of the effective field $\vec{H}$ which is solved by the Newton method, as described in section 2.4.2. When the magnetostatic approximation of the Maxwell equations is used, the maxwellian $\vec{H}$ field, along with the exchange and anisotropy field, is simply a function of $\vec{M}$, that is,

$$\vec{H} = \vec{H}(\vec{M})\ . \tag{4.53}$$

In this case, $\vec{f}$ in Eq. (4.52) is really just a function of $\vec{M}$ and is readily evaluated at $\vec{M} = \vec{M}_{n+1}^{(j)}$ at the j'th Newton iteration for the time step t_{n+1}. When the magnetoquasistatic Maxwell equations are considered, but with the additional approximation of neglecting the term $\partial\vec{H}/\partial t$ in Eq. (4.51a), which corresponds to neglecting the diffusion effect, $\vec{H}$ is a function of both $\vec{M}$ and its time derivative $\partial\vec{M}/\partial t$ so that

$$\vec{H} = \vec{H}(\vec{M}, \frac{\partial \vec{M}}{\partial t})\ . \tag{4.54}$$

This does not pose additional difficulties for the solution of Eq. (4.52) by the Newton method, since the time derivative of $\vec{M}$ in the Maxwell equations can be discretized using for instance

BDF and the nature of Eq. (4.52) is unchanged, it remains an implicit non-linear system of equations for the unknown $\vec{M}_{n+1}$. This is the reason why most works on incorporating eddy currents in micromagnetic simulations have neglected the diffusion term in the Maxwell equations.

When the complete magnetoquasistatic Maxwell equations are considered, including the diffusion term $\partial\vec{H}/\partial t$, they become a set of partial differential equations which include the time derivative of $\vec{H}$, thereby elevating $\vec{H}$ to the same level as $\vec{M}$, i.e. a variable that must be time integrated. This is what motivated Hrkac et al. [44] to solve a problem where the vector of unknowns $\vec{M}$ is appended by the unknowns $\vec{H}$ and where the LLG and Maxwell equations form a single system of equations. While strictly speaking this is the most rigorously correct approach, in practice it might not be the best one. Indeed, another approach, which is the one that will be used in this work, is to slightly relax the coupling that exists between $\vec{M}$ and $\vec{H}$ and allow $\vec{H}$ to lag by one iteration in the iterative solution process. In other words, the LLG equation and the Maxwell equations are kept as two separate sets of equations and are solved each individually by two coupled solvers. The solution process with this approach is illustrated in Fig. 4.3. The LLG equation solver integrates $\vec{M}$ in time, as described in section 2.4.2. When evaluating $\vec{f}(\vec{M},\vec{H})$ as part of the Newton method, say to find the $(j+1)$'th approximation of $\vec{M}$ at time t_n, $\vec{M}_n^{(j+1)}$, control is passed to the Maxwell equations solver which solves for the $\vec{H}_n$ field while assuming that the value of the magnetization at time step t_n corresponds to the latest available approximation $\vec{M}_n^{(j)}$.

In this approach, the computation of the $\vec{H}$ field is very similar to the case where $\vec{H}$ is simply a function of $\vec{M}$. The only difference is that here, the computation of $\vec{H}$ depends on its values at previous time steps. When comparing this approach with that of combining the LLG and the Maxwell equations in a single system, it has the advantage of avoiding any possible issue with the conditioning of a matrix built to solve $\vec{M}$ and $\vec{H}$ simultaneously, these two unknowns potentially having different orders of magnitude. Another advantage is that, assuming that the $\vec{M}$ and $\vec{H}$ fields are computed at the same number of nodes, the single system approach doubles

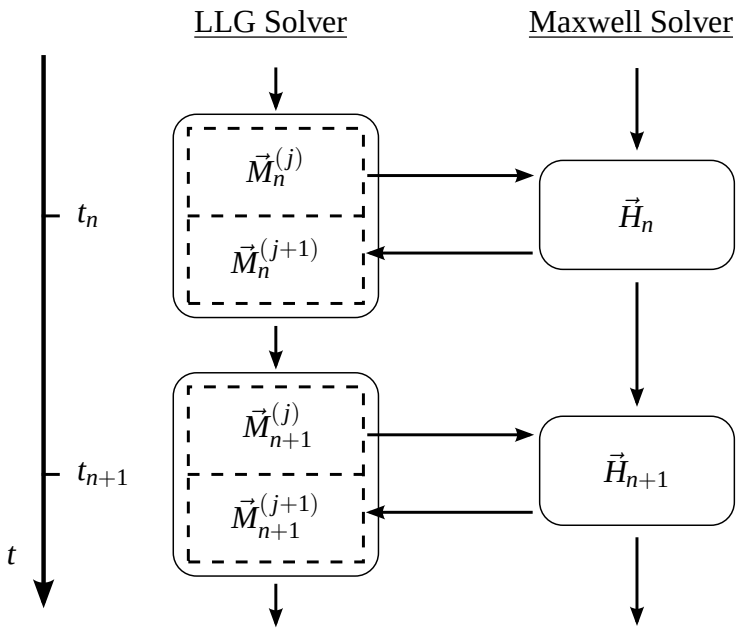

Figure 4.3: Schematic illustration of the proposed approach with two coupled solvers, one for the LLG equation and one for the Maxwell equations. At each time step, the non-linear LLG equation is solved iteratively using the Newton method. At each Newton iteration, say at time t_n, in order to compute the next approximation $\vec{M}_n^{(j+1)}$ using Eqs. (2.99) and (2.101), the magnetic field $\vec{H}_n$ is computed using the previous approximation $\vec{M}_n^{(j)}$.

the size of the problem which will be slower to solve than two smaller systems. This advantage is somewhat negated by the fact that in allowing the $\vec{H}$ field to lag behind $\vec{M}$ by an iteration in the solution process, a price will be paid in terms of speed of convergence. However, the main advantage of the proposed approach lies in the fact that as opposed to the LLG equation, the Maxwell equations are linear, and therefore solving them involves the solution of a linear system of equations. Because of this, the larger system of the single system approach is not only split into two smaller systems of equations, it is split into two systems where only one of them needs to be solved by the Newton method, which involves the solution of a linear system for each Newton iteration, while the other one only requires the solution of a single linear system.

In the proposed approach, the magnetic field is in a sense subordinate to the magnetization since it is the magnetic field that lags one iteration behind the magnetization. Also, it is the LLG equation solver that invokes the Maxwell equations solver at each Newton iteration and

therefore controls the overall solution process. The reason for this is not that the magnetization or the LLG equation is more important, it is simply because by breaking the overall system of equations into two separate systems, one of the fields $\vec{H}$ or $\vec{M}$ has to be solved iteratively, where with each iteration a solution for the second field is obtained based on the value of the first field from the latest iteration, until convergence is achieved. The magnetization $\vec{M}$ is a natural choice for the field to be solved iteratively, since it requires solving a non-linear problem and must be done iteratively anyways. One could in principle choose to instead solve the Maxwell equations iteratively, and solve the non-linear LLG equation at each iteration. This would however be less efficient than the proposed approach since the LLG equation, being non-linear, also would need to be solved iteratively.

4.5 An integral equation solver for the Maxwell equations

The approach used to model eddy currents in micromagnetic simulations uses two separate solvers, one for the LLG equation, the other for the Maxwell equations. While these two solvers communicate with each other as part of the solution process as shown in Fig. 4.3, either the LLG equation or the Maxwell equations solver can be treated as a black box. For instance, the LLG equation solver is oblivious to how the Maxwell equations solver computes its solution, as long as it returns the correct $\vec{H}$ field solution. The same can be said about the LLG equation solver, the Maxwell equations solver is not aware of how the $\vec{M}$ solution that it receives is computed. Because of this, the Maxwell equations solver could solve either the full Maxwell equations, the magnetoquasistatic Maxwell equations as in this case, or even the magnetostatic Maxwell equations without changing the overall approach of Fig. 4.3. Different numerical methods could also be used for each solver. This gives a lot of flexibility in the implementation of the solvers.

In this section and in section 4.7, two different solvers for the magnetoquasistatic Maxwell

equations will be presented, the first one based on an integral equation, the other one based on the finite element method. As will be seen, each of these two methods has its advantages and disadvantages. For instance, the integral equation approach only requires the discretization of magnetic and conductive regions, thereby allowing the modeling of eddy currents without increasing the overall size of the problem. However, the integral equation approach involves the solution of a linear system of equations where the system matrix is in the form of an integro-differential operator which can become expensive to evaluate. In the finite element method, the air region around magnetic and conductive regions need to be discretized, thus increasing the size of the problem, but in this case the system matrix is a sparse matrix that can be pre-assembled.

For the integral equation formulation, it is useful to decompose the electric and magnetic fields into two parts,

$$\vec{E} = \vec{E}_M + \vec{E}_J \tag{4.55}$$

and

$$\vec{H} = \vec{H}_M + \vec{H}_J \ . \tag{4.56}$$

Here, the M subscript denotes the fields arising due to the magnetization $\vec{M}$, which is provided by the LLG solver and is acting as a source. These fields satisfy

$$\nabla \times \vec{E}_M = -\mu_0 \frac{\partial}{\partial t} \left(\vec{H}_M + \vec{M} \right) \tag{4.57a}$$

$$\nabla \times \vec{H}_M = 0 \tag{4.57b}$$

$$\nabla \cdot \vec{E}_M = 0 \tag{4.57c}$$

$$\nabla \cdot \left(\vec{H}_M + \vec{M} \right) = 0 \ . \tag{4.57d}$$

The J subscript denotes the fields due to currents $\vec{J}$, which include eddy currents $\vec{J}_{\text{eddy}}$ and any

source current $\vec{J}_i$ that might be specified in the problem. These fields satisfy

$$\nabla \times \vec{E}_J = -\mu_0 \frac{\partial \vec{H}_J}{\partial t} \tag{4.58a}$$

$$\nabla \times \vec{H}_J = \vec{J} \tag{4.58b}$$

$$\nabla \cdot \vec{E}_J = 0 \tag{4.58c}$$

$$\nabla \cdot \vec{H}_J = 0 \ . \tag{4.58d}$$

Summing Eqs. (4.57) and (4.58), it is easy to see that the total $\vec{E}$ and $\vec{H}$ fields satisfy the magnetoquasistatic Maxwell equations, Eqs. (4.51).

Looking at Eqs. (4.57), Eqs. (4.57b) and (4.57d) are recognized as the magnetostatic equations. The field $\vec{H}_M$ is therefore none other than the magnetostatic field and is computed exactly as one would in a micromagnetic solver where eddy currents effects are neglected. In this work, the solution process for $\vec{H}_M$ is the one described in section 2.3. The difference here however is that while in the magnetostatic approximation, the electric field is disregarded as it is completely decoupled from the equations, the $\vec{E}_M$ field of Eq. (4.57a) will give rise to eddy currents and needs to be computed. From Eq. (4.57c), the divergence of $\vec{E}_M$ is zero and it can therefore be written as the curl of some vector field,

$$\vec{E}_M = -\nabla \times \vec{F} \tag{4.59}$$

where $\vec{F}$ is known as the electric vector potential. From section 2.3 (see Eq. (2.65)), $\vec{H}_M$ can be written as

$$\vec{H}_M = -\nabla \Phi_M \ . \tag{4.60}$$

Using this along with Eq. (4.59), Eq. (4.57a) can be written as

$$\nabla \times \nabla \times \vec{F} = \mu_0 \frac{\partial}{\partial t} \left(-\nabla \Phi_M + \vec{M} \right) \tag{4.61}$$

which, upon using the vector identity $\nabla \times \nabla \times \vec{a} = \nabla(\nabla \cdot \vec{a}) - \nabla^2 \vec{a}$, becomes

$$\nabla \left(\nabla \cdot \vec{F} + \mu_0 \frac{\partial \Phi_M}{\partial t} \right) - \nabla^2 \vec{F} = \mu_0 \frac{\partial \vec{M}}{\partial t} \, . \tag{4.62}$$

From Helmholtz's theorem [48], a vector field is only fully specified by both its curl and its divergence. Since only the curl of $\vec{F}$ is specified, it is not uniquely determined and we are free to determine its divergence. A convenient choice in the present situation is known as the Lorentz gauge and is

$$\nabla \cdot \vec{F} = -\mu_0 \frac{\partial \Phi_M}{\partial t} \, . \tag{4.63}$$

With this, Eq. (4.62) simplifies to

$$\nabla^2 \vec{F} = -\mu_0 \frac{\partial \vec{M}}{\partial t}. \tag{4.64}$$

which is the Poisson equation with source term $-\mu_0 \partial \vec{M}/\partial t$. Its solution is given by

$$\vec{E}_M = \frac{\mu_0}{4\pi} \nabla \times \int_V \frac{\frac{\partial}{\partial t} \vec{M}(\vec{x}')}{|\vec{x} - \vec{x}'|} d\vec{x}' \tag{4.65}$$

where the integration is over all space.

The solution for Eqs. (4.58) proceeds similarly. Because $\nabla \cdot \vec{H}_J = 0$, the magnetic field can be expressed as the curl of the magnetic vector potential $\vec{A}$,

$$\vec{H}_J = \nabla \times \vec{A} \, . \tag{4.66}$$

With this, Eq. (4.58b) becomes

$$\nabla \left(\nabla \cdot \vec{A} \right) - \nabla^2 \vec{A} = \vec{J} \, . \tag{4.67}$$

Here again, the divergence of $\vec{A}$ must be specified by a choice of gauge. The natural choice here

is $\nabla \cdot \vec{A} = 0$, in which case Eq. (4.67) simplifies to

$$\nabla^2 \vec{A} = -\vec{J} \, . \tag{4.68}$$

Again, this is a Poisson equation which has solution

$$\vec{A} = \frac{1}{4\pi} \int_V \frac{\vec{J}(\vec{x}')}{|\vec{x} - \vec{x}'|} d\vec{x}' \, . \tag{4.69}$$

Contrarily to Eq. (4.64) where the source $\vec{M}$ is a known quantity, here the current $\vec{J}$ includes both any impressed source current $\vec{J}_i$ which would be given as part of a problem and the eddy current $\vec{J}_{\text{eddy}}$ which is an unknown of the problem. For this reason, the field $\vec{H}_J$ is split into two components with corresponding magnetic vector potentials, $\vec{H}_{J,i} = \nabla \times \vec{A}_i$ and $\vec{H}_{J,\text{eddy}} = \nabla \times \vec{A}_{\text{eddy}}$, these magnetic vector potentials being given by

$$\vec{A}_i = \frac{1}{4\pi} \int_V \frac{\vec{J}_i(\vec{x}')}{|\vec{x} - \vec{x}'|} d\vec{x}' \tag{4.70}$$

and

$$\vec{A}_{\text{eddy}} = \frac{1}{4\pi} \int_V \frac{\vec{J}_{\text{eddy}}(\vec{x}')}{|\vec{x} - \vec{x}'|} d\vec{x}' \, . \tag{4.71}$$

To solve for the electric field $\vec{E}_J$, Eq. (4.66) is used to replace $\vec{H}_J$ in Eq. (4.58a) yielding

$$\nabla \times \left(\vec{E}_J + \mu_0 \frac{\partial \vec{A}}{\partial t} \right) = 0. \tag{4.72}$$

Since the vector field between parantheses is irrotational, it can be expressed as the gradient of some scalar function. The electric scalar potential Φ_J is therefore introduced such that

$$\vec{E}_J = -\mu_0 \frac{\partial \vec{A}}{\partial t} - \nabla \Phi_J \, . \tag{4.73}$$

Inserting Eq. (4.73) in Eq. (4.58c) and noting that $\nabla \cdot \vec{A} = 0$ because of the gauge choice results in

$$\nabla^2 \Phi_J = 0 \tag{4.74}$$

which states that the electric scalar potential is a solution of the Laplace equation. This equation can be solved using the finite element method provided that a suitable boundary condition is prescribed. Such a boundary condition is obtained from Eq. (4.22) in section 4.1, which states that $\hat{n} \cdot \vec{E} = 0$ at the conductor boundaries. Since $\vec{E} = \vec{E}_M + \vec{E}_J$ and with Eq. (4.73), this gives the following Neumann boundary condition

$$\frac{\partial \Phi_J}{\partial n} = \hat{n} \cdot \left(\vec{E}_M - \mu_0 \frac{\partial \vec{A}}{\partial t} \right) . \tag{4.75}$$

The solution of the Laplace problem with a Neumann boundary condition is not unique and will give rise to a singular or ill-conditioned matrix when solving with the finite element method. This problem can be avoided by imposing the solution value at one or a few nodes at a certain location on the boundary. The choice of this value is of no importance since Φ_J is used to compute $\vec{E}_J$ and from Eq. (4.73) it is clear that only its gradient is of interest. Just as was done for $\vec{H}_J$, it is useful to decompose $\vec{E}_J$ into different components,

$$\vec{E}_J = \vec{E}_{J,i} + \vec{E}_{J,\text{eddy}} + \vec{E}_{J,M} \tag{4.76}$$

defined as

$$\vec{E}_{J,i} = -\mu_0 \frac{\partial \vec{A}_i}{\partial t} - \nabla \Phi_{J,i} \tag{4.77}$$

$$\vec{E}_{J,\text{eddy}} = -\mu_0 \frac{\partial \vec{A}_{\text{eddy}}}{\partial t} - \nabla \Phi_{J,\text{eddy}} \tag{4.78}$$

$$\vec{E}_{J,M} = -\nabla \Phi_{J,\text{M}} \tag{4.79}$$

where $\vec{A}_i$ and $\vec{A}_{\text{eddy}}$ are given by Eqs. (4.70) and (4.71) and where the electric scalar potential has

been decomposed into three components which each satisfy the Laplace equation as well as the following boundary conditions,

$$\frac{\partial \Phi_{J,i}}{\partial n} = -\hat{n} \cdot \mu_0 \frac{\partial \vec{A}_i}{\partial t} \tag{4.80}$$

$$\frac{\partial \Phi_{J,\text{eddy}}}{\partial n} = -\hat{n} \cdot \mu_0 \frac{\partial \vec{A}_{\text{eddy}}}{\partial t} \tag{4.81}$$

$$\frac{\partial \Phi_{J,M}}{\partial n} = \hat{n} \cdot \vec{E}_M \ . \tag{4.82}$$

It is easily seen that $\Phi_J = \Phi_{J,i} + \Phi_{J,\text{eddy}} + \Phi_{J,M}$ satisfies the Laplace equation with the boundary condition Eq. (4.75).

At this point, all the elements are in place to setup an integral equation that will allow to solve for the eddy currents $\vec{J}_{\text{eddy}}$ and the corresponding magnetic field $\vec{H}_{J,\text{eddy}}$. While $\vec{H}_M$ is computed directly by computing an integral involving $\vec{M}$, the equations for the eddy currents are implicit. To see this and to make notation more convenient, the following linear operators are defined. From Eq. (4.65), the $\vec{E}_M$ field is computed by an integro-differential operator $\mathcal{L}_{E_M}$ consisting of the composition of the curl and integral operators applied on the time derivative of $\vec{M}$,

$$\vec{E}_M = \mathcal{L}_{E_M}(\frac{\partial \vec{M}}{\partial t}) = \frac{\mu_0}{4\pi} \nabla \times \int_V \frac{\frac{\partial}{\partial t}\vec{M}(\vec{x}')}{|\vec{x} - \vec{x}'|} d\vec{x}' \ . \tag{4.83}$$

From Eqs. (4.77) and (4.78), both $\vec{E}_{J,i}$ and $\vec{E}_{J,\text{eddy}}$ are obtained by first computing the time derivatve of the corresponding magnetic vector potential $\vec{A}_i$ and $\vec{A}_{\text{eddy}}$ from the integrals of Eqs. (4.70) and (4.71) involving $\vec{J}_i$ and $\vec{J}_{\text{eddy}}$ respectively, to which a correction is added corresponding to the gradient of $\Phi_{J,i}$ and $\Phi_{J,\text{eddy}}$ which are harmonic functions with boundary conditions that are linear functions of the time derivatives of $\vec{A}_i$ and $\vec{A}_{\text{eddy}}$. Both $\vec{E}_{J,i}$ and $\vec{E}_{J,\text{eddy}}$ are therefore given by a linear integro-differential operator $\mathcal{L}_{E_J}$ in terms of the time derivative of $\vec{J}_i$ and $\vec{J}_{\text{eddy}}$ respectively,

$$\vec{E}_{J,i} = \mathcal{L}_{E_J}(\frac{\partial \vec{J}_i}{\partial t}) = -\mu_0 \frac{\partial \vec{A}_i}{\partial t} - \nabla \Phi_{J,i} \tag{4.84}$$

$$\vec{E}_{J,\text{eddy}} = \mathcal{L}_{E_J}(\frac{\partial \vec{J}_{\text{eddy}}}{\partial t}) = -\mu_0 \frac{\partial \vec{A}_{\text{eddy}}}{\partial t} - \nabla \Phi_{J,\text{eddy}} \ . \tag{4.85}$$

Similarly, $\vec{E}_{J,M}$ is obtained as the gradient of $\Phi_{J,M}$, which is a harmonic function with a boundary condition that is a linear function of $\vec{E}_M$, itself being a function of the time derivative of $\vec{M}$ as seen from Eq. (4.83). Therefore, it is given by a linear integro-differential operator applied on the time derivative of $\vec{M}$,

$$\vec{E}_{J,M} = \mathcal{L}_{E_{J,M}}(\frac{\partial \vec{M}}{\partial t}) = -\nabla \Phi_{J,\text{M}} \ . \tag{4.86}$$

The integral equation for the eddy currents $\vec{J}_{\text{eddy}}$ is based on Ohm's law $\vec{J} = \sigma \vec{E}$, which when written in terms of its components becomes

$$\vec{J}_i + \vec{J}_{\text{eddy}} = \sigma \left(\vec{E}_M + \vec{E}_{J,i} + \vec{E}_{J,\text{eddy}} + \vec{E}_{J,M} \right) \ . \tag{4.87}$$

Using the linear operators defined above, this can be written as

$$\vec{J}_i + \vec{J}_{\text{eddy}} = \sigma \left[\mathcal{L}_{E_M}(\frac{\partial \vec{M}}{\partial t}) + \mathcal{L}_{E_J}(\frac{\partial \vec{J}_i}{\partial t}) + \mathcal{L}_{E_J}(\frac{\partial \vec{J}_{\text{eddy}}}{\partial t}) + \mathcal{L}_{E_{J,M}}(\frac{\partial \vec{M}}{\partial t}) \right] \ . \tag{4.88}$$

Using the BDF method to discretize the time derivative of $\vec{J}_{\text{eddy}}$ as in Eq. (2.94), evalutating Eq. (4.88) at time t_{n+1} and grouping $\vec{J}_{\text{eddy},n+1}$ terms on the left-hand side gives a linear system of equations that can be solved for $\vec{J}_{\text{eddy},n+1}$,

$$\begin{aligned} \vec{J}_{\text{eddy},n+1} - \mathcal{L}_{E_J}(\alpha_0 J_{\text{eddy},n+1}) = -\vec{J}_i + \sigma \Bigg[& \mathcal{L}_{E_M}(\frac{\partial \vec{M}}{\partial t}) + \\ & \mathcal{L}_{E_J}(\frac{\partial \vec{J}_i}{\partial t}) + \mathcal{L}_{E_J}(\sum_{i=1}^{r} \alpha_i \vec{J}_{\text{eddy},n+1-i}) + \mathcal{L}_{E_{J,M}}(\frac{\partial \vec{M}}{\partial t}) \Bigg] \end{aligned} \tag{4.89}$$

This linear system can be expressed in the form of a matrix equation

$$A \vec{J}_{\text{eddy},n+1} = \vec{b} \tag{4.90}$$

where the system matrix A corresponds to the operator $I - \alpha_0 \mathcal{L}_{E_J}$, with I being the identity matrix, and where $\vec{b}$ is the right-hand side of Eq. (4.89). Since the system matrix A is in the form of an operator, the matrix (which also happens to be dense) is not computed explicitly and matrix-free iterative solvers need to be used. Since in this case the operator is not symmetric, the GMRES method [49] is used. A preconditioner could be used for the GMRES method by using a sparse version of the A matrix involving only nearest neighbor contributions to the integrals, however the non-preconditioned GMRES method has been found to perform relatively well for this problem and was used in the present work. Once a solution for $\vec{J}_{\text{eddy},n+1}$ has been found, the corresponding field $\vec{H}_{\text{eddy},n+1}$ is computed using Eq. (4.66) with $\vec{A} = \vec{A}_{\text{eddy}}$ given by Eq. (4.71). The solution of the integral equation Eq. (4.89) by the GMRES method involves computing the integrals that are part of the different linear operators. All these integrals are computed using a Fast-Fourier-Transform-accelerated technique implemented on GPU's which is described by Li [22, 23].

In terms of performance, while the integrals are accelerated, the fact that several integrals have to be computed at every time step due to the iterative GMRES method makes the Maxwell equations solver the most computationally intensive part of the micromagnetic solver. For example, using a Intel Xeon E5645 CPU and a NVIDIA GeForce GTX 580 GPU, simulating 1 ns for a problem with a mesh of 3.5 million tetrahedral elements takes 21.2 hours while it only takes 0.22 hours when the eddy currents are neglected. Clearly, the computation of the eddy currents field is the performance bottleneck when eddy currents are modeled in micromagnetic simulations and the significant slowdown that their computation causes limits the size of problems that can be solved in practice. Because of this, it is worthwhile to investigate different methods of solving the magnetoquasistatic Maxwell equations. An alternative solver based on the finite element method will be presented in section 4.7.

4.6 A test problem for the micromagnetic-eddy currents solver

One of the challenges in numerical micromagnetics is to verify that solutions obtained with a given solver are indeed accurate. In general, for the solution of numerical partial differential equations, one way of doing this is to solve a problem for which the analytical solution is known. Since the LLG equation is non-linear and magnetization dynamics are usually fairly complex with domain wall motion, magnetic domain nucleation, magnetization rotation and chaotic magnetization reversal, problems for which analytical solutions exist are usually not available. To address this problem in micromagnetics, the National Institute of Standards and Technology has developed a series of standard problems for which there exist accepted solutions that have been validated through different micromagnetic solvers [50].

The same challenge evidently applies to the validation of micromagnetic solvers that take into account eddy currents. A quick look at the literature on eddy currents modeling in micromagnetic simulations, which was discussed in section 4.2, reveals that lacking a problem where the analytical solution is known, researchers have resorted to comparing simulation results obtained with and without eddy currents effects, looking for qualitative effects of eddy currents such as a faster magnetization switching time or added losses in the system, which would be equivalent to using a higher damping coefficient α in the LLG equation.

In this section, a problem to validate a micromagnetic solver with eddy currents effects is presented. It will be used to validate the approach proposed in section 4.4 both with the integral equation solver for the Maxwell equations of section 4.5 and the finite element solver which will be presented in section 4.7. Lacking an analytical solution for a problem with non-linear magnetization dynamics, which would showcase the full extent of a micromagnetic solver's capabilities, the next best test case is a problem that can be represented by a linear analytical model for which an analytical solution can be found and which can still be solved by the fully non-linear-capable micromagnetic solver. The geometry of the test problem is shown in Fig. 4.4.

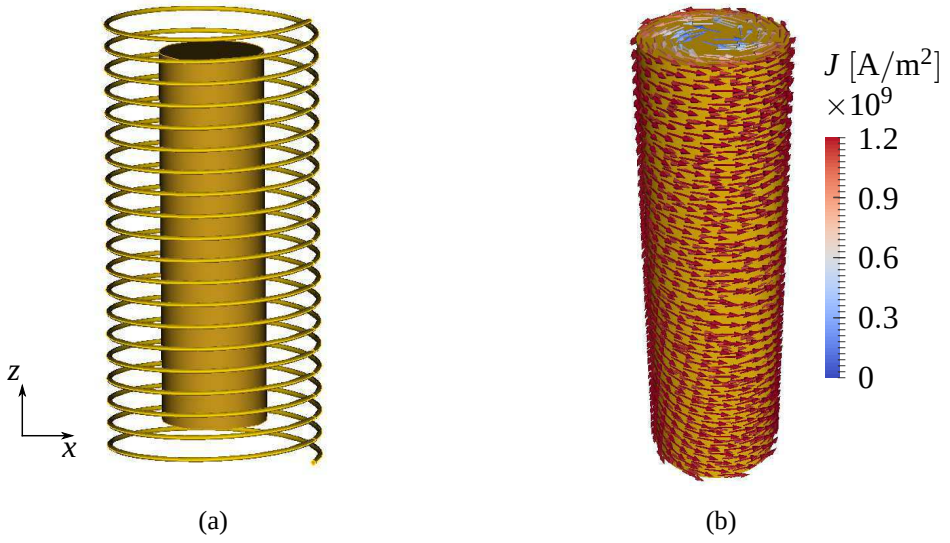

(a) (b)

Figure 4.4: (a) Long ferromagnetic cylinder excited by a current-carrying solenoidal coil. (b) Eddy currents $\vec{J}_{\text{eddy}}$ induced inside the cylinder.

It consists in a long ferromagnetic cylinder of radius a and with conductivity σ which is excited by a metallic coil carrying a time-harmonic current. The coil current will tend to generate an applied field $\vec{H}_i$ which is uniform inside the coil region and oriented in the z direction along the coil axis. Because the cylinder is conductive, this field, along with any accompanying changes in magnetization, will tend to induce eddy currents that flow azimuthally within the cylinder. In accordance with Lenz's law, which states that the currents induced by a time-varying magnetic field will tend to induce a magnetic field opposing this first magnetic field, the eddy currents will generate a field $\vec{H}_{\text{eddy}}$ that tends to oppose the coil field and is also oriented along the cylinder's axis.

If the problem is idealized by assuming that the cylinder is infinitely long and that its magnetization response is linear and described by a real-valued scalar and frequency independent permeability μ, then it has an analytical solution which is derived in Appendix A. In that solution, the total magnetic field consisting of the coil field $\vec{H}_{\text{coil}}$ and the eddy field $\vec{H}_{\text{eddy}}$ only has a z component. The objective then is to devise a micromagnetic problem that will replicate this idealized problem as closely as possible. The first issue is that in the simulation, the cylinder

cannot be made infinitely long[5]. However, by making the cylinder sufficiently long, the solution for the $\vec{H}$ field obtained in a cross-section taken at the middle point of the cylinder along its length should be close to the infinite cylinder case. A key issue is the magnetization response to the magnetic field. In the ideal problem, the magnetization response is given in terms of a real-valued, scalar and frequency independent magnetic susceptibility χ_m by $\vec{M} = \chi_m \vec{H}$ from which the permeability $\mu = \mu_0(1+\chi_m)$ is defined. Since, as discussed in Appendix A, the $\vec{H}$ field only has a z component, this implies that the magnetization also only has a z component. This is evidently impossible to replicate in a micromagnetic simulation of a ferromagnetic material since the magnitude of the magnetization is constant and equal to M_s which means that any variation of the z component of the magnetization must be accompanied by variations of the other components. In other words, the magnetic susceptibility is in reality a tensor. What can be done however is to operate in a linear region around an equilibrium magnetization state and consider the variation of the z component of the $\vec{H}$ field as the quantity to be compared with the analytical solution. While variations in the z component of the magnetization will necessarily be accompanied by variations of the x or y components, from the geometry of the problem these variations are expected to induce $\vec{H}_{\text{eddy}}$ fields with mostly x and y components. This means that the relation between the z component of $\vec{H}$ and $\vec{M}$ can be considered independently from their x and y components. This is equivalent to considering only the $\chi_{m,zz}$ component of the magnetic susceptibility tensor.

The desired linear behavior $M_z = \chi_{m,zz} H_z$ can be obtained by introducing a uniaxial anisotropy along a direction perpendicular to the cylinder axis, for instance along the x direction. When no coil field is applied, the magnetization rests at equilibrium along the x direction. As a coil field is applied, giving rise to a H_z field which includes the coil field and the eddy current field, the magnetization will tend to rotate towards z in such a way that the z component of $\vec{M}$ will be directly proportional to H_z. From the discussion of section 3.1.2 on the frequency

[5]One could of course simulate an infinitely long cylinder with a two-dimensional micromagnetic solver, however the aim here is to validate three-dimensional solvers.

dependent permeability tensor, the above rotation behavior is understood to be a simplification and only rigorously valid at zero frequency since it neglects the fact that $\vec{M}$ will actually precess as it rotates towards the z direction.

Referring to the expression for the frequency dependent $\chi_{m,zz}$ of Eq. (3.22) and the expression for the resonant frequency in Eq. (3.24), it is seen that if the resonant frequency is much higher than $\omega\alpha$, where ω represents the frequency content of the magnetic field $\vec{H}_z$, then χ_{mzz} reduces to the zero frequency susceptibility expression of Eq. (3.21) and is seen to be purely real and frequency independent. Another way to understand this is in terms of precession in the time domain. It can be shown that in the time domain, the precession amplitude is proportional to $e^{-\gamma H_K \alpha\, t/(1+\alpha^2)}$. If the time t here is interpreted as the characteristic time corresponding to the frequency content of H_z such that $t = 1/\omega$, then the above condition that the resonant frequency should be much higher than $\omega\alpha$ is seen to be equivalent to requiring that the precessional motion dies out within the characteristic time so that it can effectively be neglected.

The expressions given in section 3.1.2 for the frequency dependent susceptibility tensor components are valid only for small variations of $\vec{M}$ around the equilibrium state. Therefore, the coil field should be chosen so that it is sufficiently smaller than H_K. In the micromagnetic simulation, another complication arises due to the magnetostatic field, which in the case of a long cylinder gives rise to shape anisotropy. As discussed in Section 2.3.1, shape anisotropy depends on the shape of a magnetic region and is due to the magnetostatic field being such that a certain orientation of the magnetization is favored. Shape anisotropy can be modeled as an equivalent uniaxial anisotropy, which in the case of a long cylinder is along the axis of the cylinder with magnitude $K_{\text{shape}} = \pi M_s^2$. Since the equivalent uniaxial anisotropy is perpendicular to the net anisotropy that is desired along the x axis, from the discussion in chapter 3 on summing uniaxial anisotropies, the resulting anisotropy will have a magnitude corresponding to the difference of the magnitudes of the two anisotropies and will be oriented in the direction of the dominant anisotropy. Therefore, the magnitude of the crystalline anisotropy that is set in the x direction in

the micromagnetic simulation must correspond to the desired net anisotropy magnitude plus the shape anisotropy magnitude.

The magnetic parameters of the ferromagnetic cylinder are chosen to achieve a specific value of μ while satisfying the condition above that $\omega_0 \gg \omega\alpha$ so that the permeability can be considered frequency independent and purely real. Lets consider for example that the time-harmonic coil current has a frequency of 1 GHz and lets set magnetic parameters to obtain a relative permeability $\mu_r = 4$. A set of parameters that can be used (this choice is not unique) is a saturation magnetization $M_s = 360\,\mathrm{emu/cm^3}$, a net anisotropy $K = 2.71 \times 10^5\,\mathrm{erg/cm^3}$ and a damping coefficient $\alpha = 0.1$. With these parameters, from Eq. (3.20), the anisotropy field is $H_K = 1508\,\mathrm{Oe}$ and the magnetic susceptibility is $\chi_{mzz} = 0.239$. The attentive reader will have noticed that this value of χ_m does not result in $\mu_r = 4$ according to Eq. (4.9). This is because the cgs unit system is used here[6], in which case the relative permeability is defined in terms of the magnetic susceptibility as $\mu_r = (1 + 4\pi\chi_m)$. Since $4\pi\chi_{mzz} = 3$, we do obtain $\mu_r = 4$ with the above magnetic parameters. Also, from Eq. (3.24) the resonant frequency is given by 4.2 GHz, which is larger than $\omega\alpha = 0.1\,\mathrm{GHz}$ so that the approximation of a purely real, frequency independent permeability should be valid. This can also be seen from the plot of the magnetic susceptibility χ_{mzz} as a function of frequency, obtained from Eq. (3.22) and shown in Fig. 4.5. From this plot, it is seen that from zero frequency up to 1 GHz, the magnetic susceptibility $4\pi\chi_{mzz}$ is mostly constant and equal to 3, with an imaginary part very close to 0. This validates the idealized model where the ferromagnetic cylinder is simply characterized by $\mu_r = 4$.

To validate the micromagnetic solver with eddy currents, this test problem is solved numerically. The radius of the cylinder is chosen to be 7 µm, its length 50 µm and its conductivity $1 \times 10^7\,\mathrm{S/m}$, roughly corresponding to the conductivity of iron. To ensure a uniform coil field within the ferromagnetic cylinder, the coil is chosen to contain 50 turns uniformly wound around

[6] In this chapter, most of the equations and results are given with the SI unit system in mind. However, numerical solutions are presented in terms of cgs units since the cgs system is still prevalent in the magnetism literature and among researchers and practitioners.

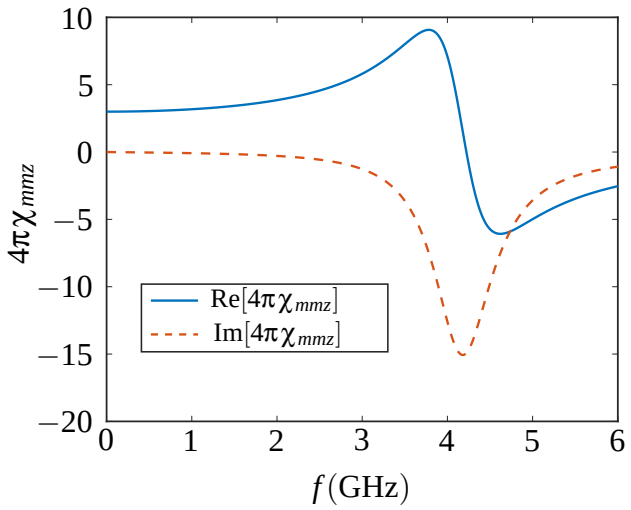

Figure 4.5: Plot of $4\pi\chi_{mmz}$ as a function of frequency obtained from Eq. (3.22) with the magnetic parameters chosen to obtain $\mu_r = 4$.

a length of 100 µm. The radius of the coil is set to 14 µm. The problem is solved for three sets of magnetic parameters which have equivalent relative permeabilities of $\mu_r = 1$, 2 and 4. The case $\mu_r = 1$ corresponds to a non-magnetic cylinder while the 2 sets of parameters for $\mu_r = 2$ and 4 are chosen such that $H_K \approx 1500$ Oe. The coil current is a 1 GHz causal sinusoidal with a peak amplitude of 10 mA which corresponds to a peak coil magnetic field of 62 Oe. This field amplitude is much smaller than H_K which means that the system is operated in a small linear region around the equilibrium point. The exchange coefficient is assumed to be zero in the simulations since the exchange interaction is not part of the idealized linear model.

The results are shown in Fig. 4.6 in the form of plots of the total H_z field, comprising the coil field and the eddy current field, as a function of the radius of the cylinder at three different time snapshots, $t_1 = 0.3$ ns, $t_2 = 0.4$ ns and $t_3 = 0.8$ ns, which are indicated in Fig. 4.6a showing the coil current signal. At each time snapshot, for each permeability value the H_z field obtained from the simulation in a cross-section of the cylinder taken along its middle point is compared with the analytical solution. The numerical solutions are seen to be in good agreement with the analytical results. Also shown is the coil field amplitude at that particular time snapshot, which corresponds to the amplitude of the coil current signal at that moment and is seen to be uniform

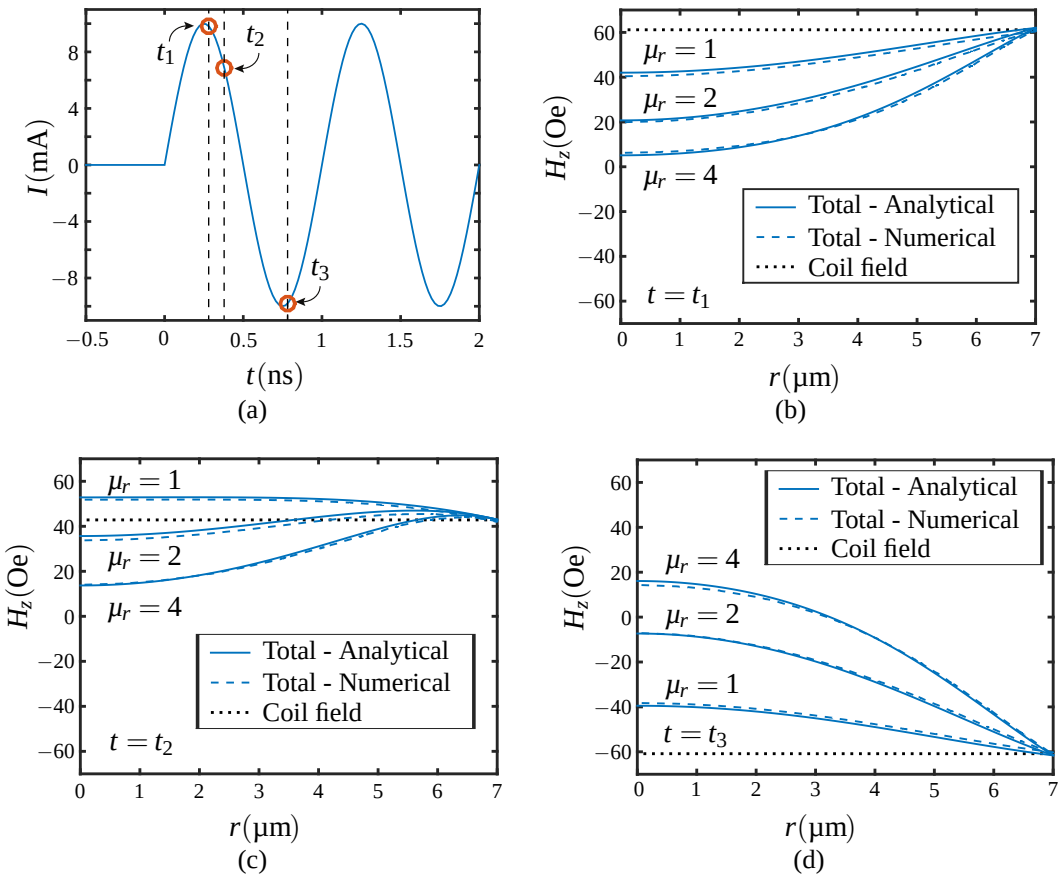

Figure 4.6: (a) Current flowing in the coil of Fig. 4.4a. It is a causal, 1 GHz sine signal and produces a concurrent time harmonic magnetic field with a peak amplitude of 62 Oe. (b–d) Axial component H_z of the total magnetic field as a function of the radius inside a cross section perpendicular to the cylinder's axis and taken at the middle point along its length, at times $t_1 = 0.3\,\text{ns}$, $t_2 = 0.4\,\text{ns}$ and $t_3 = 0.8\,\text{ns}$ respectively. Numerically obtained results are shown for 3 sets of magnetic parameters corresponding to $\mu_r = 1$, $\mu_r = 2$ and $\mu_r = 4$ and are compared with the analytical solution. Also shown is the spatially uniform z component of the coil magnetic field.

throughout the cylinder. If eddy currents were neglected, the coil field would correspond to the total magnetic field so that the eddy currents magnetic field $\vec{H}_{\text{eddy}}$ corresponds to the difference between the total magnetic field and the coil field on these plots. The fact that the $\vec{H}_{\text{eddy}}$ field is seen to be significant compared to the coil field indicates that in this case, the magnetostatic approximation of the Maxwell equations is not a good approximation and that the magnetoquasistatic approximation should be used instead. This is validated by the condition of validity for the magnetostatic approximation, Eq. (4.48) from section 4.3. Indeed, from Eq. (4.29), the skin

depth for this problem is 2.5 µm while the relevant size is the cylinder diameter which is 14 µm. Since the skin depth is comparable to the cylinder diameter, the magnetostatic approximation cannot be expected to be a good one.

At $t = t_1$, where the coil current and coil field are at their maximum value, from Fig. 4.6b it is seen that at the center of the cylinder, the total field is smaller than the applied coil field. This is due to eddy currents which produce a field which tends to cancel the applied field. At the surface of the cylinder at $r = 7\,\mu$m, the total field is equal to the coil field since, as discussed in Appendix A, the eddy currents field $\vec{H}_{\text{eddy}}$ are zero outside of the cylinder. These results can also be understood in terms of the diffusion of the magnetic field. The penetration of the field inside the cylinder depends on the skin depth. For instance, in the $\mu_r = 4$ case which corresponds to a skin depth at 1 GHz of 2.5 µm, the field H_z remains close to zero. In the $\mu_r = 1$ case, the skin depth is 5 µm and the magnetic field penetrates the cylinder more. Diffusion occurs over a time scale corresponding to the diffusion time constant defined in Eq. (4.28). Taking the diffusion length to correspond to the cylinder radius, $L = 7\,\mu$m, in the $\mu_r = 4$ case, the diffusion time constant is $\tau_m = 2.5\,$ns whereas for $\mu_r = 1$ it is $\tau_m = 0.6\,$ns. This means that the magnetic field diffuses inside the cylinder more rapidly in the $\mu_r = 1$ case and the total field will therefore track the applied coil field more closely than for the $\mu_r = 4$ case. Diffusion effectively causes the magnetic field inside the cylinder to lag in time behind the applied coil field. For instance, in the $\mu_r = 2$ case, at $t = t_1$ when the coil field is at its maximum, the total H_z field at $r = 1\,\mu$m is around 20 Oe. At time $t = t_2$, when the coil field has actually decreased in amplitude, the H_z field at $r = 1\,\mu$m has increased to 35 Oe.

To further illustrate the effect of diffusion, Fig. 4.7 shows the z component of the magnetization M_z as a function of time at different radius values inside the cylinder for the case $\mu_r = 4$. Also plotted is M_z for the case where eddy currents are neglected, that is when the magnetostatic approximation is used, in which case H_z and correspondingly the M_z response is uniform within the cylinder. The coil field, which also corresponds to H_z in the magnetostatic case, is included

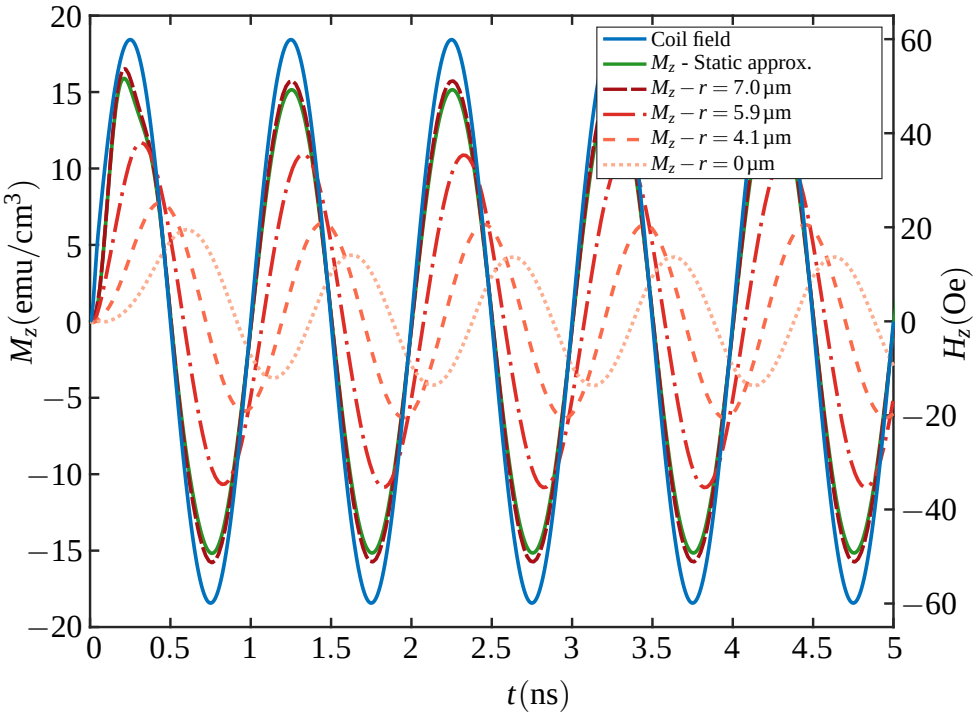

Figure 4.7: Magnetization response M_z to the coil current of Fig. 4.6a at different radius values inside the cylinder for the case $\mu_r = 4$. The z oriented magnetic field generated by the coil is plotted against the right-hand vertical axis. Also shown is the M_z response obtained using the static approximation of the Maxwell equations.

in the plot.

The magnetization response is seen to differ greatly as a function of the radial distance r inside the cylinder. At $r = 7\,\mu m$, corresponding to the surface of the cylinder, the response is seen to be very similar to the case where the magnetostatic approximation is used. This is expected since as in the case of the magnetostatic approximation, the total H_z field at the surface of the cylinder corresponds to the coil field. As points closer to the center of the cylinder are considered, the amplitude of the response decreases and the time delay with respect to the coil field increases, both of which are a result of the diffusion effect.

4.7 A finite element solver for the Maxwell equations

The integral equation formulation proposed in section 4.5 for the Maxwell equations solver has the advantage of only requiring the discretization of magnetic and conductive regions, therefore allowing eddy currents to be modeled without increasing the problem size when compared to micromagnetic simulations without eddy currents. However, while the volume integrals that need to be computed to solve the linear system can be accelerated using GPU's and fast algorithms, because the system is solved iteratively, several integral computations need to be performed at every time step which is quite demanding computationally. It is therefore natural to investigate other types of solvers for the magnetoquasistatic Maxwell equations, such as the finite element method.

In the present section, a finite element solver for the magnetoquasistatic Maxwell equations is presented which is used in the coupled micromagnetic-eddy currents solver. As in section 4.5 on the integral equation solver, the problem consists in solving the magnetoquasistatic Maxwell equations where the magnetization $\vec{M}$ is obtained from the LLG equation solver and is treated as a known source and where the current $\vec{J}$ has two parts, an impressed source current $\vec{J}_i$, which is assumed known, and the eddy currents $\vec{J}_{\text{eddy}}$. The magnetoquasistatic Maxwell equations were given in Eqs. (4.51) and are repeated here for convenience,

$$\nabla \times \vec{E} = -\mu_0 \frac{\partial}{\partial t}\left(\vec{H} + \vec{M}\right) \tag{4.91a}$$

$$\nabla \times \vec{H} = \vec{J} \tag{4.91b}$$

$$\nabla \cdot \vec{E} = \frac{\rho_s}{\varepsilon_0} \tag{4.91c}$$

$$\nabla \cdot \left(\vec{H} + \vec{M}\right) = 0\ . \tag{4.91d}$$

To solve the magnetoquasistatic Maxwell equations, the magnetic field is decomposed

into three parts, $\vec{H} = \vec{H}_M + \vec{H}_i + \vec{H}_{\text{eddy}}$. The field $\vec{H}_M$ is the magnetostatic field and is solution of

$$\nabla \times \vec{H}_M = 0 \ , \ \nabla \cdot (\vec{H}_M + \vec{M}) = 0 \ . \tag{4.92}$$

It is computed as in the magnetostatic approximation with the computation of a volume integral, as in section 2.3. The field $\vec{H}_i$ is the magnetic field induced by the impressed current source $\vec{J}_i$ and satisfies

$$\nabla \times \vec{H}_i = \vec{J}_i \ , \ \nabla \cdot \vec{H}_i = 0 \ . \tag{4.93}$$

It can be computed from the volume integral [6]

$$\vec{H}_i(\vec{x}) = \frac{1}{4\pi} \int \vec{J}_i(\vec{x}') \times \frac{\vec{x} - \vec{x}'}{|\vec{x} - \vec{x}'|^3} dv' \ . \tag{4.94}$$

Since the source current $\vec{J}_i$ is given as a data of the problem, the field $\vec{H}_i$ is pre-computed before the micromagnetic simulation. Alternatively, $\vec{H}_i$ can also be specified directly as an externally applied magnetic field. The field $\vec{H}_{\text{eddy}}$ is the magnetic field induced by eddy currents and is solution of

$$\nabla \times \vec{E} = -\mu_0 \frac{\partial}{\partial t} (\vec{H}_i + \vec{H}_M + \vec{H}_{\text{eddy}} + \vec{M}) \tag{4.95a}$$

$$\nabla \times \vec{H}_{\text{eddy}} = \vec{J}_{\text{eddy}} \tag{4.95b}$$

$$\nabla \cdot \vec{E} = \frac{\rho_s}{\varepsilon_0} \tag{4.95c}$$

$$\nabla \cdot \vec{H}_{\text{eddy}} = 0. \tag{4.95d}$$

These equations are solved for $\vec{H}_{\text{eddy}}$ using the finite element method for which a variational formulation will be given. From Eqs. (4.92), (4.93) and (4.95), it is seen that $\vec{H} = \vec{H}_M + \vec{H}_i + \vec{H}_{\text{eddy}}$ along with $\vec{E}$ satisfy the magnetoquasistatic equations, Eqs. (4.91). It should be noted that both the fields $\vec{H}_M$ and $\vec{H}_i$ could in principle be combined with $\vec{H}_{\text{eddy}}$ and included in the finite

element formulation. However, since $\vec{H}_i$ is actually pre-computed, it makes sense to compute it separately from $\vec{H}_{\text{eddy}}$. Furthermore, it allows the flexibility of providing $\vec{H}_i$ directly as an applied external field, without having to specify a source current distribution $\vec{J}_i$. In the case of $\vec{H}_M$, it is obtained by computing a single integral once per iteration in the Newton method. Indeed, $\vec{H}_M$ only depends on the magnetization $\vec{M}$ and does not need to be solved iteratively like $\vec{H}_{\text{eddy}}$ so that computing it separately from $\vec{H}_{\text{eddy}}$ is not overly costly. Also, since $\vec{H}_M$ has jump discontinuities at interfaces where $\vec{M}$ has jump discontinuities, such as at the boundary of magnetic regions, computing it separately allows $\vec{H}_{\text{eddy}}$ to be everywhere continuous. This avoids complications such as doubled degrees of freedom which would be needed to handle jump discontinuities in the finite element formulation.

In order to solve for $\vec{H}_{\text{eddy}}$ within some domain Ω, boundary conditions need to be determined. While several different approaches can be taken, in this work an homogeneous Dirichlet boundary condition is used for $\vec{H}_{\text{eddy}}$, i.e. $\vec{H}_{\text{eddy}} = 0$ is assumed at the boundary $\partial\Omega$. The domain of solution Ω is chosen to enclose the magnetic and conductive regions and chosen large enough so that the homogeneous boundary condition is a good enough approximation. Comparing Eqs. (4.93) with Eqs. (4.95), it is seen that Eq. (4.94) holds for $\vec{H}_{\text{eddy}}$ and $\vec{J}_{\text{eddy}}$ so that $\vec{H}_{\text{eddy}}$ falls off at a rate of square the distance from eddy currents distributions which means that Ω need not be overly large.

The variational formulation can be obtained by two equivalent methods: the Galerkin method and the least squares method. In the Galerkin method, the scalar product of the curl of Eq. (4.95b) and a test function $\vec{V}$ is integrated over the region Ω. This yields

$$\int_{\Omega} (\nabla \times \nabla \times \vec{H}_{\text{eddy}} - \nabla \times \vec{J}_{\text{eddy}}) \cdot \vec{V} dv = 0 \,. \tag{4.96}$$

The vector form of Green's first identity states that given two appropriately smooth vector fields

$\vec{A}$ and $\vec{B}$ [51],

$$\int_\Omega (\nabla \times \nabla \times \vec{A}) \cdot \vec{B} dv = \int_\Omega \nabla \times \vec{A} \cdot \nabla \times \vec{B} dv + \int_{\partial\Omega} (\nabla \times \vec{A} \times \vec{B}) \cdot \hat{n} ds \ . \tag{4.97}$$

Applying this to Eq. (4.96) yields

$$\int_\Omega \nabla \times \vec{H}_{\text{eddy}} \cdot \nabla \times \vec{V} dv + \int_{\partial\Omega} (\nabla \times \vec{H}_{\text{eddy}} \times \vec{V}) \cdot \hat{n} ds - \int_\Omega \nabla \times \vec{J}_{\text{eddy}} \cdot \vec{V} dv = 0 \ . \tag{4.98}$$

Since from Eq. (4.95b) $\nabla \times \vec{H}_{\text{eddy}} = \vec{J}_{\text{eddy}}$, this can be written as

$$\int_\Omega \nabla \times \vec{H}_{\text{eddy}} \cdot \nabla \times \vec{V} dv + \int_{\partial\Omega} (\vec{J}_{\text{eddy}} \times \vec{V}) \cdot \hat{n} ds - \int_\Omega \nabla \times \vec{J}_{\text{eddy}} \cdot \vec{V} dv = 0 \ . \tag{4.99}$$

While Eq. (4.99) constitutes a variational formulation that can be used to solve for $\vec{H}_{\text{eddy}}$ with the finite element method, it does not make use of Eq. (4.95d) which states that $\vec{H}_{\text{eddy}}$ should be divergence free. Because of this, as is well documented in the finite element method literature in electromagnetism [52, 53, 54], the numerical solution obtained with this variational formulation will not necessarily have a zero divergence which can lead to so-called spurious solutions. For this reason, a penalty term can be added which penalizes non-zero divergence of the $\vec{H}_{\text{eddy}}$ field, following which Eq. (4.99) becomes

$$\int_\Omega \nabla \times \vec{H}_{\text{eddy}} \cdot \nabla \times \vec{V} dv + \int_{\partial\Omega} (\vec{J}_{\text{eddy}} \times \vec{V}) \cdot \hat{n} ds - \int_\Omega \nabla \times \vec{J}_{\text{eddy}} \cdot \vec{V} dv + \int_\Omega \nabla \cdot \vec{H}_{\text{eddy}} \nabla \cdot \vec{V} dv = 0 \ . \tag{4.100}$$

This result can also be obtained using the least squares method [55]. In this method, we seek to satisfy the Maxwell equations for $\vec{H}_{\text{eddy}}$, Eqs. (4.95b) and (4.95d) in the least squares sense by minimizing the functional

$$I(\vec{H}_{\text{eddy}}) = \int_\Omega |\nabla \times \vec{H}_{\text{eddy}} - \vec{J}_{\text{eddy}}|^2 dv + \int_\Omega |\nabla \cdot \vec{H}_{\text{eddy}}|^2 dv \ . \tag{4.101}$$

From the calculus of variations, a minimum of this functional corresponds to

$$\frac{d}{d\varepsilon} I(\vec{H}_{\text{eddy}} + \varepsilon \vec{V})\Big|_{\varepsilon=0} = 0 \tag{4.102}$$

where $\vec{V}$ is any vector field. From the definition of I in Eq. (4.101), this can be written as

$$\frac{d}{d\varepsilon}\Big[\int_\Omega (\nabla \times (\vec{H}_{\text{eddy}} + \varepsilon \vec{V}) - \vec{J}_{\text{eddy}}) \cdot (\nabla \times (\vec{H}_{\text{eddy}} + \varepsilon \vec{V}) - \vec{J}_{\text{eddy}}) dv + \int_\Omega \nabla \cdot (\vec{H}_{\text{eddy}} + \varepsilon \vec{V}) \nabla \cdot (\vec{H}_{\text{eddy}} + \varepsilon \vec{V}) dv \Big]_{\varepsilon=0} = 0 \tag{4.103}$$

which when evaluated gives

$$\int_\Omega \nabla \times \vec{H}_{\text{eddy}} \cdot \nabla \times \vec{V} dv - \int_\Omega \vec{J}_{\text{eddy}} \cdot \nabla \times \vec{V} dv + \int_\Omega \nabla \cdot \vec{H}_{\text{eddy}} \nabla \cdot \vec{V} dv = 0 \, . \tag{4.104}$$

Since $\nabla \cdot (\vec{A} \times \vec{B}) = \vec{B} \cdot (\nabla \times \vec{A}) - \vec{A} \cdot (\nabla \times \vec{B})$, for sufficiently smooth vector fields $\vec{A}$ and $\vec{B}$, the divergence theorem yields

$$\int_\Omega \vec{A} \cdot (\nabla \times \vec{B}) dv = \int_\Omega \vec{B} \cdot (\nabla \times \vec{A}) dv - \int_{\partial\Omega} (\vec{A} \times \vec{B}) \cdot \hat{n} ds \, . \tag{4.105}$$

Using this, Eq. (4.104) can be written as

$$\int_\Omega \nabla \times \vec{H}_{\text{eddy}} \cdot \nabla \times \vec{V} dv + \int_{\partial\Omega} (\vec{J}_{\text{eddy}} \times \vec{V}) \cdot \hat{n} ds - \int_\Omega \nabla \times \vec{J}_{\text{eddy}} \cdot \vec{V} dv + \int_\Omega \nabla \cdot \vec{H}_{\text{eddy}} \nabla \cdot \vec{V} dv = 0 \tag{4.106}$$

which is exactly Eq. (4.100), the variational formulation obtained with the Galerkin method.

The solution process in the finite element method involves discretizing the unknown function $\vec{H}_{\text{eddy}}$ with N basis functions whose support is localized on tetrahedral elements. In the present work, linear basis functions are used such that each node is assigned a hat basis function with a support corresponding to neighboring tetrahedral elements and three degree of

freedom, one for each vector component. The test function $\vec{V}$ is then successively let to be the N basis functions which gives rise to a $N \times N$ linear system of equations that can be solved for the degrees of freedom. This involves an assembly procedure for the system matrix which involves the elemental variational formulation, which corresponds to the variational formulation of Eqs. (4.100) and (4.106) but with integration over an individual tetrahedral element K. The elemental variational formulation reads

$$\int_K \nabla \times \vec{H}_{\text{eddy}} \cdot \nabla \times \vec{V} dv + \int_{\partial K} (\vec{J}_{\text{eddy}} \times \vec{V}) \cdot \hat{n} ds - \int_K \nabla \times \vec{J}_{\text{eddy}} \cdot \vec{V} dv + \int_K \nabla \cdot \vec{H}_{\text{eddy}} \nabla \cdot \vec{V} dv = 0 \tag{4.107}$$

where ∂K is the surface of the tetrahedral element K and $\hat{n}$ is the outward pointing unit vector normal to the surface. With the eddy currents in conductive regions given by $\vec{J}_{\text{eddy}} = \sigma \vec{E}$, assuming that the electric conductivity σ is constant within each element K, the third term in Eq. (4.107) can be written as

$$\int_K \nabla \times \vec{J}_{\text{eddy}} \cdot \vec{V} dv = \int_K \sigma \nabla \times \vec{E} \cdot \vec{V} dv \, . \tag{4.108}$$

Using Eq. (4.95a) to replace for $\nabla \times \vec{E}$ gives

$$\int_K \nabla \times \vec{J}_{\text{eddy}} \cdot \vec{V} dv = -\mu_0 \sigma \int_K \frac{\partial}{\partial t} (\vec{H}_i + \vec{H}_{\text{eddy}} + \vec{H}_M + \vec{M}) \cdot \vec{V} dv \, . \tag{4.109}$$

Using this in Eq. (4.107) and using Eq. (4.95b) to replace for $\vec{J}_{\text{eddy}}$ in the surface integral term yields the following variational formulation in terms of the unknown $\vec{H}_{\text{eddy}}$, the test function $\vec{V}$ and known vector fields,

$$\begin{aligned} \int_K \nabla \times \vec{H}_{\text{eddy}} \cdot \nabla \times \vec{V} dv + \int_K \nabla \cdot \vec{H}_{\text{eddy}} \nabla \cdot \vec{V} dv = \\ - \mu_0 \sigma \int_K \frac{\partial}{\partial t} (\vec{H}_i + \vec{H}_{\text{eddy}} + \vec{H}_M + \vec{M}) \cdot \vec{V} dv - \int_{\partial K} (\nabla \times \vec{H}_{\text{eddy}} \times \vec{V}) \cdot \hat{n} \, ds \, . \end{aligned} \tag{4.110}$$

For tetrahedrons with zero conductivity, $\vec{J}_{\text{eddy}} = 0$ and the variational formulation of Eq. (4.107)

reduces to

$$\int_K \nabla \times \vec{H}_{\text{eddy}} \cdot \nabla \times \vec{V} dv + \int_K \nabla \cdot \vec{H}_{\text{eddy}} \nabla \cdot \vec{V} dv = 0 \,. \tag{4.111}$$

As was done for the integral equation solver of section 4.5, the time derivative of $\vec{H}_{\text{eddy}}$ is discretized using the BDF method. Evaluated at time $t = t_{n+1}$, the time derivative is written as

$$\frac{\partial \vec{H}_{\text{eddy}}}{\partial t} = \sum_{i=0}^{r} \alpha_i \vec{H}_{\text{eddy},n+1-i} \tag{4.112}$$

where r is the BDF order and $\vec{H}_{\text{eddy},n+1-i}$ is the solution $\vec{H}_{\text{eddy}}$ at time t_{n+1-i}. With this, the time-discretized version of the variational formulation in Eq. (4.110) is

$$\begin{aligned} &\int_K \nabla \times \vec{H}_{\text{eddy},n+1} \cdot \nabla \times \vec{V} dv + \int_K \nabla \cdot \vec{H}_{\text{eddy},n+1} \nabla \cdot \vec{V} dv + \mu_0 \sigma \alpha_0 \int_K \vec{H}_{\text{eddy},n+1} \cdot \vec{V} dv + \\ &\quad \int_{\partial K} (\nabla \times \vec{H}_{\text{eddy},n+1} \times \vec{V}) \cdot \hat{n} \, ds = -\mu_0 \sigma \int_K \left[\sum_{i=1}^{r} \alpha_i \vec{H}_{\text{eddy},n+1} + \frac{\partial}{\partial t} (\vec{H}_i + \vec{H}_M + \vec{M}) \right] \cdot \vec{V} dv \,. \end{aligned} \tag{4.113}$$

As mentioned before, the assembly process relies on approximating the eddy currents magnetic field $\vec{H}_{\text{eddy}}$ in terms of basis functions as

$$\vec{H}_{\text{eddy},n+1} = \sum_{j=1}^{N} u_j \vec{\psi}_j \tag{4.114}$$

where N corresponds to the number of degrees of freedom which is equal to three times the number of nodes in the mesh, excluding nodes on $\partial\Omega$, the $\vec{\psi}_j$'s are the vector basis functions which correspond to the scalar hat basis functions associated with each node to which either of the three unit vector components $\hat{x}$, $\hat{y}$ or $\hat{z}$ is affixed and the u_j's are the degrees of freedom. By letting the test function $\vec{V}$ be successively $\vec{\psi}_i$ with $i = 1, \ldots, N$, a linear system is obtained which is of the form

$$AU = F \tag{4.115}$$

where A is the system matrix, U is a vector containing the u_j's as its components and F is a vector representing the right-hand side of the variational formulation. This global system of equations is assembled from the elemental system which reads

$$A^K U^K = F^K \ . \tag{4.116}$$

Here, U^K contains the degrees of freedom associated with tetrahedron K. The ijth element of the A^K matrix is given by

$$a_{ij}^K = \int_K \nabla \times \vec{\psi}_j^K \cdot \nabla \times \vec{\psi}_i^K dv + \int_K \nabla \cdot \vec{\psi}_j^K \nabla \cdot \vec{\psi}_i^K dv + \mu_0 \sigma \alpha_0 \int_K \vec{\psi}_j^K \cdot \vec{\psi}_i^K dv + \int_{\partial K} (\nabla \times \vec{\psi}_j^K \times \vec{\psi}_i^K) \cdot \hat{n} ds \tag{4.117}$$

for tetrahedrons K in conductive regions and

$$a_{ij}^K = \int_K \nabla \times \vec{\psi}_j^K \cdot \nabla \times \vec{\psi}_i^K dv + \int_K \nabla \cdot \vec{\psi}_j^K \nabla \cdot \vec{\psi}_i^K dv \tag{4.118}$$

for tetrahedrons in regions with $\sigma = 0$. The elements of F^K are given by

$$f_i^K = -\mu_0 \sigma \int_K \left[\sum_{i=1}^{r} \alpha_i \vec{H}_{\text{eddy},n+1} + \frac{\partial}{\partial t} (\vec{H}_i + \vec{H}_M + \vec{M}) \right] \cdot \vec{\psi}_i^K dv \tag{4.119}$$

for tetrahderons in conductive regions and by zero for tetrahedrons in non-conductive regions. In practice, time integration involves a variable time step scheme so that the coefficient α_0 in Eq. (4.117) will in general change from one step to the next. To avoid having to re-assemble the system matrix, the global system matrix A is divided into two parts, A_1 and A_2 corresponding to the following matrix elements

$$a_{ij,1}^K = \int_K \nabla \times \vec{\psi}_j^K \cdot \nabla \times \vec{\psi}_i^K dv + \int_K \nabla \cdot \vec{\psi}_j^K \nabla \cdot \vec{\psi}_i^K dv + \int_{\partial K} (\nabla \times \vec{\psi}_j^K \times \vec{\psi}_i^K) \cdot \hat{n} ds \tag{4.120}$$

and

$$a^K_{ij,2} = \mu_0 \sigma \int_K \vec{\psi}^K_j \cdot \vec{\psi}^K_i dv \tag{4.121}$$

This effectively allows the linear system of Eq. (4.115) to be written as

$$(A_1 + \alpha_0 A_2)U = -A_2 \left[\sum_{i=1}^{r} \alpha_i \vec{H}_{\text{eddy},n+1} + \frac{\partial}{\partial t}(\vec{H}_i + \vec{H}_M + \vec{M}) \right] \tag{4.122}$$

where the matrices A_1 and A_2 are pre-assembled and the global matrix $(A_1 + \alpha_0 A_2)$ can quickly be obtained at each time step given the value of α_0. The time derivatives of $\vec{H}_i$, $\vec{H}_M$ and $\vec{M}$ in Eq. (4.122) are computed using the BDF method, although any other finite difference time discretization scheme could be used, using the values of these fields at the current and previous time steps.

The linear system of Eq. (4.122) can be solved using different techniques. For large problems, iterative solvers are a good choice, and since the matrix A of the system is not symmetric, the GMRES method [49] is employed. Different preconditioners can be used along with the preconditioned GMRES method. One option is to use a symmetric approximation of the A matrix, assembled from Eq. (4.117) where the last term involving a surface integral is neglected, as a preconditioning matrix. A potent way of solving the preconditioning linear system with this symmetric matrix is by using the conjugate gradient method with a weak convergence criterion which allows the preconditioning step of the GMRES method to involve only a few conjugate gradient iterations which are very efficient. This approach however requires the use of the flexible GMRES (FGMRES) variant of the GMRES method [49] which has higher memory requirements than the standard GMRES method. Also, while this approach works well in many cases, for problems with a fine mesh, the convergence rate of the conjugate gradient method decreases which makes its use as a preconditioning method much less efficient.

An alternative preconditiong method which was found to have a very good performance is to pre-compute incomplete LU factorizations [49] of the global A matrix, given by $(A_1 + \alpha_0 A_2)$

for a range of α_0 values, which correspond to a range of time step values. At each time step, the incomplete LU factorization is interpolated for the current α_0 value and this interpolated factorization is used as a preconditioning matrix.

Comparing performance with the integral equation solver, on the same hardware and for the same 3.5 million tetrahedral elements problem which requires 21.2 hours of computation time per ns of simulation time with the integral equation solver, the finite element solver with the interpolated incomplete LU factorization preconditioner requires 1.76 hours of computation time per ns of simulation time. Comparing this with the 0.22 hours required to simulate 1 ns without eddy currents, it is seen that while modeling eddy currents comes at a significant performance cost, it is still possible to realistically handle very large problems.

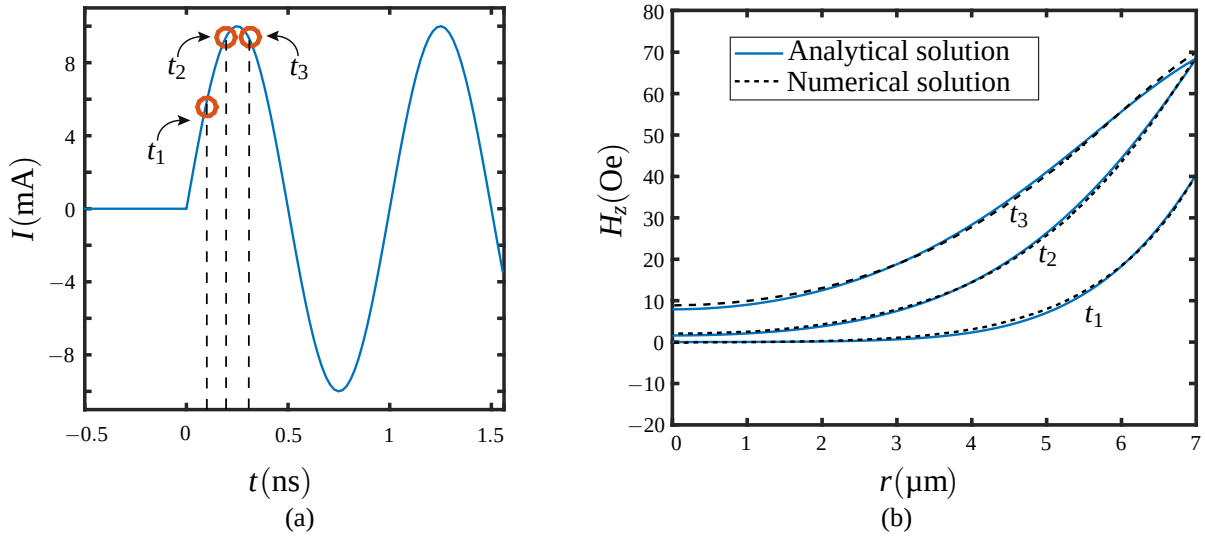

Figure 4.8: (a) Current signal flowing in the coil of the test problem. (b) Axial component H_z of the total magnetic field as a function of the radius inside a cross section taken at the cylinder's middle point along its length. The numerical results obtained with the solver are compared to the analytical solution for times $t_1 = 0.1\,\text{ns}$, $t_2 = 0.2\,\text{ns}$ and $t_3 = 0.3\,\text{ns}$. The ferromagnetic cylinder has a length of 50 µm, a radius of 7 µm, a conductivity of $1\times 10^7\,\text{S/m}$ and magnetic parameters equivalent to $\mu_r = 4$.

To validate the eddy currents-micromagnetic solver using the finite element Maxwell equations solver, the test problem of section 4.6 is solved for a ferromagnetic cylinder with conductivity $\sigma = 1 \times 10^7\,\text{S/m}$, magnetic parameters corresponding to $\mu_r = 4$, a length of 50 µm

and a radius of 7 µm. The current signal is the same 1 GHz sinusoidal signal that was used in section 4.6 and is shown in Fig. 4.8a. The resulting total H_z field is shown in Fig. 4.8b at 3 time snapshots and is seen to be in good agreement with the analytical solution.

4.8 Example of eddy currents effect

The ferromagnetic cylinder test problem of 4.6 allows to verify the validity of numerical solutions obtained with the coupled eddy currents-micromagnetic solver and also illustrates the physics of eddy currents effects, including the diffusion of the electromagnetic fields. However, the dynamics involved in that problem are fairly simple and can be represented by a linear model while the value of micromagnetics lies in its ability to model highly complex, non-linear magnetization dynamics. For this reason, in this section the effect of eddy currents on the switching behavior of a ferromagnetic nano-disk is investigated.

The problem consists in a ferromagnetic disk with a 2 µm radius, a 500 nm thickness, a perpendicular unixaxial anisotropy, i.e. along the disk axis in the z direction, with magnitude $K = 5 \times 10^5 \,\mathrm{erg/cm^3}$, a conductivity of 1×10^7 S/m, a saturation magnetization $M_s = 200 \,\mathrm{emu/cm^3}$, a damping factor $\alpha = 0.1$, and an exchange coefficient $A_{\mathrm{ex}} = 5 \times 10^{-6} \,\mathrm{erg/cm}$. As shown in Fig. 4.9b, the initial state has the magnetization mostly uniform and pointing in the $-z$ direction. At $t = 0$, an external magnetic field oriented in the $+z$ direction is applied. The applied field is shown in Fig. 4.9a and has a rise time of 50 ps. The external applied field causes the magnetization of the disk to switch to a state with uniform magnetization in the $+z$ direction. Plots of the volume averaged z component of the normalized magnetization $\langle m_z \rangle$ as a function of time for the cases with and without eddy currents are shown in Fig. 4.9(a). It is seen that eddy currents cause the switching to occur faster.

The normalized magnetization distributions for the three states indicated by circled numbers in Fig. 4.9a for the simulation with eddy currents are shown in Fig. 4.9b. The intermediate

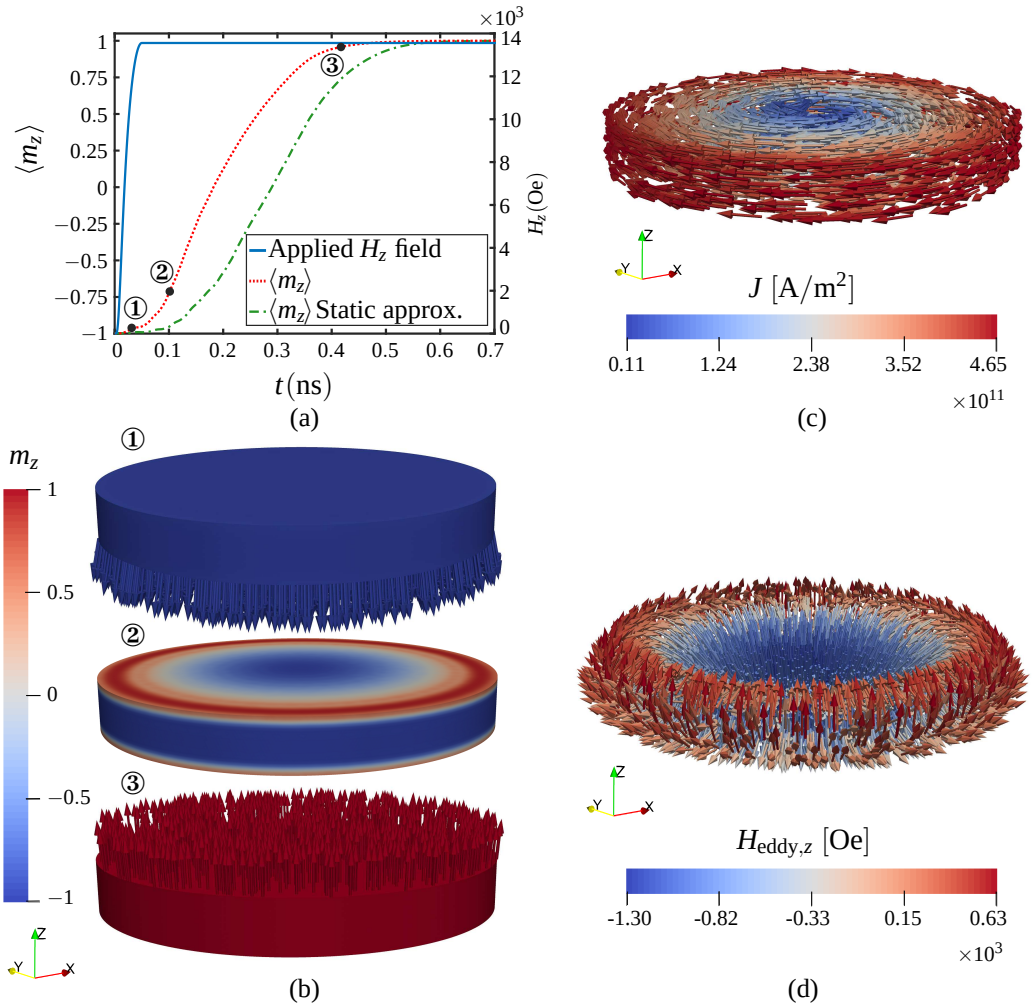

Figure 4.9: Switching of a ferromagnetic disk with a 500 nm thickness, 2 µm radius, saturation magnetization $M_s = 200\,\text{emu/cm}^3$, a z oriented uniaxial anisotropy $K = 5\times10^5\,\text{erg/cm}^3$, damping factor $\alpha = 0.1$ and exchange coefficient $A_{\text{ex}} = 5\times10^{-6}\,\text{erg/cm}$. (a) Externally applied H_z field and volume averaged z component of the normalized magnetization as a function of time for both the magnetoquasistatic approximation case and the magnetostatic approximation case. (b) Initial, intermediate and final normalized magnetization states for switching with eddy currents, as indicated by circled numbers in (a). The color indicates the value of the m_z component. (c) Eddy current density at $t = 0.02\,\text{ns}$, with color indicating the magnitude of the current. (d) Magnetic field due to the eddy currents at $t = 0.02\,\text{ns}$, with color indicating the value of the z component.

state shows that switching occurs by the nucleation of ring-shaped domains near the edge of the disk on the top and bottom surfaces. While not shown in the figure, the switching mechanism in the simulation without eddy currents is nearly identical. The expectation is that eddy currents would lead to faster switching due to increased overall losses in the system which lead to faster

relaxation to the new equilibrium state. However, from the eddy current density and the corresponding $\vec{H}_{\text{eddy}}$ magnetic field, shown in Figs. 4.9c and 4.9d respectively for time, $t = 0.02\,\text{ns}$, another mechanism for the faster switching can be identified. Indeed, it is seen that the eddy currents produce a magnetic field that is oriented in the $+z$ direction close to the edges of the disk, which helps to nucleate the ring-shaped domains seen in the intermediate state of Fig. 4.9b.

Chapter 4, in part, contains material that appears in Coupled Finite-Element Micromagnetic - Integral Equation Electromagnetic Simulator for Modeling Magnetization-Eddy Currents Dynamics, IEEE Trans. Magn., 2017, Couture, Simon; Chang, Ruinan; Volvach, Iana; Goncharov, Alexander; Lomakin, Vitaliy, as well as material that has been submitted for publication, Modeling Eddy Currents in Micromagnetic Simulations: A Coupled Micromagnetic-Maxwell Equations Solver Based on the Finite Element Method, 2018, Couture, Simon; Goncharov, Alexander; Lomakin, Vitaliy. The dissertation/thesis author was the primary investigator and author of these papers.

Appendix A

Analytical solution for the eddy currents test problem

In this section, the analytical solution for the ideal linear test problem of section 4.6 is derived. An infinitely long ferromagnetic cylinder with radius a, conductivity σ and permeability μ is considered that is excited by solenoidal coil carrying a time-harmonic current. The geometry of the problem is shown in Fig. 4.4.

An infinitely long solenoidal coil with N turns per unit length carrying a current $I(t)$ produces a predominantly uniform, z oriented axial magnetic field given by $H_{\text{coil}}(t) = NI(t)$ inside the solenoid and 0 outside the solenoid [6]. From the cylindrical symmetry of the problem, the coil field induces azimuthally oriented eddy currents which, acting as volumetric solenoidal currents, produce an axially oriented magnetic field inside the cylinder and no magnetic field outside of it. For this reason, in the ideal linear version of the test problem the $\vec{H}$ field only has a z component and it satisfies the magnetoquasistatic Maxwell equations Eqs. (4.51) with $H_z(t) = H_{\text{coil}}(t)$ as a boundary condition at the surface of the cylinder.

With Ohm's law $\vec{J} = \sigma\vec{E}$, taking the curl of Eq. (4.51b) gives

$$\nabla\nabla\cdot\vec{H} - \nabla^2\vec{H} = \sigma\nabla\times\vec{E}. \tag{A.1}$$

Since $\vec{B} = \mu\vec{H}$, Eq. (4.51d) is equivalent to $\nabla\cdot\vec{H} = 0$. Using this and Eq. (4.51a) to replace for $\nabla\times\vec{E}$, Eq. (A.1) becomes

$$\frac{1}{\sigma\mu}\nabla^2\vec{H} = \frac{\partial\vec{H}}{\partial t}, \tag{A.2}$$

which is the vector diffusion equation. The z component of $\vec{H}$ satisfies the scalar version of this diffusion equation,

$$\frac{1}{\sigma\mu}\nabla^2 H_z = \frac{\partial H_z}{\partial t} \tag{A.3}$$

and the problem is then to obtain a solution to Eq. (A.3) with the time dependent boundary condition $H_z(t) = H_{\text{coil}}(t)$ at $r = a$. For this problem to be well posed, an initial condition $H_z(t=0)$ is also required. For this purpose, it is assumed that before $t = 0$, no current flows in the coil so that the magnetic field is everywhere zero. When the current is switched on at $t = 0$, no field will have diffused inside the cylinder yet so that the initial condition is $H_z(t=0) = 0$ everywhere inside the cylinder. In cylindrical coordinates, from the symmetry of the problem H_z is expected to be a function of only the r coordinates and time. Therefore, Eq. (A.3) becomes

$$\frac{1}{\sigma\mu}\left[\frac{\partial^2 H_z(r,t)}{\partial^2 r} + \frac{1}{r}\frac{\partial H_z(r,t)}{\partial r}\right] = \frac{\partial H_z(r,t)}{\partial t}. \tag{A.4}$$

Taking the Laplace transform of Eq. (A.4) with respect to t and multiplying by $r^2\sigma\mu$, one obtains

$$r^2\frac{\partial^2}{\partial^2 r}H_z(r,s) + r\frac{\partial}{\partial r}H_z(r,s) - s\sigma\mu r^2 H_z(r,s) = 0 \tag{A.5}$$

with the boundary condition $H_z(r=a,s) = H_{\text{coil}}(s)$ and with the Laplace transform of $H_z(r,t)$

defined as

$$H_z(r,s) = \int_0^\infty e^{-st} H_z(r,t)dt. \tag{A.6}$$

Eq. (A.5) is recognized as Bessel's equation and has the general solution

$$H_z(r,s) = A(s)J_0(i\sqrt{s\sigma\mu}r) + B(s)Y_0(i\sqrt{s\sigma\mu}r). \tag{A.7}$$

where J_0 is the Bessel function of the first kind of order 0 and Y_0 is the Bessel function of the second kind of order 0. Since $Y_0(x) \to -\infty$ as $x \to 0$ and H_z must be bounded at $r = 0$, $B(s) = 0$. Applying the boundary condition at $r = a$ yields

$$A(s) = \frac{H_{\text{coil}}(s)}{J_0(i\sqrt{s\sigma\mu a})}. \tag{A.8}$$

Lets now consider a sinusoidal current signal and the corresponding sinusoidal coil field given by $H_{\text{coil}}(t) = H_0 \sin(\omega t)$. The Laplace transform of the coil field is then given by $H_{\text{coil}}(s) = H_0\omega/(s^2+\omega^2)$. Using this, Eq. (A.7) becomes

$$H_z(r,s) = H_0 \frac{\omega}{(s^2+\omega^2)} \frac{J_0(i\sqrt{s\sigma\mu}r)}{J_0(i\sqrt{s\sigma\mu a})}. \tag{A.9}$$

The solution in the time domain is obtained by computing the inverse Laplace transform

$$H_z(r,t) = \frac{1}{2\pi i} \int_{-i\infty+\tau_0}^{i\infty+\tau_0} H_z(r,s)e^{st}ds. \tag{A.10}$$

which can be done using the calculus of residues. By closing the contour with a semicircle in the left half complex plane, Eq. (A.10) can be expressed as the sum of the residues of $H_z(r,s)e^{st}$ at its singular points in the left half complex plane, including those on the imaginary axis. Two

such singular points are $s = i\omega$ and $s = -i\omega$, at which the residues are respectively

$$\operatorname*{Res}_{s=i\omega} H_z(r,s)e^{st} = H_0 \frac{J_0(i\sqrt{i\omega\sigma\mu}r)}{2iJ_0(i\sqrt{i\omega\sigma\mu}a)} e^{i\omega t} \tag{A.11}$$

and

$$\operatorname*{Res}_{s=-i\omega} H_z(r,s)e^{st} = H_0 \frac{J_0(i\sqrt{-i\omega\sigma\mu}r)}{-2iJ_0(i\sqrt{-i\omega\sigma\mu}a)} e^{-i\omega t}. \tag{A.12}$$

In addition, $H_z(r,s)$ in Eq. (A.9) has an infinite number of singular points corresponding to the zeros of $J_0(i\sqrt{s\sigma\mu}a)$. Denoting the n'th zero of the Bessel function $J_0(x)$ by α_n, the corresponding singular point of $H_z(r,s)$ is

$$s_n = \frac{-1}{\sigma\mu}\left(\frac{\alpha_n}{a}\right)^2 \tag{A.13}$$

and at each such point the residue of $H_z(r,s)e^{st}$ is

$$\operatorname*{Res}_{s=s_n} H_z(r,s)e^{st} = H_0 \frac{-\omega}{(s_n^2+\omega^2)} \frac{2\sqrt{s_n}J_0(i\sqrt{s_n\sigma\mu}r)}{i\sqrt{\sigma\mu}aJ_1(i\sqrt{s_n\sigma\mu}a)} e^{s_n t}. \tag{A.14}$$

The solution is then given by

$$H_z(r,t) = \operatorname*{Res}_{s=i\omega} H_z(r,s)e^{st} + \operatorname*{Res}_{s=-i\omega} H_z(r,s)e^{st} + \sum_{n=1}^{\infty} \operatorname*{Res}_{s=s_n} H_z(r,s)e^{st} \tag{A.15}$$

where the residues are given by Eqs. (A.11), (A.12) and (A.14). The series in Eq. (A.15) converges rapidly for $t > 0$ so that in practice, one can retain only the first few terms.

Bibliography

[1] A. Heller, "Anianus jedlik," *Nature*, vol. 53, no. 1379, pp. 516–517, 1896.

[2] D. J. Allan, "Power transformers - the second century," *Power Eng. J.*, vol. 5, no. 1, pp. 5–14, 1991.

[3] E. Pawley, *B. B. C. Engineering, 1922-72*. BBC Books, 1972.

[4] W. F. Brown, Jr., *Micromagnetics*. Interscience Publishers, 1963.

[5] G. Russakoff, "A derivation of the macroscopic maxwell equations," *Am. J. Phys.*, vol. 38, no. 10, pp. 1188–1195, 1970.

[6] J. D. Jackson, *Classical Electrodynamics*. Wiley, 1999.

[7] B. Yang, "Numerical studies of dynamical micromagnetics," Ph.D. dissertation, University of California, San Diego, 1997.

[8] S. Tehrani, J. M. Slaughter, M. Deherrera, B. N. Engel, N. D. Rizzo, J. Salter, M. Durlam, R. W. Dave, J. Janesky, B. Butcher, K. Smith, and G. Grynkewich, "Magnetoresistive random access memory using magnetic tunnel junctions," *Proc. IEEE*, vol. 91, no. 5, pp. 703–714, 2003.

[9] D. C. Ralph and M. D. Stiles, "Spin transfer torques," *J. Magn. Magn. Mater.*, vol. 320, no. 7, pp. 1190–1216, 2008.

[10] A. Crépieux and C. Lacroix, "Dzyaloshinsky-moriya interactions induced by symmetry breaking at a surface," *J. Magn. Magn. Mater.*, vol. 182, no. 3, pp. 341–349, 1998.

[11] C. Lambert, S. Mangin, B. S. D. C. S. Varaprasad, Y. K. Takahashi, M. Hehn, M. Cinchetti, G. Malinowski, K. Hono, Y. Fainman, M. Aeschlimann, and E. E. Fullerton, "All-optical control of ferromagnetic thin films and nanostructures," *Science*, vol. 345, no. 6202, pp. 1337–1340, 2014.

[12] H. Goldstein, C. Poole, and J. Safko, *Classical Mechanics*. Addison Wesley, 2002.

[13] L. Landau and E. Lifshitz, "On the theory of the dispersion of magnetic permeability in ferromagnetic bodies," *Phys. Zeitsch. der Sow.*, no. 8, pp. 153–169, 1935.

[14] T. L. Gilbert, "A phenomenological theory of damping in ferromagnetic materials," *IEEE Trans. Magn.*, vol. 40, no. 6, pp. 3443–3449, 2004.

[15] D. R. Fredkin and T. R. Koehler, "Hybrid method for computing demagnetizing fields," *IEEE Trans. Magn.*, vol. 26, no. 2, p. 415, 1990.

[16] C. Seberino and H. N. Bertram, "Concise, efficient three-dimensional fast multipole method for micromagnetics," *IEEE Trans. Magn.*, vol. 37, no. 3, 2001.

[17] H. Forster, T. Schrefl, R. Dittrich, W. Scholz, and J. Fidler, "Fast boundary methods for magnetostatic interactions in micromagnetics," *IEEE Trans. Magn.*, vol. 39, no. 5, pp. 2513–2515, 2003.

[18] B. D. Cullity and C. D. Graham, *Introduction to Magnetic materials*. John Wiley & Sons, 2009.

[19] M. V. Lubarda, "Micromagnetic modeling and analysis for memory and processing applications," Ph.D. dissertation, University of California, San Diego, 2012.

[20] W. A. Strauss, *Partial Differential Equations An Introduction*. John Wiley & Sons, 2008.

[21] R. Chang, "Finite element and integral equation formulations for high-performance micromagnetic and electromagnetic solvers," Ph.D. dissertation, University of California, San Diego, 2014.

[22] S. Li, R. Chang, A. Boag, and V. Lomakin, "Fast electromagnetic integral-equation solvers on graphics processing units," *IEEE Antennas Propag. Mag.*, vol. 54, no. 5, 2012.

[23] S. Li, "Fast algorithms and solvers in computational electromagnetics and micromagnetics on gpus," Ph.D. dissertation, University of California, San Diego, 2012.

[24] P. N. Brown, G. D. Byrne, and A. C. Hindmarsh, "VODE: A variable-coefficient ODE solver," *SIAM J. Sci. Stat. Comput.*, vol. 10, no. 5, 1989.

[25] A. C. Hindmarsh, P. N. Brown, K. E. Grant, S. L. Lee, R. Serban, D. E. Shumaker, and C. S. Woodward, "Sundials: Suite of nonlinear and differential/algebraic equation solvers," *ACM Trans. Math. Software*, vol. 31, no. 3, pp. 363–396, 2005.

[26] E. C. Stoner and E. P. Wohlfarth, "A mechanism of magnetic hysteresis in heterogeneous alloys," *Philos. Trans. R. Soc. London, Ser. A*, vol. 240, pp. 599–642, 1948.

[27] C. A. Balanis, *Advanced Engineering Electromagnetics*. Wiley, 1989.

[28] R. F. Soohoo, *Microwave Magnetics*. Harper & Row, 1985.

[29] Y. Yoshizawa, S. Oguma, and K. Yamauchi, "New fe-based soft magnetic alloys composed of ultrafine grain structure," *J. Appl. Phys.*, vol. 64, no. 10, pp. 6044–6046, 1988.

[30] H. Hoffmann, “Static wall coercive force in ferromagnetic thin films,” *IEEE Trans. Magn.*, vol. 9, no. 1, pp. 17–21, 1973.

[31] R. Harris, M. Plischke, and M. J. Zuckermann, “New model for amorphous magnetism,” *Phys. Rev. Lett.*, vol. 31, no. 3, pp. 160–162, 1973.

[32] R. Alben, J. J. Becker, and M. C. Chi, “Random anisotropy in amorphous ferromagnets,” *J. Appl. Phys.*, vol. 49, no. 3, pp. 1653–1658, 1978.

[33] G. Herzer, “Grain structure and magnetism of nanocrystalline ferromagnets,” *IEEE Trans. Magn.*, vol. 25, no. 5, p. 3327, 1989.

[34] ——, “Grain size dependence of coercivity and permeability in nanocrystalline ferromagnets,” *IEEE Trans. Magn.*, vol. 26, no. 5, pp. 1397–1402, 1990.

[35] ——, *Properties and applications of nanocrystalline alloys from amorphous precursors*. Dordrecht: Kluwer Academic Publishers, 2005, ch. The random anisotropy model, pp. 15–34.

[36] M. d’Aquino, “Nonlinear magnetization dynamics in thin-films and nanoparticles,” Ph.D. dissertation, Universita Degli Studi di Napoli, 2004.

[37] K. V. Mardia, *Statistics of Directional Data*. Academic Press, 1972.

[38] J. Fidler and T. Schrefl, “Micromagnetic modelling - the current state of the art,” *J. Phys. D: Appl. Phys.*, vol. 33, pp. 135–156, 2000.

[39] M. L. Brown, “Calculation of 3-dimensional eddy currents at power frequencies,” *IEE Proc.*, vol. 129, no. 1, pp. 46–53, January 1982.

[40] A. Fortin and A. Garon, *Les éléments finis: de la théorie à la pratique*. Laval University, 2017.

[41] E. D. Torre and J. G. Eicke, “Eddy currents in micromagnetic calculations,” *IEEE Trans. Magn.*, vol. 33, no. 2, pp. 1251–1254, 1997.

[42] G. M. Sandler and H. N. Bertram, “Micromagnetic simulations with eddy currents of rise time in thin film write heads,” *J. Appl. Phys.*, vol. 81, no. 8, pp. 4513–4515, 1997.

[43] L. Torres, E. Martinez, L. Lopez-Diaz, and O. Alejos, “About the inclusion of eddy currents in micromagnetic computations,” *Physica B*, vol. 343, 2004.

[44] G. Hrkac, M. Kirschner, F. Dorfbauer, D. Suess, O. Ertl, J. Fidler, and T. Schrefl, “Three-dimensional micromagnetic finite element simulations including eddy currents,” *J. Appl. Phys.*, vol. 97, 2005.

[45] G. Hrkac, “Combining eddy-current and micromagnetic simulations with finite-element method,” Ph.D. dissertation, Technische Universität Wien, 2005.

[46] K. Takano, X. Zhang, E.-A. Salhi, L. Guan, M. Sakai, J. Smyth, and M. Dovek, "Micromagnetics and eddy current effects in magnetic recording heads," *IEEE Trans. Magn.*, vol. 43, no. 6, 2007.

[47] H. A. Haus and J. R. Melcher, *Electromagnetic Fields and Energy*. Prentice Hall, 1989.

[48] R. E. Collin, *Field Theory of Guided Waves*, 2nd ed. Wiley, 1991.

[49] Y. Saad, *Iterative Methods for Sparse Linear Systems*. SIAM, 2003.

[50] "μMAG – Micromagnetic Modeling Activity Group, Standard problems," http://www.ctcms.nist.gov/ rdm/mumag.org, accessed: 12/20/2017.

[51] J. A. Stratton, *Electromagnetic Theory*. McGraw-Hill, 1941.

[52] J. Jin, *The Finite Element Method in Electromagnetics*. John Wiley & Sons, 2014.

[53] G. Mur, "The fallacy of edge elements," *IEEE Trans. Magn.*, vol. 34, no. 5, pp. 3244–3247, 1998.

[54] B.-N. Jiang, J. Wu, and L. A. Povinelli, "The origin of spurious solutions in computational electromagnetics," *J. Comput. Phys.*, vol. 125, no. 1, pp. 104–123, 1996.

[55] B. nan Jiang, *The Least-Squares Finite Element Method*. Springer, 1998.